Mechanisms of adhesion and invadopodia regulation

during breast cancer metastasis

by

Elena Marika Smith Voorand

Department of Biochemistry

Faculty of Medicine

McGill University

Montreal, Quebec, Canada

April 2020

A thesis submitted to McGill University in partial fulfillment of the requirements of the degree of Master of Science

TABLE OF CONTENTS

ABSTRACT

The development of metastatic disease is associated with poor outcomes for patients with breast cancer. Recently, Lipoma Preferred Translocation Partner (LPP) has been identified as a novel driver of the metastatic process in Neu/ErbB2 positive mammary tumour cells. In the context of breast cancer metastasis, it was demonstrated that LPP is a functional mediator of the convergent TGFβ1 and ErbB2 signaling pathways.

LPP, which belongs to the zyxin family of LIM domain proteins, promotes cell motility through actin skeleton remodeling, has mechanosensing properties and has been implicated in metastatic progression. Currently, in cells that have undergone an EMT, binding partners of LPP at adhesions are unknown. Herein we have generated an adhesion proximity network of LPP at dynamic adhesions to reveal proteins enriched specifically in the presence of TGFβ.

Furthermore, studies have revealed that LPP plays an additional role in ErbB2-expressing breast cancer cells. Central to the process of tumour cell invasion, is the formation of invasive and mechanosensitive structures within cancer cells termed invadopodia. Interestingly, it was shown that Src-mediated phosphorylation of LPP is critical to invadopodia formation and breast cancer metastasis. Thus, LPP regulates two actin cytoskeleton structures involved in ErbB2 breast cancer metastasis.

Importantly, adhesions and invadopodia are mechanosensitive cellular structures that can detect and mediate cellular response to changes in surrounding tissue stiffness. Thus, adhesions and invadopodia are capable of sensing and modulating cellular response to the stiffening of tissue and ECM that accompanies cancer disease progression. By developing a stiffness-tunable platform, we have characterized invadopodia formation of several breast cancer cell lines across a range of physiological- and disease-relevant stiffness. From our observations, breast cancer cells have a similar pattern of response with high invadopodia activity at low (<5 kPa) and high (>90 kPa) stiffness. Moreover, our data suggests that the activity of adhesion and invadopodia actin cytoskeleton structures can be changed with biophysical conditioning, such that cells have memory for culture at a specific stiffness.

Therefore, with this thesis I have sought to characterize proximal partners of LPP at adhesions and characterize migratory and invasive breast cancer cell phenotypes in response to substrate stiffness and biophysical priming.

RÉSUMÉ

Le développement d'une maladie métastatique est associé à un mauvais pronostic vital pour les patientes atteintes d'un cancer du sein. Récemment, Lipoma Preferred Translocation Partner (LPP) a été identifié comme pouvant entrainer le processus métastatique dans les cellules tumorales mammaires positives pour Neu/ErbB2. Dans le contexte des métastases du cancer du sein, il a été démontré que LPP est un médiateur fonctionnel des voies de signalisation convergentes TGFβ1 et ErbB2.

LPP, qui appartient à la famille zyxine des protéines à domaine LIM, favorise la motilité cellulaire en réorganisant le squelette d'actine, possède des propriétés de mécano-sensibilité cellulaire et a été impliqué dans la progression métastatique. Actuellement, chez les cellules ayant subi une EMT, les molécules interagissant avec LPP au sein des adhérences cellulaires restent inconnues. Dans cette étude, nous avons établi le réseau des protéines à proximité de LPP au sein des adhérences dynamiques pour identifier les protéines spécifiquement enrichies en présence de TGFβ.

De plus, des études ont révélé que la LPP joue également un rôle dans les cellules cancéreuses du sein exprimant ErbB2. Ainsi, la formation de structures invasives et mécano-sensibles au sein des cellules cancéreuses, appelées invadopodes, est primordiale au processus d'invasion des cellules tumorales. En effet, il a été démontré que la phosphorylation de LPP, médiée par Src, est essentielle à la formation des invadopodes et au développement des métastases du cancer du sein. Ainsi, LPP régule la formation de deux structures du cytosquelette d'actine qui sont impliquées dans le processus de formation des métastases du cancer du sein positif pour ErbB2.

Essentiellement, les adhésions et les invadopodes sont des structures cellulaires mécano-sensibles qui peuvent détecter et entrainer une réponse cellulaire aux changements de la rigidité des tissus environnants. Ainsi, les adhésions et les invadopodes sont capables de détecter et de moduler la réponse cellulaire à la rigidification des tissus et de la matrice extracellulaire qui accompagne généralement la progression de la maladie cancéreuse. En développant une plateforme avec rigidité ajustable, nous avons caractérisé la formation d'invadopodes chez plusieurs lignées cellulaires de cancer du sein soumises à différentes raideurs physiologiques liées à la maladie. D'après nos observations, les cellules cancéreuses du sein ont un patron de réponse similaire avec une forte activité des invadopodes à faible (<5 kPa) et forte (> 90 kPa) rigidité. De

plus, nos données suggèrent que l'activité de l'adhésion et des structures du cytosquelette d'actine des invadopodes peut être modifiée par le conditionnement biophysique, de sorte que les cellules ont une mémoire de la culture sur un milieu avec une rigidité donnée.

Par conséquent, avec les travaux présentés dans cette thèse, j'ai cherché à caractériser les partenaires proximaux de LPP au niveau des adhésions cellulaires et à caractériser les phénotypes migratoires et invasives des cellules du cancer du sein en réponse à la rigidité et à l'induction biophysique du substrat.

ACKNOWLEDGMENTS

Dr. Peter Siegel has been an exemplar graduate supervisor and mentor for my MSc degree. His unending enthusiasm, genuine inquisitiveness and impressive intellect has been inspiring. Dr. Siegel extended his support during difficult troubleshooting, and in parallel, he offered intellectual freedom in the laboratory to drive my scientific projects and further my professional development. Science is his favorite topic of conversation and if we could get him to stray from it, he also gave great personal and professional advice to all his students.

As my co-supervisor, Dr. Claire Brown has openly shared with me her wealth of microscopy knowledge and excitement for furthering new techniques and use of technologies. I have been impressed with her honest interest in promoting collaborative and interdisciplinary work. Her efforts to improve the microscopy discipline through networking and knowledge-sharing initiatives are admirable. The McGill ABIF staff have also been very generous with their help.

I would like to thank my Committee Members Dr. Josie Ursini-Siegel and Dr. William Muller for their guidance and enthusiasm during my degree. Their comments and interest pushed me in my last semester to explore as much as I could experimentally with my research.

I am thankful for the multiple sources of funding I received to pursue my degree at McGill. These include the Canderel Studentship, the Canadian Institute of Health Research (CIHR) CGS-Master's Award, the Fonds de la Recherché en Santé du Quebec (FRQS) Master's Training Award, the McGill Biochemistry GREAT Travel Awards, and the Canderel Travel Award.

Dr. Matthew Annis has been integral to my MSc studies. I am extremely grateful for his mentorship and the investment he demonstrated in both my research and personal successes. His humour and knack for problem-solving cleared up many crises for myself and my labmates. When we discussed dead ends in my research, Matt would suggest I put that aspect of my research aside for a few months until I got over my frustrations. Somehow these long talks inspired me to do the exact opposite and dive right back into the problem until it was solved. I think every research lab needs a Matt Annis!

A big thank you to Alexander Kiepas; I have really appreciated his help and dedication to the project we shared. Our discussions were thought-provoking and we have a great synergy of strengths to move projects and publications forward bit-by-bit. Alex was extremely generous with his time and success by including me in projects, conferences, publications and opinions on complimentary graph colours. Dr. Afnan-Abu Thuraia brought fresh excitement to the end of my project. Her hard work and determination are inspiring. I wish her all the best with her project moving forward.

Haruka Yoshie, Newsha Koushki, and Dr. Adele Khavari, from Dr. Allen Ehrlicher's lab

in the McGill Department of Bioengineering, are excellent collaborators and made my project feasible. I am very grateful for their assistance and weekly involvement with experiments. Dr. Anne-Claude Gingras and her student, Kento Abe, taught me the technique of BioID and were very generous with their time and effort to ensure my mass spectrometry samples were processed.

Both current and past Siegel Lab members have been fantastic colleagues and friends. Over the years, they have shared genuine support and a love for science with me. Thank you to Dr. Sébastien Tabariès, Dr. Marco Biondini, Matthew Dankner, Dr. Camille Lehuédé, Dr. Brian Hsu, Dr. Sylvia Andrzejewski, Leeana El-Houjeiri, Brennan Lavoie, Clark Thompson, Rima Ezzeddine, Jennifer Huxham, Yun Yun Shen, Alexander Nowakowski, Rebecca Zhuang, Sara Petrecca, and Noah Neubarth. In addition, Rebecca Deagle, Abira Rajah, Jessica Lyda, and Firas Mubaid were the fantastic Brown lab members I had the opportunity to work alongside and share ideas with.

My parents, Pia-Leena and Tom, as well as my sister, Hailey, have offered immeasurable support during my studies. I would like to thank them for reminding me of my strengths, pushing my boundaries and grounding me during difficult times.

PUBLICATIONS CONTRIBUTED TO

Kiepas, A., **Voorand, E.,** Senecal, J., Ahn, R., Annis, M.G., Jacquet, K., Tali, G., Bisson, N., Ursini-Siegel, J., Siegel, P.M., Brown, C.M. **The ShcA adaptor protein cooperates with LPP to mediate adhesion dynamics and invadopodia formation.** Manuscript in revision, JBC. 2020.

Kiepas, A., **Voorand, E.,** Mubaid, F., Siegel, P.M., Brown, C.M. **Optimizing live-cell fluorescence imaging conditions to minimize phototoxicity**. Manuscript accepted, J. Cell Sci. 2020.

Lewis, K., Kiepas, A., Hudson, J., Senecal, J., Ha, J., **Voorand, E**., Annis, M.G., Sabourin, V., Ahn, R., La Selva, R., Tabaries, S., Siegel, M., Dankner, M., Brown, C., Siegel, P.M., Ursini-Siegel, J. **p66ShcA functions as a contextual promoter of breast cancer metastasis**. Manuscript in press, Breast Cancer Res. 2019.

AUTHOR CONTRIBUTIONS

Thank you to the lab members and collaborators at the GCRC and other research institutes. Their assistance was critical for collecting and analyzing data.

The thesis has been written by Elena Voorand. The experimental design and results of the thesis were planned by Elena Voorand, Dr. Peter Siegel, and Dr. Claire Brown and gathered by E. Voorand.

Dr. Peter Siegel and Dr. Claire Brown edited the manuscript in its entirety, except for the French abstract, which was edited by Dr. Sébastien Tabariès.

Kento Abe, from Dr. Anne-Claude Gingras' laboratory at Mount Sinai Hospital, processed the BioID samples and performed analysis of the BioID mass spectrometry data to provide the results used to generate figures by Elena Voorand. Protocols for PDMS design were followed from Haruka Yoshie in Dr. Allen Ehrlicher's laboratory. Haruka Yoshie and Newsha Koushki were integral to generating the PDMS substrates used in Chapter 3. Dr. Afnan Abu-Thuraia and Matthew Dankner assisted with the *ex vivo* experiments (both acquisition and analysis) included in the thesis. Alexander Kiepas generated the figures used in Chapter 4. These figures include: 4.1 TCGA breast cancer data and 4.2.

LIST OF FIGURES AND TABLES

ABBREVIATIONS

ABD	α-actinin Binding Domain
BM	Basement Membrane
BSA	Bovine Serum Albumin
cDNA	Complimentary DNA
DCIS	Ductal Carcinoma *in Situ*
DMEM	Dulbecco's Modified Eagle Media
ECM	Extracellular Matrix
eGFP	enhanced Green Fluorescent Protein
EMT	Epithelial to Mesenchymal Transition
ErbB2	Avian Erythroblastic Leukemia Viral Oncogene Homolog 2
FA	Focal Adhesion
HER2	Human Epidermal Growth Factor Receptor 2
IDC	Invasive Ductal Carcinoma
IgG	Immunoglobulin G
LASP	LIM and SH3 Domain Protein
LPP	Lipoma Preferred Partner
MMP	Matrix Metalloproteinase
MMTV	Mouse Mammary Tumour Virus
MS	Mass Spectrometry
MT1-MMP	Membrane tethered—Matrix metalloproteinase (MMP14)
Neu	Neuroblastoma/Glioblastoma Derived Oncogene Homolog
NMuMG	Normal Murine Mammary Gland
NT	neu Transformed
PEI	Polyethylenimine
PRR	Proline Rich Region
PTB	Phosphotyrosine Binding
pY	Phospho-Tyrosine

RPMI	Roswell Park Memorial Institute
ShcA	Src Homology 2 Domain and Collagen Containing Transforming Protein 1
shRNA	short hairpin RNA
siRNA	silencing RNA
Smad	Mothers Against Decapentaplegic Homolog
SMC	Smooth Muscle Cell
Src	v-src Sarcoma (Schmidt-Ruppin A-2) Viral Oncogene Homolog (avian)
STRING	Search Tool for the Retrieval of Interacting Genes/Proteins
TGFβ1	Transforming Growth Factor Beta 1
TNBC	Triple-Negative Breast Cancer
TβR1	TGFβ Type I Receptor
TβR2	TGFβ Type II Receptor
Tyr (Y)	Tyrosine
VASP	Vasodilator-Stimulated Phosphoprotein
WASP	Wiskott-Aldrich Syndrome Protein
WT	Wildtype

CHAPTER 1: LITERATURE REVIEW

1.1 Breast Cancer

In Canada, breast cancer will account for an estimated one quarter of all new cancer diagnoses in 2019. Unfortunately, 1 in 8 women are estimated to develop breast cancer and 1 in 33 will die from it[1]. Worldwide, breast cancer is within the top 5 cancers associated with mortality in 2018[2]. These statistics highlight the need for research into the mechanisms driving breast cancer and its progression to metastatic disease.

1.1.1 Classifications of breast cancer

When comparing patient tumours, breast cancer is a heterogeneous disease and this heterogeneity exists even within a single patient's tumour. Heterogeneity can make treatment courses difficult to determine. To overcome this difficulty, gene expression profiling was used to initially classify tumours into groups with unique prognostic and therapeutic implications. The five main groups are Luminal A, Luminal B, HER2-enriched, Triple-negative/Basal-like, and Normal-like[3].

Together, Luminal cancers are the most prevalent cancers and have better survival rates when compared to HER2-enriched and basal-like cancers. Luminal A and B are ER-positive, but Luminal B cancers have increased expression of proliferation-associated genes[4]. Thus, Luminal B tumours are associated with poorer outcomes. The HER2-enriched subtype represents cancers in which the Her2 receptor has been amplified and may or may not express the Estrogen-Receptor (ER) and Progesterone-Receptor (PR). Approximately 10-15 % of breast cancers make up this subtype. Basal-like tumours adopt the genetic profile of basal epithelial cells and are most often triple-negative (lack ER/PR and low expression of HER2). The prevalence of this subtype is 15-20 % of breast cancers and the outcome for patients in this category is very poor[4]. In addition, the Claudin-low subtype does not express ER/PR and is low in HER2 expression. What differentiates this group is high expression of mesenchymal markers and low expression of Claudins 3, 4, and 7[5]. Normal-like cancers have increased adipose tissue gene expression, but otherwise are similar to normal tissues (5% prevalence)[4]. These subtypes have helped predict response to chemotherapy and recurrence rates in patients, but unfortunately, further classification of tumours has been needed to account for additional heterogeneity and lack of drug targets.

More advanced molecular profiling of these cancers, with integrated transcriptomic and genomic profiling of 2,000 breast tumours, has provided better classification of breast cancers. In

fact, 10 novel subtypes of breast cancer were discovered[6, 7]. Despite this improvement in classification, many other sources of heterogeneity are not routinely profiled. Excluded from profiling were unique methylation patterns of DNA, clonal diversity, and epigenetic differences. Each of these factors have contributed to disease outcome and response to treatment[8-11]. Thus, profiling methods that incorporate testing for many of these factors is needed. An integrative analysis, sequencing and/or *in situ* methods, that includes bulk tumour and single-cell samples would improve molecular profiling of breast tumours. However, cost and time of integrative molecular profiling are a current hurdle in achieving better tumour profiling[12, 13].

All in all, advancements in tumour profiling are being made to better understand the underlying drivers and evolution of breast cancers. Cellular signaling synergies, compensatory pathways and flexibility in diverse environments are all tumour cell mechanisms that could be profiled. When combined with an understanding of these cellular mechanisms, improved profiling could lead to better treatment outcomes and new drug targets.

1.1.2 ErbB2 and TGFβ signaling pathways synergize to promote breast cancer metastasis

ErbB2/Her2/Neu is a transmembrane receptor of the EGFR family that also includes EGFR, ErbB1, and ErbB3[14]. The erythroblastic oncogene B 2 (ErbB2) was isolated from the avian genome and has also been named Her2, which originates from the protein's similarity to the human epidermal growth factor receptor, and Neu in the context of isolation from a rodent glioblastoma cell line (neural). Signaling by ErbB2 mediates cellular processes such as cell proliferation, motility, adhesion and transformation[15-18]. The kinase activity of this receptor family is activated by homo- or heterodimerization following ligand binding. Autophosphorylation of the cytoplasmic c-terminal tail serves as a docking site for adaptor proteins that initiate numerous signaling cascades. Of note, activation leads to recruitment of proteins that contain SH2 and PTB binding domains. The extracellular structure of the ErbB2 receptor differs from the other family members. The ErbB2 structure cannot bind ligands as its confirmation resembles an open "ligand-bound" state of the EGFR family members[19, 20]. Therefore, ErbB2 is the preferred binding partner of the EGFR family[21]. In situations where ErbB2 is overexpressed, homodimerization can occur, leading to increased signaling.

Expression of ErbB2 is often elevated in breast cancer[22, 23]. Transgenic mouse models of mammary tumourigenesis were generated using an MMTV promoter and oncogenic Neu(V664E)[24]. This model increases the frequency of ErbB2 homodimerization, thereby amplifying signaling. This model, and several other important models, has demonstrated that ErbB2 activation can initiate tumours and advance progression[25-30]. Notably, in combination with other signaling pathways, these effects are augmented.

Transforming Growth Factor Beta (TGFβ) signaling controls many cellular processes. The signaling axis begins with TGFβ cytokine engagement of cell surface TGFβ receptors. There are three isoforms of this cytokine: TGFβ1, 2 and 3. These ligands bring together Type 1 and Type 2 TGFβ receptor serine/threonine kinases. Following complex formation, the Type 2 receptor phosphorylates the kinase domain of the Type 1 receptor, which subsequently propagates the canonical signaling through Smad signaling molecules. The Smads act within a heterodimeric complex that translocate to the nucleus and function as transcription factors for various genes[31]. These genes control differentiation, proliferation, apoptosis, matrix remodeling, motility and immune functions. Non-canonical signaling, or non-SMAD signaling, is achieved through MAP kinase, Rho-like GTPase, and phosphatidylinositol-3-kinase/AKT pathways and can cooperate with canonical signaling to determine the final cellular response to TGFβ[32].

In normal cells, TGFβ exerts an anti-proliferative effect, but in cells that have undergone mutational hits, TGFβ no longer suppresses proliferation[33, 34]. Instead, TGFβ can elicit an epithelial-to-mesenchymal transition (EMT) where cell-to-cell contact is lost following changes in expression of cadherins; this mesenchymal transformation favours single-cell migration and upregulation of proteases leads to matrix remodeling and invasive cell behavior. These EMT-associated changes enhance cancer cell invasion and metastasis[35-37].

Several pathways modulate the ErbB2 pathway to enhance disease aggressiveness in human cancers. Among these pathways, there is clear evidence for TGFβ modulation of the ErbB2 pathway. In fact, data demonstrates that these pathways synergize in breast cancer, leading to poorer relapse-free and overall survival in Her-2 cancers compared to patients without TGFβ activation[38]. This synergy, observed by “TGFβ active” gene signatures, can also be applied to basal-like and some Luminal B cancers[38].

The paradoxical role of TGFβ in these cancers arises from genetic and epigenetic events that switch TGFβ from a tumour suppressor to a promoter[39, 40]. In other words, the growth suppressive effects are turned into pro-oncogenic effects. These effects can also be accentuated by other surrounding cell types such as stromal, immune, endothelial and smooth muscle cells responding to the presence of TGFβ[41]. A closer look at the ErbB2 and TGFβ pathways reveals cooperation to enhance migration and invasion of cancer cells[38, 42-46]. In MCF10A cells, TGFβ was identified in a genetic screen to induce cell migration in cooperation with ErbB2[45]. This cooperation induced Rac1 activity, resulting in actin stress fiber formation and increased lamellipodia activity[46]. Importantly, this cooperativity is recapitulated in ErbB2 mouse models (MMTV-neu) when TGFβ is constitutively activated; higher lung metastatic burden and increased intravasation/extravasation events are associated with the activation of these pathways[47, 48]. These studies definitively connect the synergy between the ErbB2 and TGFβ signaling pathway to metastatic disease progression.

1.1.3 Breast Cancer Metastasis

The majority of cancer related deaths are attributed to progression to metastatic disease[49]. Metastasis is a multi-step process that requires growth of the primary tumour, invasion of cancer cells into the surrounding tissue, intravasation into the blood stream, extravasation from the blood stream and establishment of a secondary site in the body. Each of these steps requires cancer cell survival and motility in diverse and challenging microenvironments[50].

Two models describe cancer cell dissemination. The first model, linear progression, suggests that cancer cells undergo alterations during primary tumour growth, which select cellular phenotypes that promote survival and dissemination of cancer cells to distant sites. The disseminated cells can undergo further evolution with respect to their genetic and epigenetic state when compared to the primary tumour. Meanwhile, the parallel progression model of metastasis suggests that cancer cells leave the primary site very early during disease progression. This argues that genetic and epigenetic alterations occur independently within the early disseminated cancer cells compared to those that remain part of the primary tumour. Therefore, these primary tumour and disseminated cells undergo separate evolution[51].

In order of preference, the most common sites of metastasis for breast cancer are bone, lung, liver, and brain[52]. Unfortunately, the 5-year survival rate of Stage IV, metastatic breast

cancer is only 27%[53]. Thus, prevention of metastatic disease is an important step to reducing breast cancer-related deaths.

1.2 Migration and invasion as key cellular processes in metastasis

1.2.1 Adhesions and invadopodia mediate cell movement

Cancer cell motility is essential to cell escape from the primary tumour and travel to a secondary site. A myriad of motility mechanisms are in place for this escape, which include multiple cell types, stroma, and soluble factors, to name a few[54]. For this thesis, I closely examine two cellular structures, adhesions and invadopodia, which are known to mediate motility via migration and invasion in mesenchymal cancer cells[55-58].

Migration is a physiological process involved in many normal cellular events such as embryogenesis, wound healing and immune surveillance[59]. However, migration can also be detrimental in certain disease processes, including cancer. During the metastatic cascade, cancer cells can adopt multiple modes of cell migration, which includes collective migration, amoeboid migration and mesenchymal migration, depending on cues and context[54]. Collective migration is defined by cell-to-cell contacts and adherens junctions that are retained by a sheet of cells following a leader cell[60]. Both cancer cells and fibroblasts have been identified as leader cells and this migration mode has been modelled by several groups *in vivo*[61-63]. Amoeboid migration relies on blebbing of the cell to navigate the ECM rapidly. This type of movement is single cell, with weak contact between cell and ECM[64, 65]. The third type of movement is mesenchymal migration. This type of movement is adopted by epithelial cells that have undergone an EMT and therefore no longer make cell-to-cell contact. In tumours, this occurs 10-40% of the time[66]. Mesenchymal cells move via integrin engagement and actomyosin contraction bridged by adhesions. *In vivo* imaging has revealed that this type of migration often occurs on collagen fibrils, thereby mimicking 2D substrates[64]. The morphology of these cells is more elongated when compared to other models of 3D migration[67]. Importantly, cancer cells have the plasticity to switch between these three modes of migration depending on the microenvironment they encounter[67].

The studies outlined in this thesis are focused on the mesenchymal mode of migration in cells that have undergone an EMT following TGFβ stimulation. In this context, these cells are

highly migratory, invasive and metastatic. This has allowed us to study adhesion components and adhesion responses to stimuli that help drive the metastatic process.

The second cellular structure that mediates cancer cell invasion is the invadopodia. Similar to podosomes, invadopodia are actin-rich protrusions that form perpendicular to the cellular surface[68]. While podosomes mediate normal cellular processes in monocytic, endothelial and SMC cell types, invadopodia are associated with effective ECM degradation by transformed cells[69]. In confining environments, invadopodia are the proteolytically active and F-actin–rich protrusions from the cell membrane that allow cells to overcome epithelial and endothelial barriers[68]. Many of the critical components found in adhesions are also found in invadopodia[69]. Therefore, these structures are most often identified as unique from adhesions, or other structures, using cortactin and Tks5 immunofluorescent staining which is highly specific for invadopodia[68]. When visualized together, cortactin and Tks5 are distinct puncta at the cell-ECM interface and are co-localized with F-actin.

Many invadopodia studies have been completed *in vitro*, but several studies have shown the relevance of invadopodia structures *in vivo*[57, 70]. For example, using the chorioallantoic chick embryo assay, invadopodia structures were shown intravascularly to mediate extravasation of cancer cells[71]. With knockdown of cortactin, Tks4 or Tks5, these structures are no longer formed and cells cannot extravasate from the blood stream[71]. Tissue slices, as well as intravital imaging, have further corroborated the presence of invadopodia structures at tissue barriers. Finally, there is correlation between the propensity of cancer cells to form invadopodia and poor overall survival of breast cancer patients[56]. Removal of core invadopodia components reduces the metastatic burden in these breast cancers[71, 72].

Invadopodia are critical mediators of metastasis and an important structure to elucidate. Broad MMP inhibitors have been unsuccessful therapeutically in metastasis, but more targeted inhibition of Src has had some success[73]. As mentioned, removal of core components to invadopodia effectively reduce metastatic burden; thus, there is continued interest in understanding how these structures could be targeted and inhibited. Therefore, we have sought to understand what stimuli trigger invadopodia formation and ECM degradation in the context of breast cancer.

1.2.2 Adhesion assembly and dynamics

In the mesenchymal mode of cell migration, cell-matrix adhesion assembly begins with integrins binding the ECM under the leading edge lamellopodia structure of the cell. Once bound, a signaling cascade results in the actin cytoskeleton reorganizing itself parallel to the cell-ECM interface for the generation of traction force used to propel the cell body forward. These steps in the assembly of an adhesion represent a concerted process involving upwards of 150 components[74]. Ultimately, cell movement, or migration, is achieved.

Several kinds of cell-matrix adhesions exist. These adhesions include nascent adhesions, focal complexes, focal adhesions and fibrillar adhesions. Listed in order of increasing size: 1) nascent adhesions are sub-resolution and are less than or equal to 250 nm in diameter, 2) focal complexes are a bit larger than nascent adhesions and can be oval in shape, 3) focal adhesions are about 0.5 – 1 micron along one axis and several microns along the other and 4) fibrillar adhesions are similar to focal adhesions but greater than 5 microns long. Nascent adhesions and focal complexes are located at the periphery of the cell (lamellipodia) and are highly dynamic with the potential to mature to a more stable focal adhesion. In comparison, focal adhesions are located at the ends of actin stress fibers and contribute significantly to cellular migration function. Finally, fibrillar adhesions are generally located under the central cell body, are built along long actin fiber bundles and are linked to extracellular fibronectin[75]. For the remainder of this thesis, I will use the general term adhesions to describe the various adhesion types that have functions associated with cellular migration.

The initial attachment of integrins to the ECM triggers clustering of integrins at the cellular membrane, which then serves as a platform for other adaptor and scaffolding proteins to connect the ECM to the cytoskeleton. The multitude of proteins involved in this process include talin, paxillin, tensin, p130cas, and α-actinin, for example. Furthermore, a complex series of structural and signaling proteins enter and leave the adhesion to mediate adhesion maturation, stabilization and tension, some of which are outlined in Figure 1.1. Signaling molecules essential to the coordination of these adhesion proteins include FAK and Src[76, 77]. Together, these components orchestrate continual reorganization of the cell cytoskeleton to facilitate mesenchymal migration along 2D substrates, such as collagen fibers, encountered in tissue.

Increasing cellular migration speed requires increasing both FA assembly and disassembly rates. Typically adhesions assemble and disassemble over a period of minutes to hours, with

nascent adhesions having the shortest lifetime of approximately 60 seconds[78]. Common migration stimulants include overexpression of structural adhesion components and essential signaling components, such as FAK, or stimuli such as EGF and TGFβ[55, 79-81]. Previous work by our group has shown that components, such as the ShcA and LPP adaptor proteins, are critical mediators of the migration response to TGFβ in mesenchymal cells[44, 82, 83]. Without these two adaptor proteins, ErbB2-postive cancer cell migration in response to TGFβ is stunted. In support of the migration phenotype seen with loss of ShcA and LPP, adhesion dynamics and cell speeds were measured to reveal the interplay of the proteins in adhesions (in revision, JBC, E. Voorand author contributions, Kiepas *at al.* **The ShcA adaptor protein cooperates with LPP to mediate adhesion dynamics and invadopodia formation**). Advancement in imaging and proteomic techniques are uncovering further mechanisms and levels of regulation for adhesion dynamics that contribute to increased cell migration.

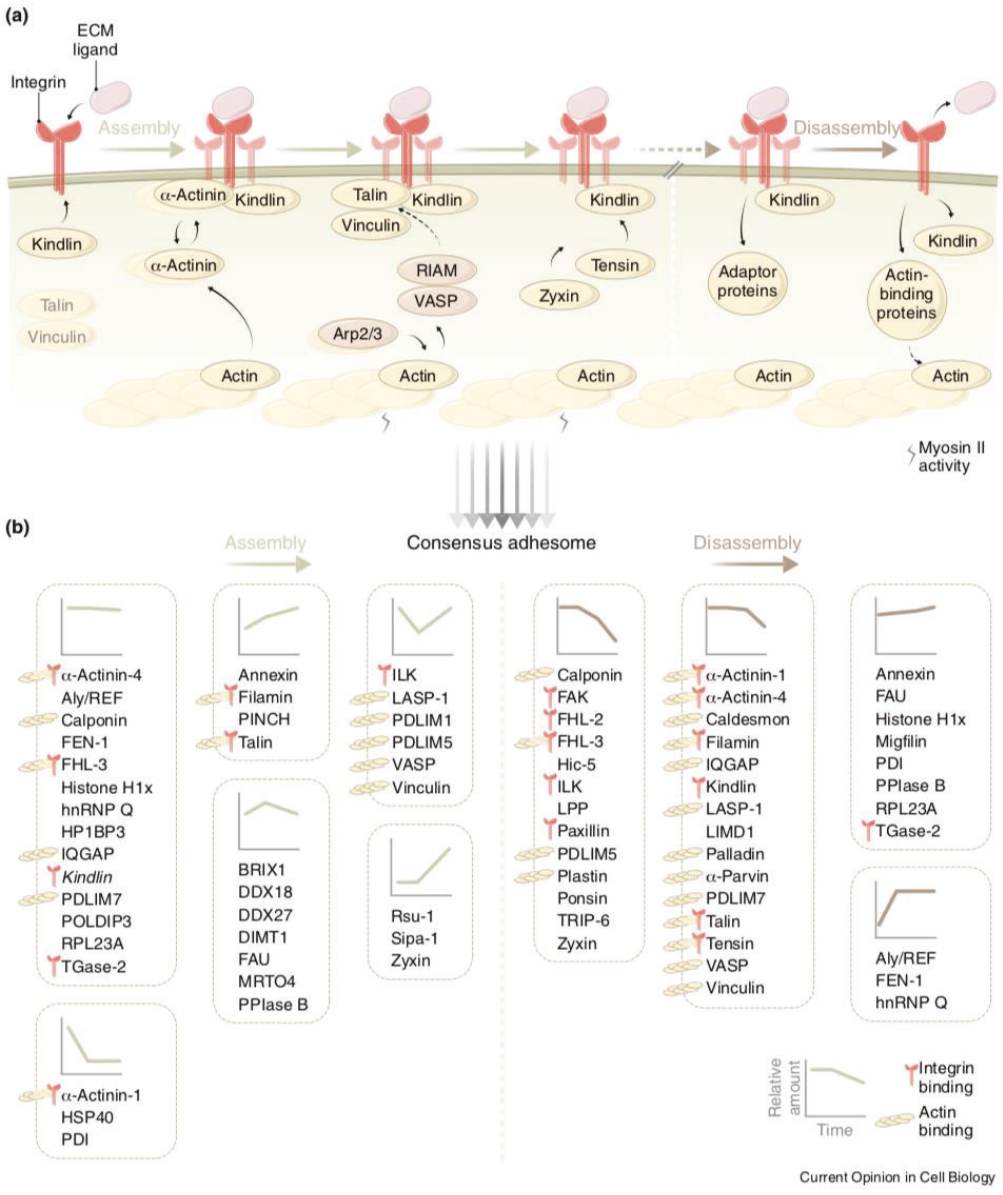

Figure 1.1 Temporal proteomic profiling of adhesions. Recruitment of adhesion-associated proteins based on the assembly and disassembly phase of the adhesion. Data compiled from multiple proteomic studies[84].

1.2.3 Invadopodia assembly and dynamics

Invadopodia are highly dynamic structures that require regulation and coordination of many cellular components. These structures form within 1-3 minutes and persist up to hours. Three stages mark invadopodia formation, the first is initiation, followed by actin assembly and, finally,

maturation (Fig. 1.2). The initiation stage involves recruitment of N-WASP, cofilin and Arp2/3 complex in response to growth factor, cellular transformation or ECM signaling that occurs concurrently with integrin engagement ($\alpha_5\beta_1$ and $\alpha_3\beta_1$) of the ECM[85]. These components, along with cortactin form the actin-nucleating core to continue the assembly phase. The assembly phase, which relies on the Arp2/3 complex activity, results in actin polymerization and elongation. Lastly, a number of proteases are trafficked to the cellular membrane for release and consequent proteolysis of the ECM during maturation of invadopodia[68, 86]. Overall, the sequence of assembly and disassembly of invadopodia is elusive and characterization of the components, signaling and timing is needed.

Proteases released by invadopodia include many MMPs, seprase, cathepsins, and ADAM (a disintegrin and metalloprotease) family proteins[69]. Of the 28 known MMPs, 14 have been implicated in cancer progression. Specifically, MMP 1, 2, 3, 7, 9, 13 and 14 have been linked to tumour progression, metastasis and poor patient prognosis[87-90]. MMP14, MMP2 and MMP9 are most enriched at invadopodia structures to mediate ECM, such as collagen type I and gelatin, degradation[91]. The interplay between proteases and regulation of trafficking is a complex process that is also under study.

Src plays an important role in phosphorylation of components during invadopodia assembly and is both necessary and sufficient for this process. Furthermore, constitutively activated or overexpressed Src was shown to increase invadopodia activity, resulting in enhanced ECM degradation[92-94]. Many microenvironmental factors initiate Src-mediated phosphorylation and activity of invadopodia; these factors include hypoxia, growth factors, ECM, matrix rigidity and cell-to-cell contact[68]. Our studies have implicated ShcA (p46/52 isoforms) and LPP as key invadopodia components in ErbB2-positive cells and have shown that Src-mediated phosphorylation of LPP is required for effective invadopodia induction (in revision, JBC, E. Voorand author contributions, Kiepas *at al.* **The ShcA adaptor protein cooperates with LPP to mediate adhesion dynamics and invadopodia formation**)[83]. Further research into the exact mechanisms of phosphorylation and recruitment of these components is under way. In addition, environmental cues, such as stiffness, can trigger these events. Thus, invadopodia have the capacity to respond to many distinct cues, which trigger invadopodia formation and activity, indicating the sensitivity and adaptability of this cellular structure.

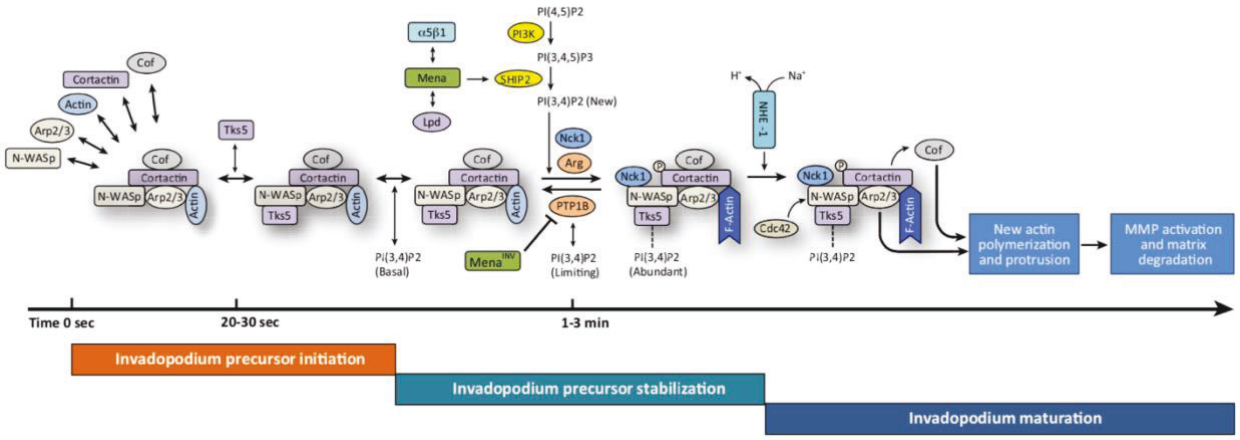

Figure 1.2 Steps in the formation of invadopodia structures. The multitude of actin-associated and signaling components are shown on the timescale of formation. Figure adapted from Eddy *et al*., 2017[68].

1.3 LPP functions within adhesion and invadopodia structures

1.3.1 LPP overview

LPP, or Lipoma Preferred Partner, was discovered in lipomas as a fusion transcript of High Mobility Group AT-Hook2 (HMGA2)[95]. LPP is an 80 kDa protein expressed in all human tissues, except blood and brain, with elevated expression in Smooth Muscle Cells (SMCs)[96]. The protein was classified as a zyxin family member due to its domain structure and similarity in LIM domain sequence[97]. Other proteins in the zyxin family include Trip6, Ajuba, LIMD1, WT1P and migfilin. Functions associated with the family include regulation of the cytoskeleton, cellular motility, mechanotransduction, proliferation and tumourigenesis[98-102].

LPP has several domains contributing to the protein's function as a cytoskeletal adaptor protein. Most proximal to the N-terminus of LPP is a short amino acid sequence, termed the α-Actinin Binding Domain (ABD) (Fig 1.3), which specifies the association between LPP and α-actinin to coordinate binding to the actin cytoskeleton. Further towards the C-terminus of LPP is the Nuclear Export Signal (NES) in the Proline Rich Region (PRR) of LPP. LPP is thought to have some nuclear roles, but is not predominantly found in the nucleus[103]. The three LIM domains at the C-terminus of LPP are zinc-finger motifs that localize LPP to adhesions to varying degrees[104, 105].

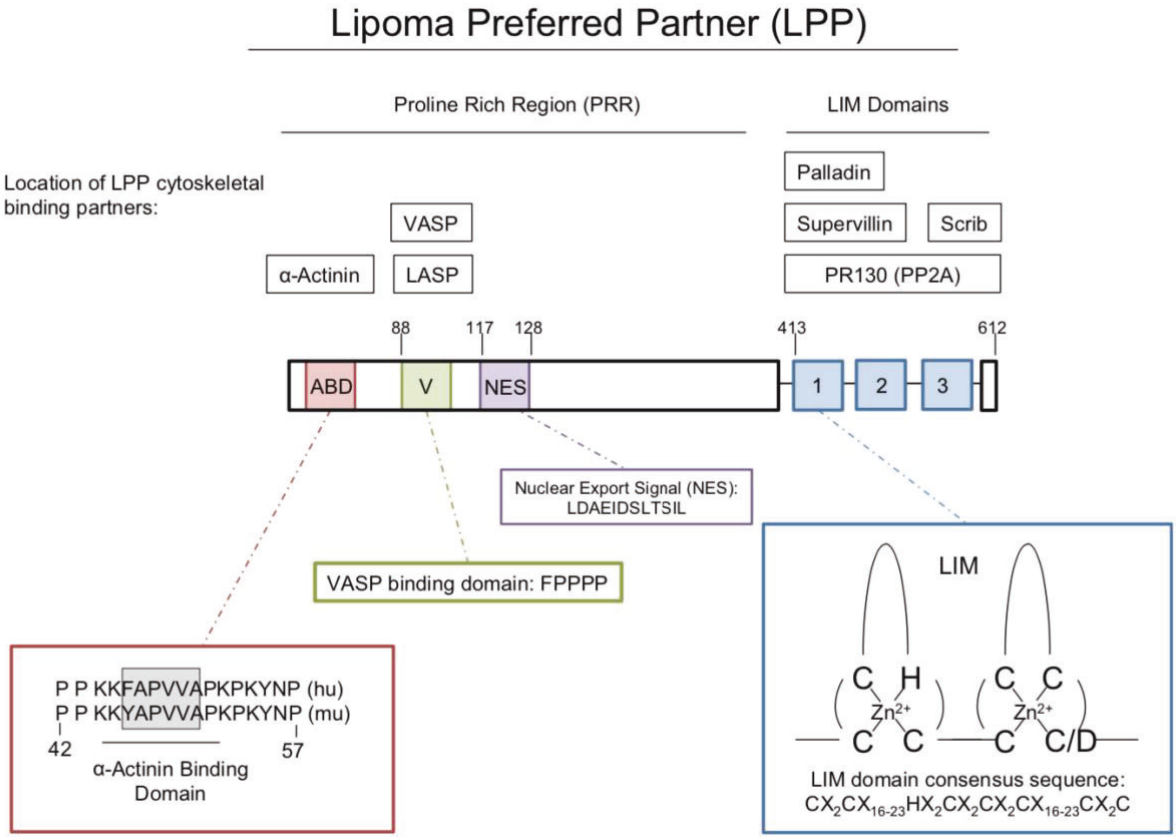

Figure 1.3 Domains of LPP and sequence of the ABD and LIM domains. Figure adapted from Ngan et al., 2018[106].

1.3.2 LPP in breast cancer metastasis

In two ErbB2-positive breast cancer cell models, NMuMG-ErbB2 and NIC, LPP expression was reduced to study the impact of LPP loss *in vivo*. Stable reduction of LPP did not impair TGFβ-induced EMT or compromise cell proliferation[83]. When injected in immunocompromised mice, LPP was found to be dispensable for primary breast tumour growth, but required for efficient lung metastasis[83]. Circulating Tumour Cell (CTC) populations were also collected after Mammary Fat Pad (MFP) injection to determine the cellular intravasation efficiency of LPP KD cells. With diminished LPP expression, CTC populations were low indicating a role for LPP in intravasation into the bloodstream. In addition, experimental metastasis assays that test cellular extravasation capacity revealed that reduced LPP expression impaired the

ability of cancer cells to colonize the lungs. These results implicate LPP as a promoter of efficient metastasis in the context of ErbB2 positive cancer.

1.3.3 Dual role for LPP

To understand the role of LPP in cancer metastasis, Ngan et al. had previously studied the migration and invasion profiles of ErbB2-positive cells[82]. LPP was found to play a critical role in both migration and invasion in Neu/ErbB-2 positive mammary tumour cells induced with TGFβ.

Under TGFß stimulation, LPP localizes to adhesions and controls adhesion dynamics via interaction with α-actinin to increase cell migration speed[82]. Localization of LPP is dependent on intact LIM domains as evidenced by mutational study[82]. Additionally, migration and invasion in Boyden chambers is abrogated with loss of the ABD and binding to the actin cytoskeleton[82]. Thus, interaction with α-actinin is crucial to LPP function.

A closer look at mechanisms of invasion revealed that LPP is localized at invadopodia structures. Using fluorescent gelatin degradation assays, LPP was colocalized with Tks5, an invadopodia marker, at sites of ECM degradation. Moreover, in an *ex ovo* chick chorioallantoic membrane (CAM) assay, LPP expression was needed for invadopodia-mediated extravasation to overcome blood vessel walls. Interestingly, mutation of key tyrosine phosphorylation sites on LPP revealed that these phosphorylation sites, Y245/301/302, are necessary for invadopodia formation. With further investigation, TGFβ-induced Src phosphorylation was the mechanism of phosphorylation; importantly, mutation of these tyrosine sites reduced lung metastases. In contrast, phosphorylation of these three tyrosine sites are not required for cell migration in response to TGFβ. Therefore, Src tyrosine kinase phosphorylation of LPP at three tyrosine sites (Y245/301/302) is required for invadopodia formation, but not migration[83].

Together, LPP-mediated cellular invasion can be uncoupled from migration. Both cellular invasion and migration rely on an intact ABD, but only invasion relies on Src tyrosine phosphorylation. Indeed, the dual role of LPP at both adhesion and invadopodia structures is similar to other studied proteins. Indeed, proteins such as cortactin, VASP and α-actinin, also function at both structures[55, 107-110].

1.3.4 Known protein interactors of LPP

As a modular adaptor protein, LPP has the potential to interact with multiple proteins directly and indirectly. Within the LPP sequence, are binding sites for α-actinin, LIM and SH3 protein (LASP), palladin, PP2A, scrib, supervillin, and vasodilator-stimulated protein (VASP) (Fig 1.3). Each of these binding partners have associated cellular functions and implications in cancer (Table 1.1).

Functionally, these protein interactors (Table 1.1) are implicated at adhesions or cell-to-cell contacts and serve as adhesion building blocks or regulators of adhesion dynamics. Examples of potential LPP regulatory proteins are supervillin and PP2A. These interactions act to increase adhesion assembly and disassembly rates, but direct regulation of LPP has not been shown. Like LPP, α-actinin, VASP, and supervillain function at invadopodia in addition to adhesion structures. Beyond these known protein interactors, the specific mechanisms of LPP regulation and LPP network of protein interactions have yet to be elucidated.

Table 1.1 Known protein interactors of Lipoma Preferred Partner (LPP)

Protein Interactor	Cellular Localization	LPP Domain of Interaction	Function	Implications in Cancer
α-actinin [107, 108, 111-118]	Leading edge of cells, lamellopodia, filapodia, FA, invadopodia, stress fibers	PRR – between aa 41-57 (LPP) **via** central rod containing spectrin 2 and 3 repeats (α-actinin)	Crosslinks actin to promote cell migration and FA maturation	Overexpression in many types of cancers
LASP (LIM and SH3 Protein) [98, 119, 120]	Focal adhesions, podosomes, lamellopodia, shuttled to nucleus	PRR – XPPPP motif (LPP) **via** SH3 domain (LASP)	Actin binding and cytoskeletal reorganization	Overexpression in breast and ovarian cancers; enhances cell migration and invasion
Palladin [121-124]	FA, stress fibers, cell adhesions	LIM domains 1 & 2 (LPP) **via** N-terminal region (Palladin)	Controls cells shape, adhesion, motility, contraction and invadopodia formation	Initiation of pancreatic cancer and metastatic progression of breast cancer
Scrib [125-131]	Cell-to-cell contacts	C-terminus (LPP) **via** PDZ domain (Scrib)	Cell adhesion, cell shape and cell polarity	Both tumour suppressor and promoter in cutaneous, lung and prostate; dysregulation in breast cancer formation and metastasis
Supervillin [132-135]	Cytosol, FA, invadopodia	LIM domains (LPP & TRIP6, not zyxin) **via** residues 342-571 (supervillin)	Control of actin organization and binds myosin 2 to control cell contractility and podosome formation	Hypoxia-induced upregulation promotes migration and invasion in hepatocellular carcinoma
VASP [110, 136-142]	Lamellopodia, filapodia, FA, invadopodia	PRR - 2 Acta repeats (FPPPP) **via** EVH1 domain (VASP)	Cell motility, cell adhesion, actin polymerization, promotes F-actin elongation	Formation of breast, colon and lung cancer
PP2A [98, 143]	Focal contacts, perinuclear, nucleus	LIM domains (LPP) **via** Zinc-finger-like motif N-terminus (PP2A)	Adhesion and migration control (both positive and negative regulation)	Increases cancer cell migration

1.3.5 Roles in mechanosensing

Zyxin is an example of a well-studied mechanosensitive protein[99, 100, 144-147]. Under mechanical stress, zyxin has been shown to relocate from adhesions to actin filaments and recruit VASP to reinforce actin stress fibers[147]. This relocation is dependent on the intact LIM domains of zyxin. These studies have distinguished zyxin as a regulator of cell response to changes in mechanical properties within the environment encountered by cells.

As a zyxin family member, LPP has the potential to also mechanotransduce at two mechanosensitive structures, adhesions and invadopodia. Characterization of LPP as a mechanosensitive protein was first performed by Hooper *at al*.[148, 149]. In the context of the myocardium, LPP expression is induced with mechanical load (hemodynamic load) of the heart in aortic-banded rats. Additionally, mechanical stretching of cardiac fibroblasts can control LPP expression level and subcellular localization. Further study of LPP in SMCs revealed changes in LPP subcellular distribution in response to stiffness; on stiff substrates LPP is localized to long-broad adhesions, while on soft substrates LPP is localized to small adhesions[150]. Whether LPP directly regulates concerted responses to mechanical cues is unknown. Structural studies of LPP would elucidate potential conformational changes, while KD studies would distinguish adhesion and invadopodia regulation in response to mechanical stimulation.

1.4 Physical Properties of Breast Cancer

1.4.1 Breast tissue and tumour have distinct biophysical properties

The tumour microenvironment evolves with cancer progression from the initial transformation of normal tissue, to tumour invasion, dissemination and metastasis. A key part of the microenvironment evolution, which has been historically understudied, includes the physical properties of the tissue. These diverse physical properties of the microenvironment are created by expansion of the tumour and changes to the ECM[151]. With tumour growth, areas of distinct stiffness form, with the periphery and invasive front of the tumour being the stiffest region[152]. Additionally, enhanced collagen I deposition, a fibrotic phenotype and Tumour Associated Collagen Signatures (TACS) mark tumour progression and further increase the tissue stiffness cancer cells encounter[153, 154]. This stiffening of breast tissue with disease progression alters cell phenotypes such as tumour growth, tumour invasion and tumour response to drug treatment[155-158].

1.4.2 Stiffness of breast cancer metastatic sites

The common sites of breast cancer metastasis include brain, liver, lung and bone. These metastatic sites are distinct from each other in terms of biochemistry, tissue architecture, cell composition and nutrient supply. The unique biophysical properties of these sites have also become of interest for study.

Several research disciplines have measured the stiffness of the metastatic sites to map tissue properties and follow disease progression. Methods include shear-wave elastography[159], rheometry[160] and Atomic Force Microscopy (AFM)[152]. Each of these methods measure tissue stiffness at different magnitudes of scale – from bulk tissue to single-cell to subcellular structures. The resulting stiffness map of these metastatic sites ranges from 1 kPa in the brain, to the GPa scale in bone, while breast (0.1-10 kPa), lung (1-10 kPa), and liver (5-20 kPa) stiffness fall between the two extremes of brain and bone (Fig. 1.4). Thus, cancer cells seeding the different metastatic sites are exposed to a diverse range of stiffness.

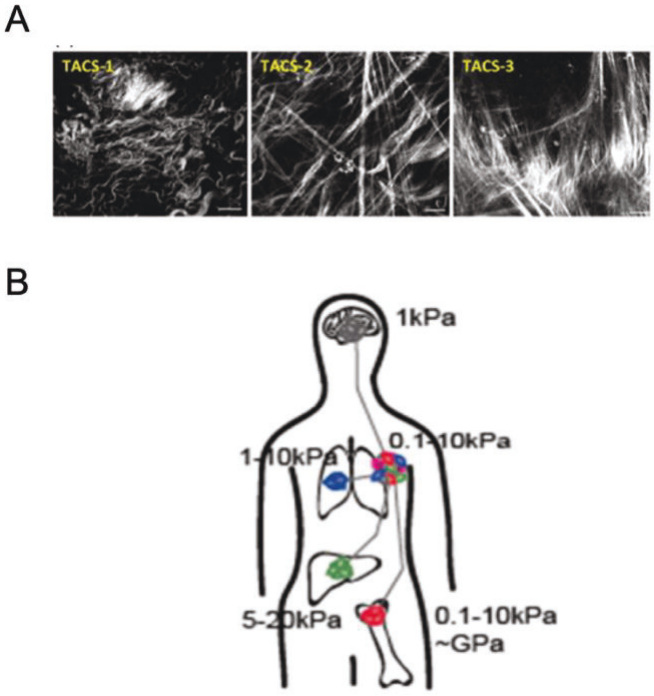

Figure 1.4 Stiffness of cancer and metastatic sites**. (A)** Tumour Associated Collagen Signatures (TACS) accompany disease progression with collagen realignment. **(B)** Common sites of breast cancer metastasis have unique stiffness. Figure taken from Lele *et al.* **[161].**

1.4.3 Single cells can sense and respond to stiffness

It has long been described that cells are durotactic, meaning cells move towards areas of greater stiffness[162]. This directed movement is mediated by the cells' ability to sense and respond to changes in stiffness. Integrins are an integral part to this mechanosensing process as they link the ECM to the actin cytoskeleton and often initiate downstream intracellular signaling[163-165]. Given the role of integrins, it is no surprise that both adhesion and invadopodia are cellular structures capable of mechanosensing and initiating a cellular response to substrate stiffness[166-170].

Controlled protein conformational changes in adhesion proteins is a mechanism of mechanosensing. These changes in conformation serve as a platform for recruitment of proteins for intracellular propagation of signal; for example, vinculin and talin unfolding for adhesion maturation and p130-CRK unfolding for phosphorylation by Src family kinases[171-174]. Other signaling molecules such as FAK, Src, paxillin and Rho GTPases (Rac, Rho and Ras) are also recruited in response to stiffness[175, 176]. Through Ras signaling, and downstream engagement of ERK and other MAPKs, proliferation and survival is promoted in several cell types[177, 178]. Activation of adhesion signaling has been shown in Neu mouse mammary tissue in response to increasing tissue stiffness by elevated $_{p130}$Cas and FAK$_{pY397}$ staining[154]. An example of a dynamic adhesion response to stiffness is bolstering of cellular contractility to alter migration rate and cell shape[179]. Both immediate and long-term responses to stiffness are therefore possible through adhesion sensing of the underlying biophysical properties of the substrate.

In addition to adhesions being mechanosensitive, some groups have characterized invadopodia as mechanosensitive structures. Alexander *et al.* (2008) has characterized differences in invadopodia activity on hard versus soft substrates using CA1d cells [168]. In addition, in other cell types, such as macrophages, podosomes are capable of mechanosensing[180]. Moreover, invadopodia are sensitive across a broad range of stiffness without a response plateau as demonstrated by Parekh et al. (2011). MCF10A CA1d invadopodia activity was tested on 1/9.9/28 kPa, 3.1/5.6 MPa, and 1.9/69 GPa with activity changing throughout the range. Whether invadopodia directly sense changes in substrate stiffness in a positive feedback mechanism or increase invadopodia activity as a downstream response to mechanosensing is still to be determined. With increasing stiffness, TWIST1 was found to induce gene expression of invadopodia assembly components (ADAM12) in Hs578T and HMLE cells[181]. To support this

in vitro finding, TWIST1 and ADAM12 mRNA expression is tightly correlated in human breast cancer samples. To note, ADAM12 is also induced in response to TGFβ-induced EMT[182]. These studies suggest that the TWIST1 response to stiffness is responsible for changes in invadopodia activity, but the potential for reverse intracellular signaling cascades, triggered by increase in invadopodia activity, have not yet been explored.

Another physical cue sensed by cells is viscoelasticity. Viscoelasticity is a time-dependent property, related to stiffness, which takes viscosity of a substrate into account. Wisdom *et al*. demonstrated that, with stiffness held constant, MDA-MB-231 cells change their mode of migration in response to viscoelasticity[183].Other physical parameters, such as fractionability (fracture energy) of a substrate, have potential for regulating cell behavior and platforms to study these properties are under development.

1.4.4 Mechanomemory

Short term cellular responses to biophysical cues have been demonstrated, but whether these changes in biophysical cues serve as a priming effect to confer cell biophysical memory is an interesting avenue of research.

Nasrollahi *et al*. (2017) have shown that epithelial cells can be primed on a substrate of a specific stiffness so that the cells, when introduced to new substrate stiffness, have distinct collective cell migration characteristics, adhesion sizes, actomyosin expression, and retention of nuclear YAP based on the priming substrate stiffness. For example, cells primed on hard substrates (50 kPa) have more ordered collective migration, higher actomyosin expression, larger adhesions and nuclear localization of YAP was more persistent when compared to cells primed on soft matrices (0.5 kPa). With YAP depletion, this memory for past mechanical environment is lost, demonstrating the dependence on YAP for biophysical memory [184].

The pathways by which mechanical signals can be transduced to the nucleus to encode biophysical memory could include changes in nuclear mechanics, nuclear lamina components, and global chromatin state[185, 186]. Stowers *et al*. (2019) suggest that epigenetic signatures are associated with enhanced stiffness of 3D matrices. Their group has demonstrated that soft 3D matrices, which mimic *in vivo* stiffness, recapitulate the chromatin state seen *in vivo* and as matrices increase in stiffness, chromatin accessibility increases. This accessible chromatin state promotes a tumourigenic phenotype through Sp1-HDAC3/8 pathways. The implication of

epigenetic changes linked to change in mechanical properties opens many avenues for research into how mechanical memory is stored.

Aside from nuclear changes, mechanical memory can be encoded in the cell cytoskeletal and adhesion components as well. In the context of adhesions, mechanical force alters the conformation of several adhesion proteins so that the conformation retains memory for a past biophysical environment. For example, conformational changes in talin result in a different response to future biophysical forces[187]. Of note, catch bonds are another example of structures that have the capacity for mechanical memory. Repeated mechanical force can increase catch bond lifetime for $\alpha_5\beta_1$ integrin with fibronectin[188]. Taken together, these studies broaden the potential mechanisms for mechanical memory encoding and suggest that biophysical conditioning is a potential component of the metastatic cascade.

1.4.5 The implications of stiffness for breast cancer disease progression

The stiffening of breast tissue with cancer progression may be a mechanism by which tumour metastasis is enhanced[154, 189]. Specifically, oncogenes make use of the same signaling pathways engaged by mechanotransduction, thus, cancer cell signaling can be enhanced with stiffening of tissue[190]. Additionally, a reciprocity exists between stiffening of cancer cells (through cellular tension) and increasing rigidity of the ECM from the applied cellular tension, thereby furthering invasive cell phenotypes[191]. The impact of repeated and persistent changes in ECM and tissue stiffness on cell function and adaptation are not yet known. Studies directed at cancer cell response to drug therapy, cultivation of Cancer Stem Cells (CSCs) and promotion of dormancy at distant sites of metastasis have begun to explore the potential impacts of mechanically diverse microenvironments[192-197].

1.5 Rationale for study

Adhesions and invadopodia are crucial cellular structures required for the metastatic process. Both structures are capable of sensing and responding to the wide variety of stimuli encountered in the microenvironment. Recently, LPP has been established as a central protein in the regulation of these two structures controlling migration, invasion and metastasis. However, little is known about the precise mechanisms of LPP and the protein interactions that mediate these mechanisms. Therefore, in this thesis a BioID mass spectrometry approach was used to identify

potential interacting proteins of LPP and narrow candidate proteins for future functional studies. In addition to the study of LPP, the impact of stiffness on the regulation of cell migration and invasion were explored. Biophysical cues, such as stiffness, are intrinsic to the tumour microenvironment and normal tissues. Thus far, cell responses to these cues are not well characterized. Therefore, this thesis outlines the development of a stiffness-tunable platform used to characterize the invadopodia response of several breast cancer cell models over a physiological- and disease-relevant stiffness range. I have demonstrated that several cell models retain the same pattern of invadopodia activity across this stiffness range. Also poorly understood is the long-term impact of cell exposure to a specific biophysical environment. Several studies are beginning to suggest that cancer cells have memory for stiffness such that cell behavior is altered in new environments based on memory of past biophysical environments. There are many implications that could stem from cell memory for stiffness in the context of metastatic disease. To address this, preliminary testing of cell mechanomemory was completed in this thesis to measure the extent of biophysical conditioning that *in vivo* environments provide. The developed stiffness-tunable platform was used to measure cell migration speed and amount of invasion of the MDA-MB-231 cell model conditioned *in vivo*, in a soft brain substrate, and *in vitro*, on stiff cell culture dishes. Using this assay, we have demonstrated that cells long-term cultured in environments of unique stiffness migrate and invade differently across a stiffness range when compared to each other. Collectively, this thesis characterizes potential interacting proteins of LPP at adhesions and the impact of substrate stiffness on cell migration and invasion activity.

CHAPTER 2: MATERIALS AND METHODS

2.1 Cell Lines and Culture Conditions

Normal murine mammary gland (NMuMG) cells were obtained from the American Type Culture Collection (ATCC; Cat. no.: CRL-1636). ErbB-2 transformed NMuMG breast cancer cells were grown in high glucose (4.5 gL^{-1}) Dulbecco's Modified Eagle Medium (DMEM; Cat. No.: 319-005-CL, Wisent Bioproducts) supplemented with 5% fetal bovine serum (FBS; Cat. No.: 10082-147, Thermo Fisher Scientific), 10 $\mu g\ mL^{-1}$ insulin (Cat. No.: 511-016-CM, Wisent Bioproducts), 1 mM L-glutamine (Cat. No.: 609-065-CM, Wisent Bioproducts), 1% penicillin-streptomycin (Cat. No.: 10378-016, Thermo Fisher Scientific) and 0.2% amphotericin B (Cat. No.: 450-105-QL, Wisent Bioproducts).

HCC1954 breast cancer cells were grown in Roswell Park Institute Medium (RPMI 1640; Cat. No.: 350-000-CL, Wisent Bioproducts) supplemented with 10 % FBS.

Isolation of 4T1-derived liver- (2776) and lung-metastatic (526) cell populations have been described previously (Tabariès *et al*., 2015).

Mycoplasma screening was routinely performed every three weeks using MycoAlert mycoplasma detection kit (Cat. no.: LT07-318, Lonza).

2.2 Immunoblotting

Cells were lysed in cold TNE lysis buffer by scraping. Cell lysates (25 μg) were resolved by 7.5 % SDS-polyacrylamide gel electrophoresis and transferred onto polyvinylidene difluoride membranes (Cat. no.: IPVH00010, Millipore). Membranes were blocked in 5% Bovine Serum Albumin (BSA) for 1 hour and incubated with the following antibodies overnight at 4°C: LPP (1:1,000; Cat. No.: 3389S, Cell Signaling), Pdlim7 (1:1,000; rabbit custom antibody from Dr. Hans-George Simons), Vinculin (1:2,000; Cat. No.: V9131, Sigma), α-adaptin (1:5,000; Cat. No.: 610502, BD Biosciences), Trip6 (1:1,000; Cat. No.: A300-865A, Bethyl Laboratories), Cdgap (1:1,000; Cat. No.: HPA036380, Sigma) Ctnna1 (1:1,000, Cat. no.; 3240, Cell Signaling), and α-tubulin (1:20,000; Cat. no.: T9026, Sigma-Aldrich). Streptavidin HRP (Cat. No.: N100, ThermoFisher) and the appropriate HRP-conjugated secondary antibodies (1:10,000; Jackson Immuno Research Laboratories) were added to the membranes for 1 h. Finally, the membranes were visualized using SuperSignal™ West Pico PLUS Chemiluminescent Substrate (Cat. no.: 34578, Thermo Fisher Scientific).

2.3 Plasmid Construction

BirA-LPP fusion plasmids: WT and mutant LPP (A, B, C, D, 245F, 5F, mLIM1, and ΔABD) sequences were amplified from pMSCV-eGFP-LPP plasmid (previously used in Ngan *et al*. 2017) and inserted into pCDNA5-FLAG-BirA using the primers: *Not*I-LPP FWD primer 5'-3': ATTGCGGCCGCGATGTCTCACCCATCTTGG and LPP-*Xho*I REV primer 5'-3': TAGACTCGAGCTACAGGTCAGTGCTTGCCTTG. FLAG-BirA-LPP was then subcloned into pMSCV-blast for virus production.

BirA (alone) control was amplified from the pCDNA5-FLAG-BirA vector using the primers: BirA FWD primer 5'-3': TAGCCTCGAGCCATGGACTACAAAGACGATGAC and LPP- REV primer 5'-3': GTACCGAATTCCTACAGGTCAGTGCTTGCCTTG and subcloned into the pMSCV-blast vector. Constructs were retrovirally infected into ErbB2-transformed NMuMG cells and maintained in 40 μg/mL of blasticidin (Cat #: BLA477.100, Bioshop Canada Inc.).

2.4 BioID Sample Preparation

Mouse breast cancer cells (NMuMG-ErbB2) were generated for the BioID experiments as follows: NMuMG parental cells were infected with a pMSCV-hygro viral vector harboring the rat orthologue of ErbB2 (which possesses the activating transmembrane point mutation V664E). In addition, endogenous LPP was stably knocked down (generated by the laboratory of Dr. Peter Siegel, McGill University).

The NMuMG-ErbB2 LPP KD cells were stably infected with pMSCV-blast Lipoma Preferred Partner N-term BirA fusion plasmids using a Retro-X Universal Packaging System (Cat. No.:631530, Clontech). For retroviral infection, NMuMG-ErbB2 cells were incubated with polybrene (8 $\mu g \cdot mL^{-1}$) and virus containing media for 24 hours. Infected cells were maintained in 40 μgmL^{-1} of blasticidin (Cat. No.: BLA477.100, Bioshop Canada Inc.) for one week of selection and then frozen.

Three days prior to biotin treatment, NMuMG-ErbB2 LPP-BirA cells were thawed in Dulbecco's modified Eagle's medium supplemented with 10% fetal bovine serum (FBS), 10 mM HEPES, 1 mM sodium pyruvate, 1 mM L-glutamine, 10 μgml^{-1} insulin, penicillin-streptomycin, and amphotericin B (Fungizone).

Biotin labeling was done in 15 cm^2 cell culture plates, as outlined in Fig. 3.2, with at least five replicates made per sample per biological replicate. The samples included NMuMG-ErbB2

LPP KD, **NMuMG-ErbB2 LPP KD expressing pMSCV-BirA**, **NMuMG-ErbB2 LPP KD expressing pMSCV-BirA-LPP wildtype**, and NMuMG-ErbB2 LPP KD expressing **pMSCV-BirA-LPP-ΔABD**. Two samples of each cell line were made with one as a control and the other stimulated with 2 ng·mL^{-1} of TGFβ1 for 24 h before experiments were performed (Cat. No.: 100-21, PeproTech HZ-1011).

Sub-confluent cells (~70 %) were induced with Biotin over 24 hours (with or without TGFβ1 24 h pre-treatment and concurrent TGFβ1 treatment for pre-treated samples) and harvested at ~90 % confluency. Cells were rinsed in 20 mL of PBS, then collected by cell scraping in 1 mL of PBS, spun down for 5 minutes at 1500 G, PNS aspirated, pellet weighed, and snap frozen in liquid nitrogen before storing the samples at -80°C. NMuMG-ErbB2 with no treatment were used as a control for endogenous biotinylation. Eight samples in total were made with two biological replicates for each condition.

Cell pellets were then processed for streptavidin pulldown and mass spectrometry. All buffers were made in HPLC grade water, all pipette tips were non-autoclaved, and all glassware was rinsed (no plastic except for Falcon tubes). Fresh modRIPA was used to resuspend cells according to pellet weight (100 µL/100 mg of pellet). Samples were sonicated for three cycles, 5 sec ON, 3 sec OFF at 30 % AMP. Each sample was treated with 1 µL RNaseA (Cat. no.: EN0531, ThermoFisher) and 1 µL Turbonuclease was added and then incubated at 4°C for 15 min with rocking. SDS was added to bring the concentration from 0.1 % to 0.4 % and then the samples, mixed by inversion for 5 min and spun at 1500 G for 15 min. 25 µL of Streptavidin Sepharose High Performance (GE-17-5113-01) beads used per sample (50 µL of 50% bead slurry). Streptavidin beads were washed three times in RIPA buffer with centrifugation at 400 G for 30 s for the bead phase. After washing, beads were suspended at a 3:1 ratio of buffer to bead. Beads were then added and samples were rotated at 4°C for 3 h. Input control, used for immunoblotting, was taken prior to bead addition. Beads were washed 2X with RIPA buffer, 1X with 2% SDS wash buffer, 2X with RIPA buffer, 1X with TENTE-wash buffer, and 3X with freshly made 50 mM ammonium bicarbonate (pH 8-8.8). Trypsin (5 µL of 200 ng·µL^{-1}, Cat. no.: T6567, Sigma) was added to beads and samples were incubated overnight at 37°C. The next day, 2.5 µL of 200 ng˙µL^{-1} trypsin were added and incubated at 37°C for three hours.

Beads were spun down and the supernatant transferred to a new tube for 0.1 Vol of 50% formic acid addition and speedvac drying for 2-3 h at RT. Peptides were resuspended in 5% formic acid and stored at -80°C prior to the mass spectrometry experiments.

modRIPA (1:500 ProtInhib -40 µL/20 mL-, 1:100 PMSF – 200µL/20 mL)

Final Concentration	Stock Concentration	**Vol. for 20ml** (~15.24ml H2O)
50 mM Tris	1 M	1 ml Tris
150 mM NaCl	5 M	600 µl NaCl
0.5 mM EDTA	0.25 M	40 µl EDTA
1 mM EGTA	0.25 M	80 µl EGTA
1 mM MgCl2	0.5 M	40 µl MgCl2
1% NP40	10%	2 ml 10% NP40
0.1% SDS	10%	200 µl SDS
0.4% NaDOC	10%	800 µl NaDOC

RIPA-wash

Final Concentration	Stock Concentration	**Vol. for 20 ml** (~15.32 ml H2O)
50 mM Tris	1 M	1ml Tris
150 mM NaCl	5 M	600 µl NaCl
1 mM EDTA	0.25 M	80 µl EDTA
1% NP40	10%	2 ml 10%NP40
0.1% SDS	10%	200 µl SDS
0.4% NaDOC	10%	800 µl NaDOC

SDS-wash

Final Concentration	Stock Concentration	**Vol. for 10 ml** (~7.75ml H2O)
25 mM Tris	1 M	250 µl Tris
2% SDS	10%	2 ml SDS

TNTE-wash

Final Concentration	Stock Concentration	**Vol. for 20 ml** (~ 18.15ml H2O)
50 mM Tris	1 M	1 ml Tris
150 mM NaCl	5 M	600µl NaCl
1 mM EDTA	0.25 M	80 µl EDTA
0.1% NP40	10%	200 µl NP40

Mass spectrometry results were generated in Dr. Anne-Claude Gingras' laboratory. These results were then viewed on the ProHitz Visualization website (website developed at the Lunenfeld-Tanenbaum Research Institute) and dotplots were generated and exported as figures (Figure 3.2 and 3.3). The SAINT (Significance Analysis of INTeractome) score and BFDR (Bayesian False Discovery Rate) were used for further prioritization and visualization of proteins.

A SAINT score, developed specifically for AP-MS data, accounts for the probability that the identified protein is a *bona fide* interactor of the bait protein[198]. This score was used in a Cytoscape software along with the AvgSpec values for the generation of Figure 3.4 and S3 (SAINT only). AvgSpec values are the average number of spectral counts (number of times the protein is detected by the MS) and are used as a semi-quantitative measure of the number of proteins being labeled. To display known protein interactions, both the Nanostring and BioGRID databases were queried (Figure 3.3B, C and S3, respectively). Together, these MS data tools were used to prioritize and visualize LPP BioID candidates.

2.5 Single-Cell Speed Tracking

Manual Cell Tracking:

NMuMG-ErbB2 BirA-LPP cells were seeded onto μ-slide 8-well plates (Cat. no.: 80821, IBIDI) coated with 5 μg/cm$_2$ fibronectin (Cat. no.: F-0895, Sigma-Aldrich) diluted in 1X PBS. Cells settled and adhered over a 12 h period prior to recombinant human TGFβ1 (2 ng mL^{-1}; Cat. no.: 100-21, PeproTech) treatment and imaging. A Zeiss AxioObserver fully automated inverted microscope equipped with a Plan-Neofluar 10x/0.3NA Ph1 objective lens, Axiocam 506 CCD (Carl Zeiss, Jena, Germany) and Chamlide TC-L-Z003 stage top environmental control incubator (Live-cell Instrument, Seoul, South Korea) was used to acquire images every 10 minutes for a 30 h period.

Speeds of cells expressing the different BirA-LPP fusion constructs were obtained manually in Fiji using the plugin "Manual Tracking". The x,y coordinates of the cell tracks were then processed in MATLAB (v. 8.6, Rel. R2015b; The MathWorks, Natick, MA).

Automated Cell Tracking:

The OperaPhenix Harmony software was used to image and automate cell tracking of single cells on PDMS. Imaging of PDMS samples was set to a 10 h window, with 10 min interval and 15 fields-of-view (FOV) per well. Technical duplicates of cells were plated in two wells and results combined (30 FOV per condition). Cells were incubated at 37˚C and 5 % CO_2 and imaged with a 10x/0.3NA air objective lens and sCMOS camera. M mode of cell detection was used on the Digital Phase Contrast (DPC) images. M method (defined by Harmony 4.9 software: universal method used for fluorescent or DPC images and is excellent for splitting objects). Each FOV was

manually checked for appropriate cell detection and tracking prior to analysis (i.e. checked for appropriate cell outlining for all cells in the FOV, cell detection occurred in each frame, and cell splitting was appropriately followed). Any FOV that inconsistently detected cells, using the method above) was then eliminated from analysis. Cell speed was calculated from track data.

2.6 Immunofluorescence Staining

At the end-point of the assay, cells cultured in 35 mm coverglass-bottom dishes on fibronectin or 488-gelatin were fixed with 4 % paraformaldehyde (PFA) for 10 minutes. Samples were permeabilized with 0.3 % Triton X-100 for 10 min and then washed with freshly prepared 100 mM glycine three times. Following washing, cells were blocked with 10 % FBS in PBS for 1 h and the appropriate primary antibody was added for incubation at 4˚C overnight. LPP (1:500; Cat. No.: 8B3A11, Cell Signaling) and cortactin (1:500; Cat. No.: ab230992, Abcam) antibodies were used to detect adhesions or invadopodia, respectively. The secondary antibody used against LPP primary was Alexa Fluor 546 (Cat. No.: A11036, ThermoFisher) and was applied for 1 h at RT. Streptavidin 647 (Cat. No.: S32357, Invitrogen) was used to visualize biotinylation, while Phalloidin 488 (Cat No.: A12379, Invitrogen) and Phalloidin Atto-647 (Cat. No.: 65906, Sigma) were used to visualize F-Actin. These conjugates were also applied for 1 h at RT. Cells were preserved in PBS and 0.05 % sodium azide (Cat. No.: SAZ001, Bioshop) for imaging.

Images were acquired on a Zeiss LSM 710 confocal microscope with a Plan Apochromat 63x/1.4 NA objective lens. Parameters used for imaging included: 1 airy unit pinhole, 850 master PMT gain, 1 digital gain, 3.15 µs pixel dwell time, and 4 line scan averaging. The 488 nm laser line from a 25 mW argon ion laser was used to image gelatin and F-Actin, a 1 mW HeNe green 543 nm laser was used to image LPP and a 5 mW HeNe red 633 nm laser was used to image F-actin and biotin. Acquired images were saved as 1024x1024 12-bit images and adjusted in Fiji for contrast and scaling. Image properties included a zoom of 1.0 and pixel size of 0.132x0.132. Emission characteristics included 2, 7 and 2.5% laser intensity for 493-549, 566-599, and 638-759 emission filters, respectively. 488/594, 458/543, and 488/543/633 beam splitters were used for the 488, 543 and 633 channels, respectively.

2.7 Gelatin Degradation Assay

Gelatin-degradation assays were performed on fluorescently conjugated gelatin-coated 35

mm cover-glass bottom cell culture dishes (FD35-100 WPI). Briefly, sterile 35 mm cell culture dishes were coated with a mix of 0.1 mg/ml poly-D-lysine (Cat. #: P6407, Sigma) and 5 mg (cm^2) Fibronectin (Cat. #: FC010, Millipore) in PBS for 20 min, followed by incubation with 0.4% Glutaraldehyde for 10 min. Oregon Green 488 conjugated gelatin (Cat. #: G13186, Invitrogen), was diluted by 1:20 with 0.1% unconjugated gelatin (Cat. #: 07903, Stem Cell Technologies) and used to coat coverslips at 37°C for 10 min. Coverslips were then incubated with 10 mg/ml sodium borohydride for 2 min, followed by 70% ethanol for 20 min. Three washes with 1X PBS were performed between each step. DMEM media was added to the coverslips at 37°C for 1 h before cell plating.

HCC1954, 2776 and 526 breast cancer cells were plated (32,000 cells) onto gelatin-coated coverslips and incubated at 37°C for 24 h and then fixed with 4 % PFA for 10 min.

Image acquisition was performed with ZEN imaging software on a Zeiss LSM710 confocal microscope and a plan-Apochromat 63/1.4 NA oil immersion objective lens (Carl Zeiss Inc.).

2.8 Quantification of Gelatin Degradation

Quantification of gelatin area degraded was performed using Imaris v8.3.1 (Bitplane) surfaces function. A threshold for each FOV was determined manually and visually inspected to ensure only degraded areas were selected for each inverted image (signal void inverted to positive signal for quantification). The background subtraction function was used to create surfaces. Total number of voxels exported from Imaris and surface area were calculated using the x,y dimensions of images.

2.9 shRNA-mediated KD of BioID Candidates

Prioritized BioID candidates and known LPP interactors were chosen for stable KD in 2776 cells. TMP constructs were obtained from the McGill Platform for Cellular Perturbation (MPCP). Lentivirus was produced as described elsewhere[199].

Target	Gene ID	TRC Clone ID	Efficacy of KD in 2776 (qualitative)
Vinculin	22330	TRCN000001593	Excellent
		TRCN000001594	None
		TRCN0000295656	Excellent
		TRCN0000288326	Good
		TRCN0000288325	None
Pdlim7	67399	TRCN0000182783	None
		TRCN0000200375	None
		TRCN0000322545	Good
		TRCN0000322470	Good
		TRCN0000375190	OK
Trip6	22051	TRCN0000277396	Excellent
		TRCN0000277329	Good
		TRCN0000277397	Good
		TRCN0000277330	Excellent
		TRCN0000277331	Good
Cdgap	12549	TRCN0000105800	Good
		TRCN0000105801	None
		TRCN0000105802	Good
		TRCN0000105803	Excellent
		TRCN0000105804	Good
Ctnna1	12385	TRCN0000108741	None
		TRCN0000108742	None
		TRCN0000108743	Good
		TRCN0000108744	Excellent

2.10 PDMS Casting and Surface Activation

PDMS Casting: Protocol adapted from Yoshie H. *et al.* (2019) for preparation of PDMS silicone and outlines in Figure S1 (Appendix). Part A and B of a high purity dielectric soft silicone gel kit (Cat. No.: GEL-8100, Nusil Technology) were mixed in a 1:1 weight ratio and mixed by rotation at a low speed. A curing agent from a Sylgard 184 silicone encapsulant kit (Cat. No.: 184 SIL ELAST KIT, Dow Corning) was added according to the required substrate modulus (stiffness) presented in the % crosslinker table of Yoshie H. *et al*. (2019). The mixture was then slowly rotated end-over-end for 30-45 min.

Depending on plate format, PDMS was applied to Type 0 coverglass 24x 60 mm (Cat. No.: 63751-01, Electron Microscopy Sciences) for characterization of the HCC1954, 2776, and 526 breast cancer cell mediated gelatin degradation or a multi-well format (24 well glass-bottom plates) (Cat. No.: 0030741021, Eppendorf) for the MDA-MB-231 mediated degradation following *in vivo* biophysical conditioning. To achieve uniform 70 μm thick PDMS casting on coverglass, spin-coating at 300 rpm for 1 min was required with an acceleration/deceleration of 50 rpm/s from 0 to 300 rpm. Following casting, the PDMS was cured on the coverglass at 100˚C for 2 h. To cast and cure in the multi-well format, PDMS was applied by dropper (~20 μl) to equally apply the viscous PDMS across the wells. Equal distribution of volume is necessary to keep the PDMS thickness consistent between wells for imaging at the same focal height. Once the entire surface area of the wells was covered, the plates were kept at RT for one day, followed by incubation for three days at 60 ˚C in a level oven.

PDMS Coating: Parameters tested for PDMS surface coating are outlined in Fig. S1 and Table S1 (Appendix). Uniform 488-gelatin coating of PDMS, without irregularities, was needed for imaging nm scale degradation patterns. Optimization of the 488-gelatin coating was difficult to achieve as PDMS is an extremely hydrophobic surface and is pliable at low stiffness leading to cracking or clustering of the gelatin.

Uniform 488-gelatin and fibronectin coating was achieved with Piranha surface cleaning followed by use of two crosslinkers. First, the PDMS surface was activated with a Piranha solution (1:3:5 ratio of water:hydrogen peroxide:sulfuric acid). Sulfuric acid (Cat. No.: A300-500, Fisher Scientific) was first added to water, followed by hydrogen peroxide (Cat. No.: H325-500, Fisher Scientific) (extremely exothermic reaction). Piranha solution was then applied to the PDMS in excess and incubated at RT for 15 min. De-ionized water was used to rinse the PDMS after

activation. A 1% PEI solution (Cat. No.: 408727, Sigma) (branched polymer) was applied for 10 min, followed by crosslinking with 0.04% glutaraldehyde (Cat. No.: G5882, Sigma) for 10 min. Substrates were finally rinsed three times with 1X PBS. The thickness of each component (glass, PDMS and gelatin) is shown as a schematic in Figure 3.5.

For migration studies, human fibronectin was applied at 5 μg/cm2 to the PDMS and for degradation studies, 488-gelatin was prepared during surface activation and crosslinking. Gelatin was prepared as follows: 488-gelatin (G-13186 Molecular Probes, stored at -80°C) was diluted in 0.1% unlabeled gelatin (Cat. no.: 07903, Stem Cell Tech) at a ratio of 1:15 fluorescent/non-fluorescent gelatin, filtered with a 0.22 μm filter and pre-heated at 37 ˚C for 30 min. The human fibronectin or 488-gelatin was then applied to the activated and crosslinked PDMS surface in excess (total PDMS surface covering) and incubated overnight at 4˚C. The next day, the remaining gelatin or fibronectin solution was aspirated and the surface was rinsed 3X with PBS and sterilized for cell plating.

2.11 Statistical Analysis

Statistical significance (P-value) was determined using unpaired two-tailed Student's *t*-test in Graphpad 7. The data is presented with error bars representing the s.e.m. in all figures and means are represented by the column height.

CHAPTER 3: RESULTS

3.1 NMuMG-ErbB2 breast cancer cells successfully express BirA-LPP constructs for BioID Assays.

LPP is an important component of adhesions and is required for regulation of cell migration speed in response to TGFβ[82, 106]. When LPP expression is reduced, cells can no longer respond to TGFβ by increasing adhesion dynamics and cell speed, ultimately, impairing metastasis to the lung (in revision, JBC; E. Voorand author contributions, Kiepas *at al.* **The ShcA adaptor protein cooperates with LPP to mediate adhesion dynamics and invadopodia formation**)[82, 83, 106]. This phenotype is also apparent when the α-actinin binding domain of LPP is lost (ΔABD) (in revision, JBC, E. Voorand author contributions, Kiepas *at al.* **The ShcA adaptor protein cooperates with LPP to mediate adhesion dynamics and invadopodia formation**). Although localized to adhesion, this mutant cannot effectively increase adhesion dynamics in response to TGFβ. Given that LPP is critical to adhesion regulation, we sought to identify novel partners that regulate LPP interactions with the cytoskeleton including interactions that depend on the ABD.

A BioID approach was chosen to identify proteins that come within the proximity of LPP at adhesions. To achieve this, the WT and ΔABD versions of LPP were chosen for comparison to identify proximal proteins that contribute to the effective regulation of highly dynamic adhesions. Three viral expression constructs were generated in an MSCV backbone for the BioID experiments: BirA-WT-LPP, BirA-ΔABD-LPP and BirA (Figure 3.1A). When compared by immunoblot, stable expression of each fusion in the NMuMG-ErbB2 (KD endogenous LPP) cell line was similar to the level of endogenous LPP expression (Figure 3.1B). Moreover, treatment with biotin for 24 h induced biotinylation of many proteins as seen with a streptavidin immunoblot of whole cell lysates (Figure 3.1B). In addition, alternate BirA-fusions with phosphorylation mutants and a LIM domain mutant of LPP, controlling invadopodia formation and LPP localization, respectively, were generated for further BioID studies (Figure S2). By immunofluorescence (IF of LPP and streptavidin), the WT and ΔABD BirA-LPP fusions were appropriately localized to cellular adhesions and mediated biotin-labeling of proteins within these structures, while the BirA control had no localization with staining for LPP and Biotin (Figure 3.1C). Cell migration speeds of the BirA-LPP expressing NMuMG-ErbB2 breast cancer cells, in response to TGFβ, also confirmed functional rescue of the endogenous LPP KD (Table 3.1). Taken together, the expression and function of BirA-LPP fusion proteins and control BirA proteins were successfully validated for use in the BioID proteomic approach.

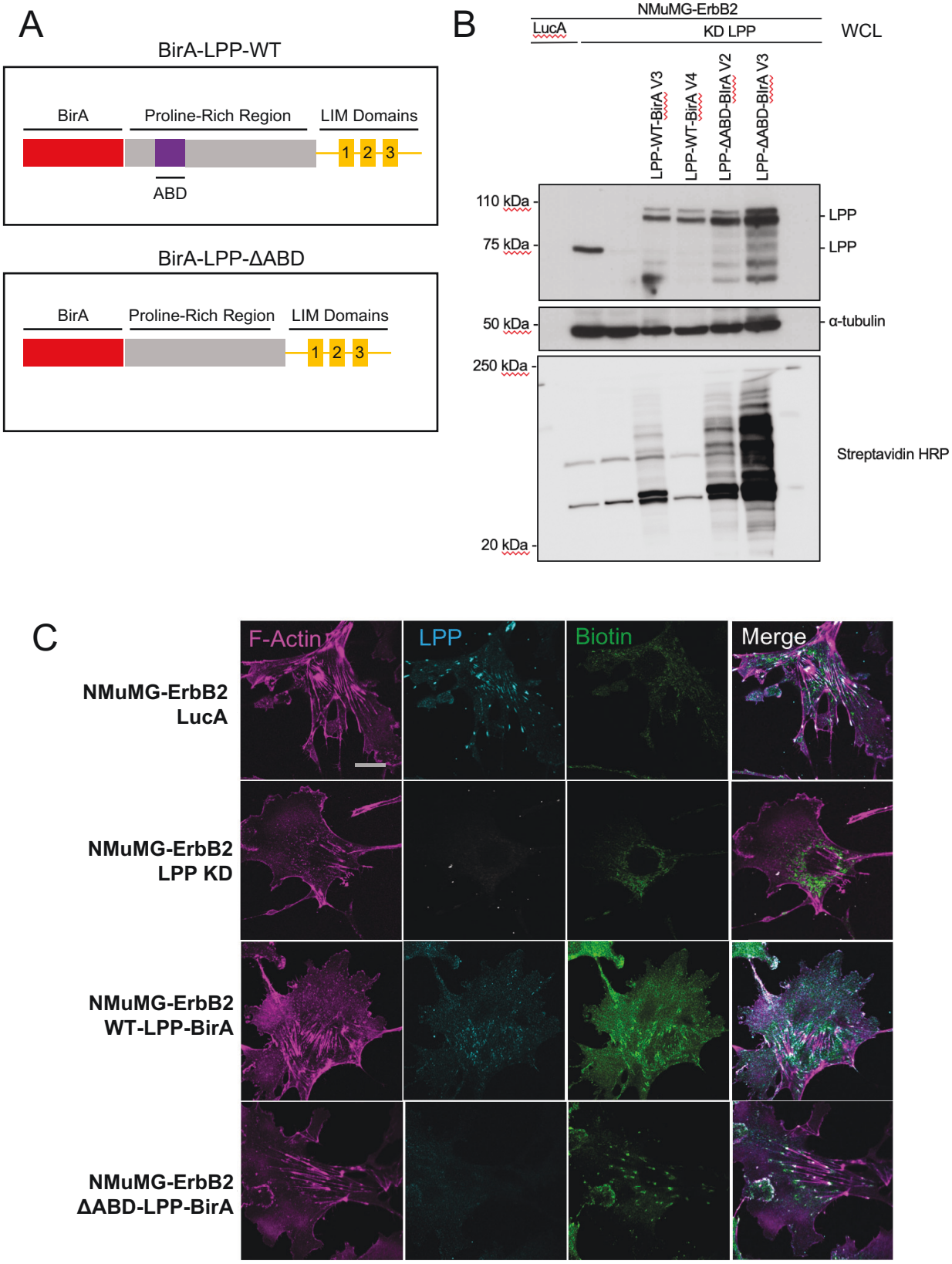
A
BirA-LPP-WT
BirA
Proline-Rich Region
LIM Domains
1
2
3
ABD
BirA-LPP-ΔABD
BirA
Proline-Rich Region
LIM Domains
1
2
3
B
NMuMG-ErbB2
LucA
KD LPP
WCL
LPP-WT-BirA V3
LPP-WT-BirA V4
LPP-ΔABD-BirA V2
LPP-ΔABD-BirA V3
110 kDa
75 kDa
LPP
LPP
50 kDa
α-tubulin
250 kDa
Streptavidin HRP
20 kDa
C
F-Actin
LPP
Biotin
Merge
NMuMG-ErbB2
LucA
NMuMG-ErbB2
LPP KD
NMuMG-ErbB2
WT-LPP-BirA
NMuMG-ErbB2
ΔABD-LPP-BirA

Figure 3.1 NMuMG-ErbB2 cells successfully express BirA-LPP constructs for BioID Assays. **(A**) BirA-LPP-WT and BirA-LPP-ΔABD (loss of α-actinin binding domain) fusion proteins. (**B)** Immunoblot of LPP-BirA fusion protein expression and biotinylation pattern of NMuMG-ErbB2 cells. Cells were treated with 50 μM biotin for 24 h and subsequently lysed. An antibody against LPP was used to detect the BirA-LPP fusion protein and streptavidin conjugated to HRP was used to detect biotinylated proteins. Loading control is α-tubulin. LPP-WT-BirA V3 and LPP-ΔABD-BirA V2 were selected for the BioID assay based on expression level in comparison to endogenous LPP. **(C)** Localization of BirA-LPP fusion protein and biotin-labeled proteins at focal adhesions when treated with TGFβ and biotin, visualized by immunofluorescence. An LPP antibody and 647-conjugated streptavidin was used for immunofluorescence. F-Actin is shown in magenta, LPP in cyan and biotin in green. Images were taken on a Zeiss Confocal Laser Scanning Confocal Microscope (CLSM) using a Plan-Apochromat 63x/1.4 NA oil DIC objective lens (1 pixel = 0.132 μm). Scale bar is 20 μm.

Table 3.1 Cell migration speeds of NMuMG-ErbB2 expressing BirA-LPP fusions in response to TGFβ treatment

	Average Cell Velocity Between 20 and 30 hr (μm/h)	
	- TGFβ	+ TGFβ
LucA	17.4	28.8
LPP KD	15.2	23.8
BirA-LPP-WT	17.2	30.2
BirA-LPP-ΔABD	16.25	14.91
eGFP-LPP	16.1	31.0

3.2 LPP BioID mass spectrometry reveals changes in the pattern of proximal proteins with both TGFβ treatment and loss of the LPP actinin-binding domain.

To elucidate potential partners of LPP that mediate adhesion dynamics in response to TGFβ, NMuMG-ErbB2 LPP KD cells expressing the BirA-LPP fusions were subjected to several treatment combinations prior to mass spectrometry (MS). Both the BirA-WT and BirA-ΔABD expressing NMuMG-ErbB2 cells were left untreated or were pre-treated with TGFβ for 24 h to ensure biotin labeling was enriched in highly dynamic adhesions (migratory phenotype) throughout the subsequent biotin labeling period (Figure 3.2A). During the subsequent 24 h biotin treatment, TGFβ was included in the media for cells that received pre-treatment (Figure 3.2A). Following biotin treatment, cells were lysed and processed for MS of the biotin labeled proteins. To note, NMuMG-ErbB2 LPP KD and NMuMG-ErbB2 FLAG-BirA expressing cells were used as controls for endogenous biotinylated proteins and non-specific biotin-labeling, respectively.

Our MS findings revealed differences in the proteins proximal to LPP in the presence of TGFβ and with mutation of the actinin-binding domain (Figure 3.2B). In agreement with a TGFβ-induced EMT, biotin labeling of junctional proteins such as Jcad, Xpo1, and Tjp1 was reduced for WT and ΔABD LPP in response to TGFβ stimulation (Figure 3.2B). Gene Ontology (GO) term analysis confirmed that the large majority of biotinylated proteins that emerged in response to TGFβ were components or regulators of adhesions or actin cytoskeleton structures, with some hits falling into the category of stress granule (Pabpc4 and Cpeb4) and P-body proteins (R3hdm1, Marf1, Dcp1a, Tnrc6a/b, and Cnot1) proteins (data not shown). Interestingly, there is a large overlap in protein labeling between the WT and ΔABD versions of LPP, with few unique proteins identified for either (Figure 3.2B). These results are supported by a ~75 % overlap in proteins identified from one of our previous BioID MS experiments (data not shown).

3.3 LPP BioID candidates prioritized based on differences between WT and ΔABD LPP-BirA protein labeling with TGFβ treatment.

LPP BioID candidates were sorted by greatest difference in biotin labeling between the WT and ΔABD LPP fusion expressing cells in the presence of TGFβ (Figure 3.3A). Prioritizing the candidates in this manner narrowed the candidate list to those that might functionally contribute to regulation of adhesion dynamics. The prioritized list of candidates was then subjected to STRING network analysis to query known protein interactions and build an interaction network

for LPP. The first subshell included only known interactions between the candidates revealed by BioID and LPP (Figure 3.3B). The second subshell included known interactors of the potential LPP binding proteins identified by BioID candidates (Figure 3.3C) from the STRING database. The layering of subshells in this manner gave context to the generated interaction network. Furthermore, BioGRID was queried in a similar manner (first and second subshell interactions) as a second alternate database to strengthen the LPP adhesome protein network (Figure S3 [appendix]). Thus far, prioritization of candidates based on enrichment in the WT LPP condition has established a potential interaction network for LPP at focal adhesions in the presence of TGFβ.

3.4 In the presence of TGFβ, proteins in proximity with LPP are distinctly enriched with the WT versus actinin-binding domain mutant (ΔABD) LPP-BirA.

Functional verification of the BioID interaction network is needed to validate if each potential LPP interacting candidate functionally contributes to adhesion regulation. Therefore, a second round of prioritization of candidates was performed before functional validation through shRNA approaches. This prioritization was achieved by visualizing the fold change (FC) in spectral counts (biotin labeling) of WT LPP over ΔABD LPP conditions (Figure 3.4). From this FC analysis, we could rank those candidates that were enriched in the WT LPP (Table S2) or ΔABD LPP (Table S3) condition were ranked. Kank1, Rassf8, Sorbs1, Ppp2r2d, and Pdlim7 were the five most enriched for WT LPP; meanwhile, Acta2, Actg2, Dcp1a, and Arhgap31 were the five most enriched for ΔABD LPP (Figure 3.4).

Of these identified proteins, Pdlim7, Arhgap31, Vcl, Trip6, and Ctnna1 were selected for functional testing based on antibody availability and expression level in the NMuMG-ErbB2 and the 2776 4T1-derived metastatic subpopulation breast cancer cells. Subsequently, expression of Pdlim7, Arhgap31, Vcl, Trip6, and Ctnna1 was successfully diminished in the 2776 (liver-aggressive 4T1 mouse model) for future functional validation by single-cell tracking and *in vivo* metastasis assays (Figure S4). Collectively, these analyses have generated an adhesion interactome for LPP and led to the prioritization of BioID hits for functional *in vitro* and *in vivo* validation to understand the protein complex and protein interactions that mediate breast cancer cell metastasis.

A

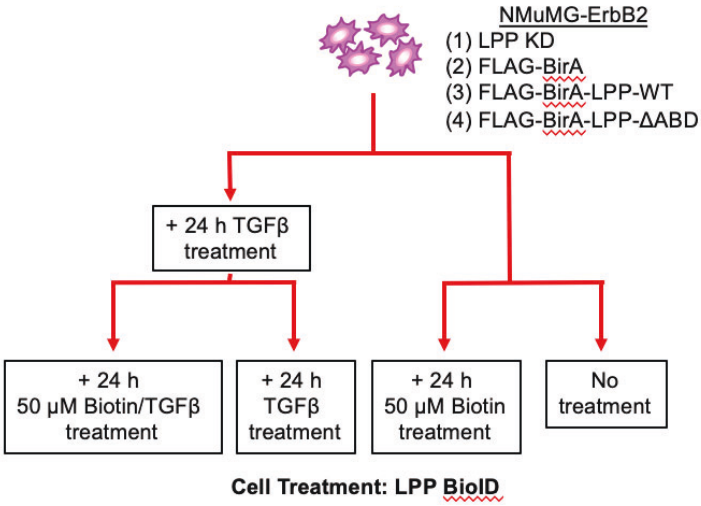
NMuMG-ErbB2
(1) LPP KD
(2) FLAG-BirA
(3) FLAG-BirA-LPP-WT
(4) FLAG-BirA-LPP-ΔABD
+ 24 h TGFβ treatment
+ 24 h 50 μM Biotin/TGFβ treatment
+ 24 h TGFβ treatment
+ 24 h 50 μM Biotin treatment
No treatment
Cell Treatment: LPP BioID

B


Bait
MSPLIT_LPP
MSPLIT_LPP_dADB
MSPLIT_LPP_TGFb
MSPLIT_LPP_dADB_TGFb
Prey
Tln2
Tns1
Trip6
Pxn
Ahnak
Ctnna1
Acta2
Usp7
Arhgap31
Actg2
Fam83h
Usp37
Gstp2
Arhgap21
Krt42
Dok1
U2af1
Bnip2
Ruvbl2
Mcm7
G3bp2
Krt76
Ptgs2
Pdlim7
Itsn1
Hspa1a
Hspa1b
Usp9x
Gzmg
Prag1
Usp54
Ppp2r2d
Rassf8
Enah
R3hdm1
Xpo1
2900026A02Rik
Plekha7
Pabpc4
Rpn1
Tns2
Alms1
1700071K01Rik
Kank1
Arpc4
Maml3
Cpeb4
Dcp1a
Ncor2
Marf1
Ankdd1a
Vasp
Ppp2r3a
Sec16a
Prrc2b
Tnrc6a
Cgn
Sorbs2
Sorbs1
Limd1
Jcad
Tnrc6b
Bcar1
Tns3
Shroom2
Vcl
Kank2
Dlg5
Tjp1
Etl4
0
AvgSpec
50
Relative abundance
≤ 0.2
≤ 0.8
> 0.8
BFDR

Figure 3.2 LPP BioID mass spectrometry reveals changes in the pattern of proximal proteins with both TGFβ treatment and loss of the LPP actinin-binding domain. **(A)** NMuMg-ErbB2 cells expressing BirA-LPP-WT and BirA-LPP-ΔABD fusion proteins were treated with or without TGFβ for 24 hours prior to 24 hours of 50 μM biotin treatment. NMuMG LPP KD cells were used as a control for endogenous biotinylated proteins. **(B)** Post-treatment, cell pellets were collected and sent for streptavidin pull-down and mass spectrometry sample preparation. Background endogenous biotinylation was removed with NMuMG LucA control and mass spectrometry results were normalized to the spectral counts of an NMuMg-ErbB2 BirA control. Legend displays dot colour to represent average spectral count, dot size to represent relative abundance and outer dot colour to represent the BFDR of each protein identified. Dot plot was generated using ProHitz Visualization tool.

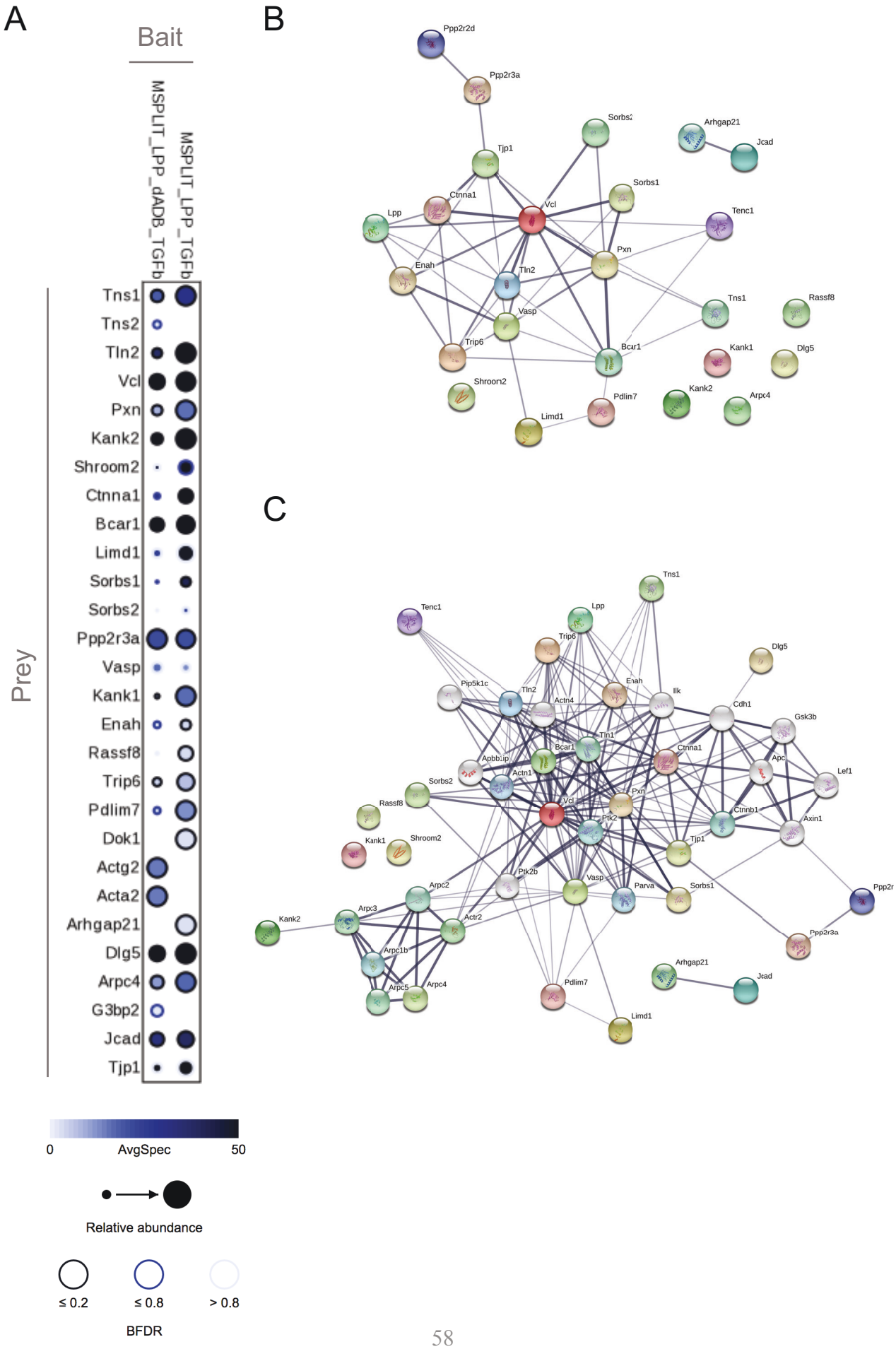
A
Bait
MSPLIT_LPP_dADB_TGFb
MSPLIT_LPP_TGFb
Prey
Tns1
Tns2
Tln2
Vcl
Pxn
Kank2
Shroom2
Ctnna1
Bcar1
Limd1
Sorbs1
Sorbs2
Ppp2r3a
Vasp
Kank1
Enah
Rassf8
Trip6
Pdlim7
Dok1
Actg2
Acta2
Arhgap21
Dlg5
Arpc4
G3bp2
Jcad
Tjp1
0
AvgSpec
50
Relative abundance
≤ 0.2
≤ 0.8
> 0.8
BFDR
B
Ppp2r2d
Ppp2r3a
Sorbs2
Arhgap21
Jcad
Tjp1
Sorbs1
Ctnna1
Vcl
Lpp
Tenc1
Pxn
Enah
Tln2
Tns1
Rassf8
Vasp
Trip6
Bcar1
Kank1
Dlg5
Shroom2
Kank2
Pdlim7
Arpc4
Limd1
C
Tns1
Tenc1
Lpp
Trip6
Dlg5
Pip5k1c
Tln2
Actn4
Enah
Ilk
Cdh1
Gsk3b
Tln1
Bcar1
Ctnna1
Apbb1ip
Actn1
Apc
Lef1
Sorbs2
Pxn
Rassf8
Vcl
Ptk2
Ctnnb1
Axin1
Kank1
Shroom2
Tjp1
Ptk2b
Vasp
Parva
Sorbs1
Ppp2r
Arpc2
Arpc3
Actr2
Kank2
Ppp2r3a
Arpc1b
Arhgap21
Jcad
Arpc5
Arpc4
Pdlim7
Limd1

Figure 3.3 Prioritization of LPP BioID candidates based on differences between WT and ΔABD LPP-BirA protein labeling following TGFβ treatment. **(A)** Dot plots include only BioID candidates that differ noticeably in biotin labeling between WT and ΔABD LPP-BirA. AvgSpec is displayed by colour of the dot, relative abundance by the size of the dot and the BFDR by the colour of the ring surrounding the dot. Dot plot spectral counts are normalized to the NMuMG-ErbB2 BirA (alone) control. Dot plot generated using ProHitz Visualization tool. **(A)** First subshell of STRING database protein interactions for LPP and the prioritized BioID candidates and **(B)** the second subshell of protein interactions for the BioID candidates which includes other proteins identified by STRING.

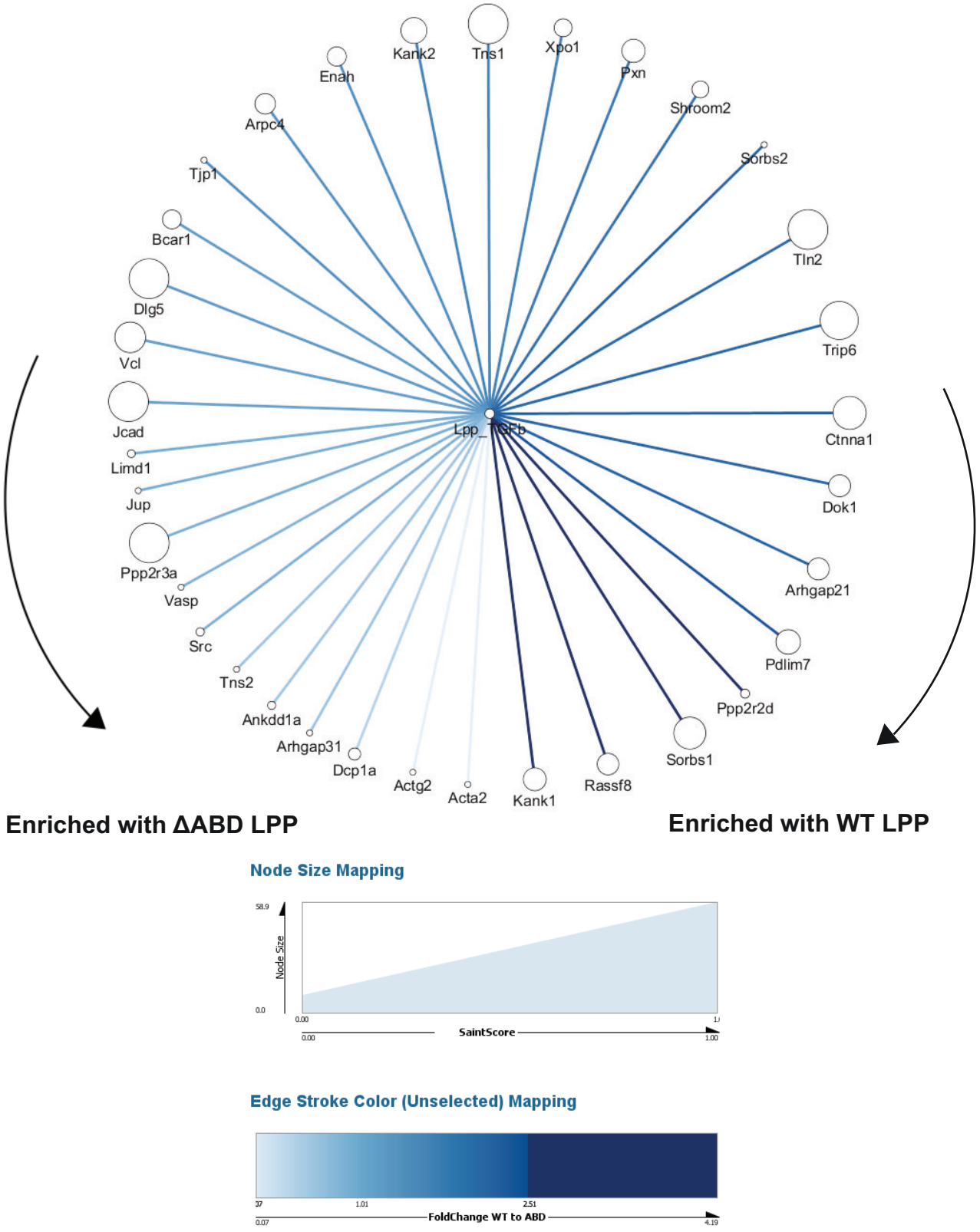

Figure 3.4 In the presence of TGFβ, proteins in proximity with LPP are distinctly enriched with the WT versus actinin-binding domain mutant (ΔABD) LPP-BirA. Proteins identified with the LPP BioID are displayed in order based on enrichment of biotin labeling (Fold Change of average spectral counts) for WT versus ΔABD BirA-LPP. Ordering is displayed as Edge colour and the SAINT score for each protein is displayed as node size.

3.5 Degradative invadopodia activity of HCC1954 cells is modulated based on underlying substrate stiffness in the presence of TGFβ.

Invadopodia are mechanosensitive cell structures that modulate activity based on underlying substrate stiffness[168]. Using an ErbB2 positive model of breast cancer, we sought to characterize invadopodia degradation activity over a physiologically-comprehensive range of stiffness. We first extended the gelatin-based invadopodia assay to a range of stiffness that represents tissue from physiological breast stiffness (~ 1-5 kPa) to invasive disease progression (IDC) (~150 kPa)[152]. To achieve this, PDMS was chosen as a stiffness-tunable substrate to coat with a thin layer of fluorescent gelatin for invadopodia assays. Due to its chemical properties, PDMS is versatile and can be used to model stiffness in ranges that are difficult to achieve with traditional polyacrylamide or hydrogel substrates. The resulting PDMS substrate design allowed imaging of invadopodia at 5, 10, 20, 30, 50, 70, 90 and 100 kPa stiffness (Figure 3.5A).

HCC1954 breast cancer cells were left untreated or were pre-treated with TGFβ for 24 h prior to plating on PDMS substrates. Interestingly, stiffness alone was not enough to trigger invadopodia formation in HCC1954 (Figure 3.5B, -ß). Indeed, with experimentation on glass substrates HCC1954 breast cancer cells do not form invadopodia unless treated with TGFβ (data not shown). Interestingly, the TGFβ-treated HCC1954 breast cancer cells exhibited detectable degradation activity on lower stiffness (<10 kPa) and peak degradation activity on higher stiffness (>70 kPa) substrates, while invadopodia activity was lowest between 20 and 50 kPa stiffness (Figure 3.5C). These results suggest that invadopodia can sense a wide range of stiffness and modulate degradative activity in response to each stiffness.

3.6 4T1 metastatic subpopulation cells have similar degradative responses to substrate stiffness.

To test whether this pattern of invadopodia response to stiffness is intrinsic or unique to all cell types, two 4T1-derived breast cancer sub-populations (Triple-Negative Breast Cancer subtype) were used. Our findings demonstrated that the 4T1-2776 (liver-aggressive) (Figure 3.6A, B) and 4T1-526 (lung-aggressive) (Figure 3.6C, D) cells maintained the pattern of response to stiffness seen with the HCC1954 human breast cancer cell model. Both 4T1-2776 and 4T1-526 breast cancer cells exhibited elevated degradative activity on low stiffness substrate (5 kPa) and peak degradative activity on high stiffness (100 kPa), with minimal degradative activity within the

mid-range of stiffness (48 kPa) (Figure 3.6). These cell lines were tested in the absence of TGFβ, as these models have highly active invadopodia on glass substrates without stimulation (data not shown). These results suggest that the pattern of invadopodia activity in response to substrate stiffness is retained by multiple cell types.

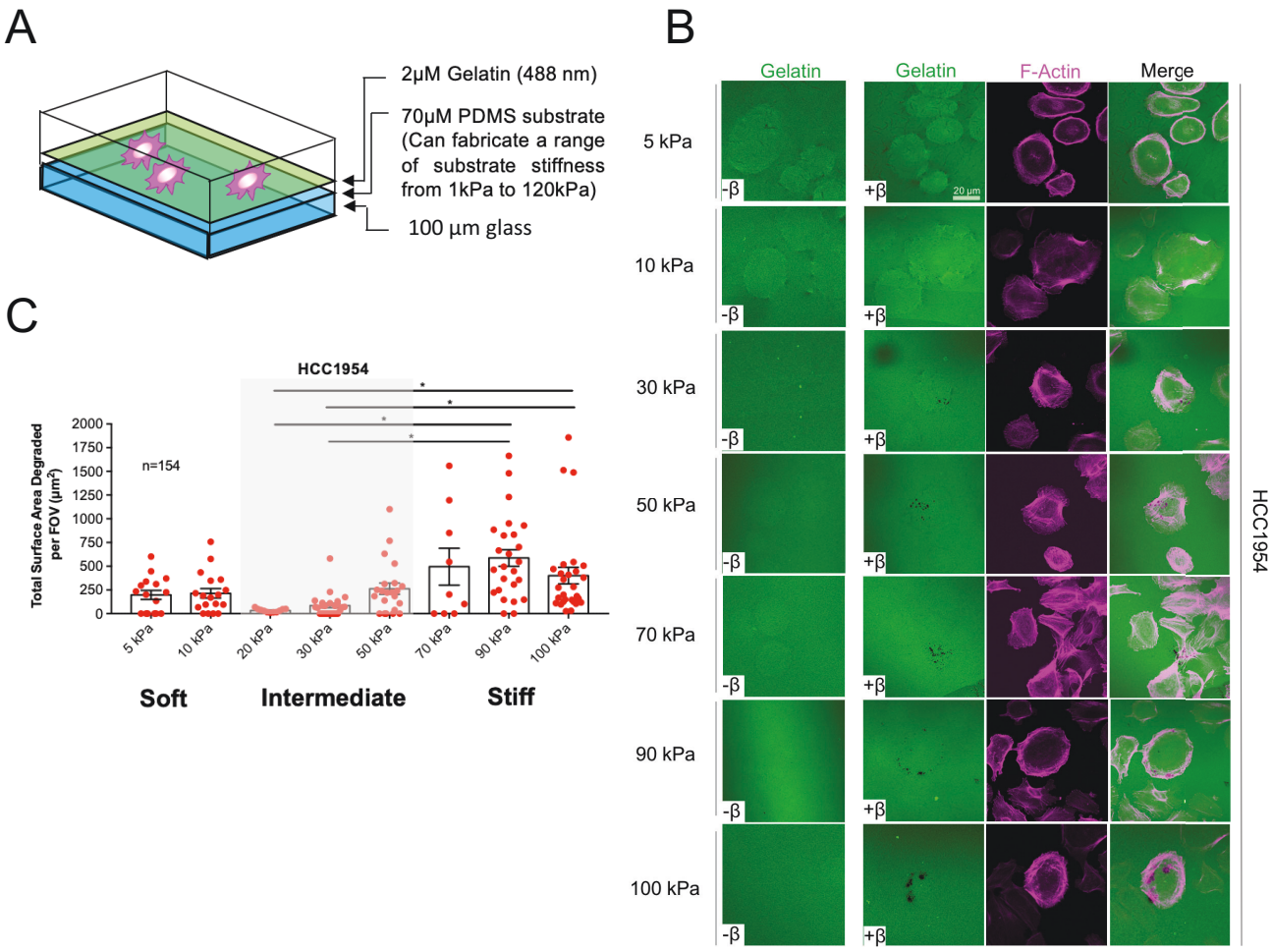

Figure 3.5 Degradative invadopodia activity of HCC1954 cells is modulated based on underlying substrate stiffness in the presence of TGFβ. **(A)** PDMS substrate design for the gelatin degradation assay. **(B)** HCC1954 invadopodia activity in response to stiffness with and without 24 h of TGFβ pre-treatment. 488-gelatin is represented in green and F-Actin in magenta. Scale bar is 20 μm. **(C)** Quantification of HCC1954 gelatin degradation over the stiffness range. 154 FOV were quantified from three independent experiments. (*, $P < 0.05$, two-tailed Student's *t*-test).

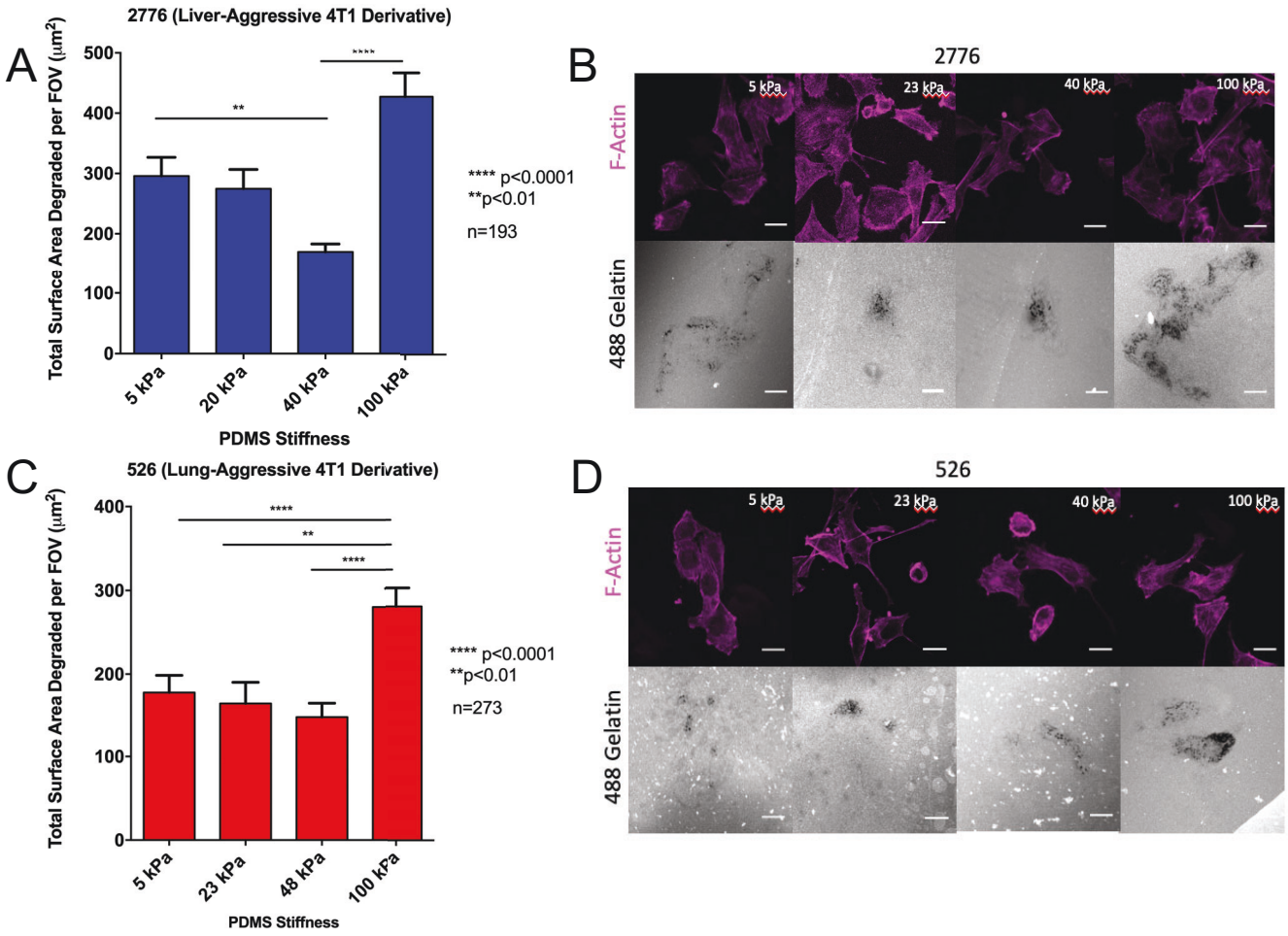

Figure 3.6 4T1 metastatic sub-populations have similar degradative responses to substrate stiffness. Cells were plated on 488-gelatin-coated PDMS with substrate stiffness of 5, 23, 40, and 100 kPa for 24 h followed by fixation and staining with 647-phalloidin. Total surface area degraded per FOV was quantified by the surface area of signal void in the 488-gelatin channel. Surface area degraded by liver-aggressive 2776 cells (193 FOV quantified) **(A)** and lung-aggressive 526 cells (273 FOV quantified) **(C)** on different underlying stiffness from three independent experiments. (**, $P < 0.01$, ****, P<0.0001, two-tailed Student's *t*-test). Representative images of cell degradation for 2776 **(B)** and 526 **(D)** cells. Magenta is F-Actin staining and grey is 488-gelatin. Scale bar is 20 μm.

3.7 MDA-MB-231 cells regulate migration speed in response to stiffness based on biophysical conditioning.

Initial studies of mechanical memory suggest that mechanical "priming" of cells can have long-term effects on phenotype[184, 200]. We sought to test the impact on migratory and invasive phenotypes of breast cancer cells mechanically primed *in vivo* and to test whether this priming could be reverted. This mechanical "priming" effect was tested by conditioning MDA-MB-231 human breast cancer cells (triple negative model) by long-term growth in mechanically soft *in vivo* brain and comparing them to MDA-MB-231 cells directly that were grown continually on mechanically stiff plastic tissue culture dishes. The explanted MDA-MB-231 cancer cells were termed "*ex vivo"* and cells grown on tissue culture dishes "plastic". Furthermore, *in vivo* conditioned cells were cultured *ex vivo* for 1 week on 1 kPa PDMS surfaces (mimicking brain stiffness) or on stiff plastic dishes (~10^8 kPa) to test whether migratory phenotypes could be further modulated. These cells are represented as "*ex vivo* 1 kPa" and "*ex vivo* plastic", respectively. After conditioning, the MDA-MB-231 breast cancer cells in each condition were used for migration speed and invadopodia degradation assays on PDMS of different stiffness (Figure 3.7). These stiffnesses included 1 kPa, 23 kPa, 48 kPa, 100 kPa, 3 MPa and Glass (~65 GPa)[201] . Importantly, there were no observed differences in proliferation of the MDA-MB-231 cells once seeded on the surfaces of different stiffness across the entire range (data not shown).

Our data demonstrate that the cell migration speed of biophysically-conditioned MDA-MB-231 breast cancer cells has a pattern that reflects the mechanical exposure the cells received *in vivo* (Figure 3.8). The average migration speed across the stiffness range of *ex vivo* and *ex vivo* 1 kPa cells was above 40 μm/h, with the exception of *ex vivo* on glass substrate, which had a migration speed of ~ 35 μm/h (Figure 3.8A). In contrast, plastic and *ex vivo* plastic conditioned cells tended to decrease migration speeds to less than 40 μm/h, and sometimes less than 30 μm/h, on substrates of specific stiffness (Figure 3.8A), suggesting that the migratory phenotype of *ex vivo* cells could be reverted with one week of plastic conditioning. Specifically, the MDA-MB-231 breast cancer cells moved most slowly on 23 and 48 kPa substrates and, similar to the *ex vivo* cells, had a slower average speed on glass (Figure 3.8A). These patterns of response to substrate stiffness were also visualized by the relative frequency distribution of the cell speeds (Figure 3.8B). The conditioning of cells explanted directly from the mouse brain was also observed in a second biological replicate (BR) isolated from a second cohort of mice (Figure S5). Together,

these results suggest that a mechanically soft environment (*in vivo* brain tissue or 1 kPa PDMS) primes a highly migratory phenotype that is maintained by cells that encounter a broad distribution of substrate stiffness encountered. In contrast, cells primed in a mechanically stiff environment can adjust migratory speed in response to a range of new substrate stiffness. Experiments are ongoing to assess the behavior of MDA-MB-231 breast cancer cells isolated directly from bone metastases (stiff tissue environment) relative to the phenotypes observed with MDA-MB-231 breast cancer cells isolated from brain tissue (soft tissue environment).

3.8 Biophysical conditioning modulates MDA-MB-231 cell degradative response to stiffness.

In addition to migratory responses, the activity of degradative invadopodia was tested for *in vivo* biophysically conditioned cells (Figure 3.7). In general, *ex vivo* MDA-MB-231 breast cancer cells had less invadopodia-mediated degradation than *ex vivo* plastic and plastic conditioned cells (Figure 3.9A). On glass substrates, *ex vivo* MDA-MB-231 breast cancer cells had much higher degradative activity compared on all substrates with a stiffness below that of glass (Figure 3.9 B, C). Thus, invadopodia activity was not completely diminished by *in vivo* brain tissue conditioning. Furthermore, the pattern of invadopodia response to stiffness under 3 MPa mimicked the degradative pattern discovered for the HCC1954, 2776 and 526 breast cancer models (Figure 3.5C, 3.6A, C, and 3.9B). In contrast, results from the *ex vivo* plastic and plastic conditioned breast cancer cells demonstrated large amounts of degradative activity, with similar numbers of actively degrading cells per FOV across the substrate stiffness range tested. The total surface area degraded for these cells had a large variance for each stiffness highlighting cell-to-cell variation (Figure 3.9B). This variance could also be attributed to moderate changes in substrate (gelatin/ligand) density. Density has the potential to fluctuate based on PDMS reactive group density (dependent on underlying PDMS stiffness) that could affect local gelatin concentration; however, this slight fluctuation does not directly alter the gelatin layer stiffness. Although Gelatin images suggest that the upper threshold of degradative activity was reached for active cells (indicated by large areas completely devoid of gelatin signal) (Figure 3.9A). These results suggest that cells exposed to the biophysical environment in brain tissue are only highly invasive on very stiff substrates but can be conditioned to degrade on a range of stiffness if conditioned on plastic dishes for one week. In fact, *ex vivo* cell conditioning on plastic for one week changed the cell degradative phenotype to

essentially match cells that had been serially passaged on stiff plastic dishes. Therefore, by measuring the degradative ability of these conditioned cells, we have confirmed that mechanical conditioning of MDA-MB-231 modulates the invasive phenotype of cells when presented with new substrate stiffness.

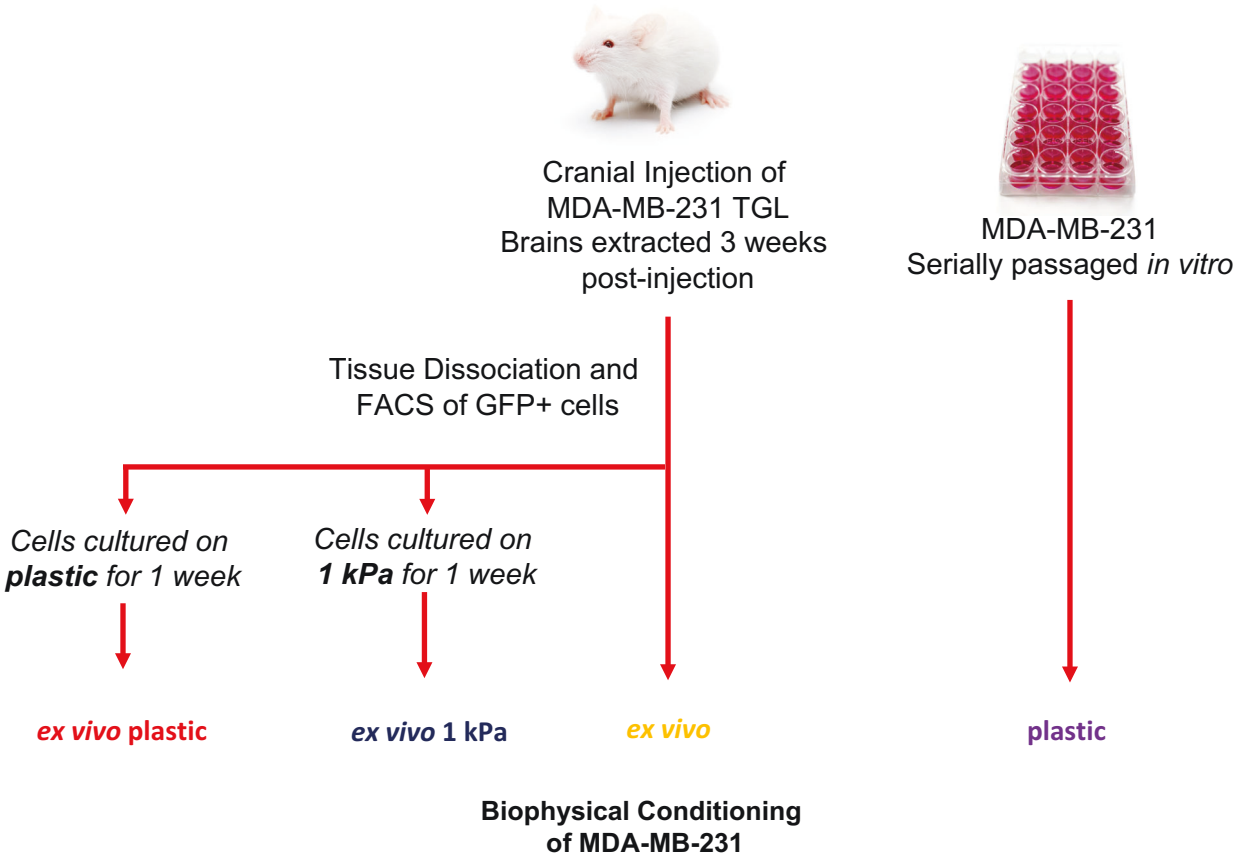

Figure 3.7 Experimental design for the biophysical conditioning of MDA-MB-231 cells. MDA-MB-231 TGL cells were cranially injected in NSG mice. Three weeks post-injection, mouse brains were extracted and the brain section containing tumour was dissociated in order to FACS isolate GFP+ MDA-MB-231 TGL. The *ex vivo* MDA-MB-231 cells were either directly plated on a PDMS substrate stiffness series for analysis (termed: *ex vivo*) or cultured on plastic (termed: *ex* vivo plastic) or 1 kPa PDMS (termed: *ex vivo* 1 kPa) substrate for one week prior to plating on the PDMS stiffness series for analysis. These represent three conditions of biophysical training. MDA-MB-231 serially cultured on plastic were used as a comparison for cell response to the PDMS stiffness series and are termed plastic. The PDMS stiffness series included 1 kPa, 23 kPa, 48 kPa, 100 kPa, and 3MPa. Glass was used as a control for stiffness. PDMS substrates used for analysis of single-cell migration and gelatin degradation were coated with fibronectin or 488-gelatin, respectively.

A

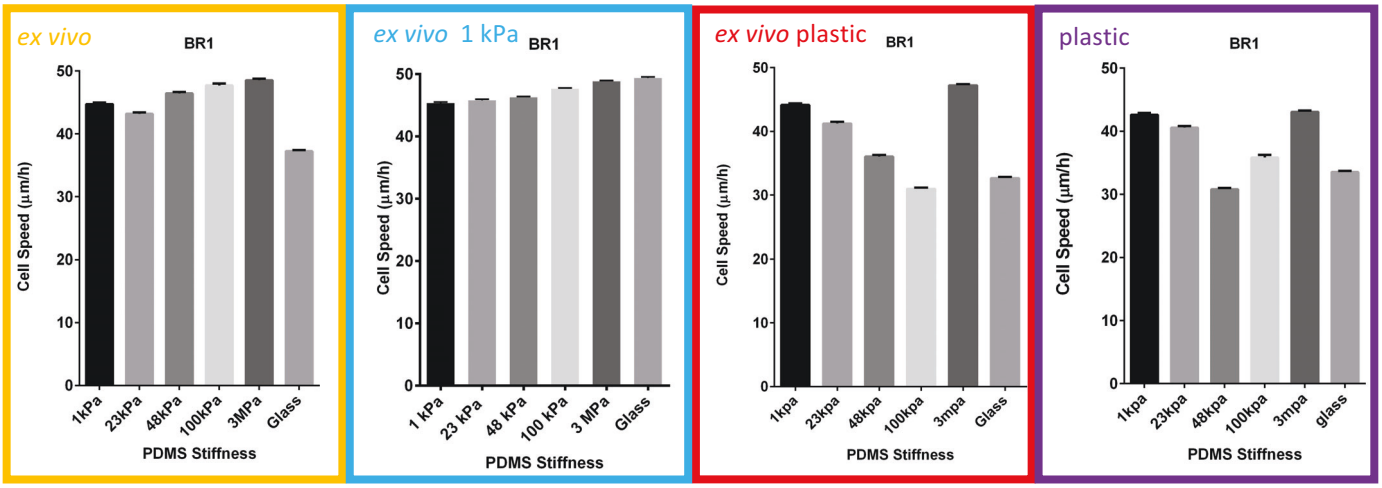
ex vivo
BR1
Cell Speed (µm/h)
1kPa
23kPa
48kPa
100kPa
3MPa
Glass
PDMS Stiffness
ex vivo 1 kPa
BR1
1 kPa
23 kPa
48 kPa
100 kPa
3 MPa
Glass
PDMS Stiffness
ex vivo plastic
BR1
1kpa
23kpa
48kpa
100kpa
3mpa
Glass
PDMS Stiffness
plastic
BR1
1kpa
23kpa
48kpa
100kpa
3mpa
glass
PDMS Stiffness

B

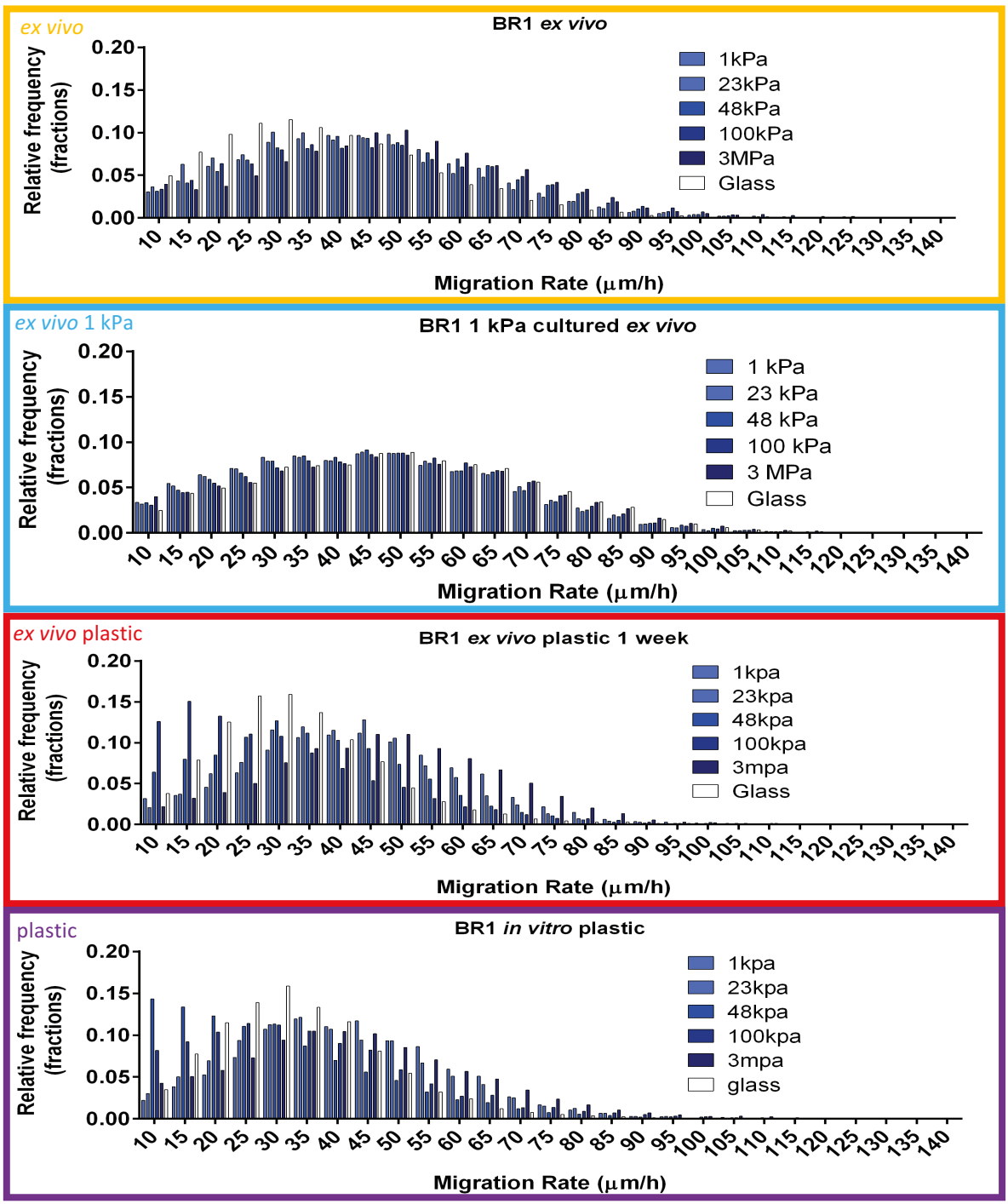
ex vivo
BR1 ex vivo
Relative frequency (fractions)
1kPa
23kPa
48kPa
100kPa
3MPa
Glass
Migration Rate (µm/h)
ex vivo 1 kPa
BR1 1 kPa cultured ex vivo
1 kPa
23 kPa
48 kPa
100 kPa
3 MPa
Glass
Migration Rate (µm/h)
ex vivo plastic
BR1 ex vivo plastic 1 week
1kpa
23kpa
48kpa
100kpa
3mpa
Glass
Migration Rate (µm/h)
plastic
BR1 in vitro plastic
1kpa
23kpa
48kpa
100kpa
3mpa
glass
Migration Rate (µm/h)

Figure 3.8 MDA-MB-231 cells regulate migration speed in response to stiffness based on biophysical conditioning. MDA-MB-231 *ex vivo* cells were taken either directly *ex vivo* from mouse brain tissue, or were cultured for one week on plastic or 1 kPa PDMS, and subsequently cultured on PDMS of different stiffness (*ex vivo* and *ex vivo* plastic, and *ex vivo* 1 kPa, respectively). The migration speed of these cells were compared to MDA-MB-231 serially cultured on plastic culture dishes (plastic) and placed on PDMS of different stiffness. **(A)** Average cell speed (μm/h) of MDA-MB-231 from distinct biophysical environments (*ex vivo*, *ex vivo* plastic, *ex vivo* 1 kPa and plastic) on PDMS of 1 kPa, 23 kPa, 48 kPa, 100 kPa, 3 MPa, and Glass (Gpa stiffness) coated with human fibronectin. **(B)** Frequency distribution of cell migration speed (A) with a bin size of 5 μm/h. One biological replicate represented with 93,597 *ex vivo* 1 kPa, 47,017 *ex vivo*, 43,908 *ex vivo* plastic, and 43,353 plastic cell tracks followed for calculation of cell speed.

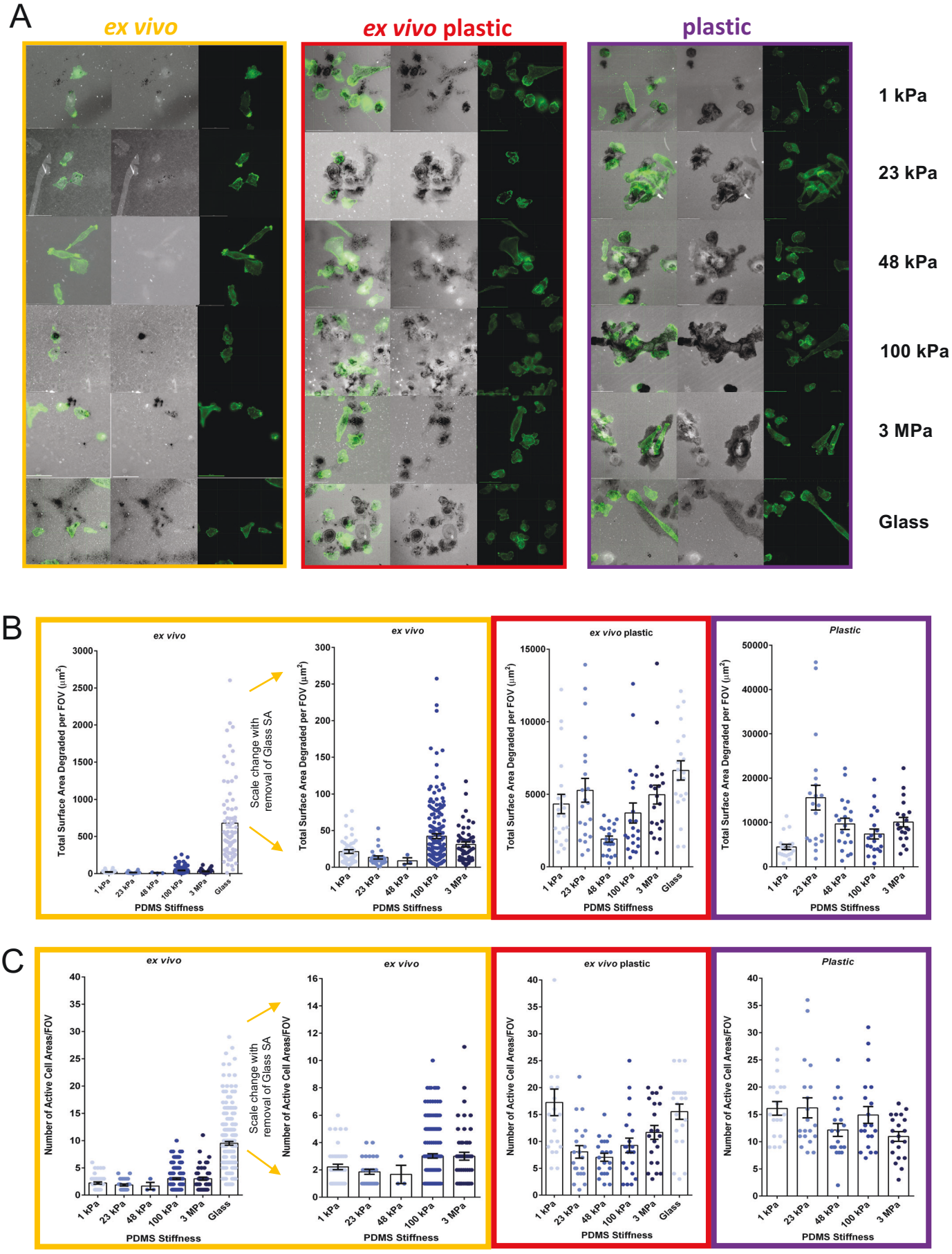
A
ex vivo
ex vivo plastic
plastic
1 kPa
23 kPa
48 kPa
100 kPa
3 MPa
Glass
B
ex vivo
ex vivo plastic
Plastic
Total Surface Area Degraded per FOV (μm²)
Scale change with removal of Glass SA
PDMS Stiffness
1 kPa
23 kPa
48 kPa
100 kPa
3 MPa
Glass
C
Number of Active Cell Areas/FOV

Figure 3.9 Biophysical conditioining modulates MDA-MB-231 cell degradative response to stiffness. MDA-MB-231 *ex vivo* cells were taken either directly *ex vivo* from mouse brain tissue, or were cultured for one week on plastic, and subsequently cultured on PDMS of different stiffness coated with 488-labeled gelatin (*ex vivo* and *ex vivo* plastic, respectively). Gelatin degradation of the *ex vivo* and *ex vivo* plastic cells was compared to MDA-MB-231 serially cultured on plastic (plastic) and placed on 488-gelatin-coated PDMS of different stiffness. **(A)** Representative images of 488-gelatin degradation by MDA-MB-231 from distinct biophysical environments (*ex vivo*, *ex vivo* plastic and plastic) on PDMS of 1 kPa, 23 kPa, 48 kPa, 100 kPa, 3 MPa, and Glass. Scale bar represents 50 μm. **(B)** 488-gelatin degradation of the cells was quantified by the Surface Area (SA) of the void in 488-gelatin signal. **(C)** The number of active cells in a given Field of View (FOV) were manually counted for each image quantified for surface area (B). One biological replicate represented with 321, 80, and 80 images quantified for SA and Number of Active Cell Areas/FOV for *ex vivo*, *ex vivo* plastic and plastic, respectively.

CHAPTER 4: DISCUSSION AND FUTURE DIRECTIONS

Proximity map of LPP within cellular adhesions

Migratory and invasive phenotypes of cancer cells rely on specific organization of the actin cytoskeleton. Thus far, we have demonstrated that LPP is a critical component of actin cytoskeleton regulation that mediates breast cancer metastasis[82, 83, 106]. However, the underlying mechanisms of this regulation are unknown.

A BioID approach was taken to elucidate details of this mechanism by identifying proteins within proximity of LPP at highly dynamic adhesions. The resulting protein interactome demonstrated that there is an enrichment of unique adhesion proteins for WT LPP (localized at highly dynamic adhesions) versus an α-actinin binding domain mutant LPP (localized at less dynamic adhesions) with TGFβ treatment. These proteins were prioritized for future functional validation by ranking the fold change in labeling from highest to lowest. Among the prioritized candidates are Kank1, Ppp2r2d (subunit of PP2A), Sorbs1 (CAP/Ponsin), Tns1 (Tensin 1), Pdlim7 (Enigma) and Trip6 (Thyroid Hormone Receptor Interactor 6). Kank1and Sorbs1 are adhesion proteins that exhibit force-dependent regulation within adhesions, while Ppp2r2d (a subunit of PP2A) has been studied as an interacting protein of LPP via LIM domain interaction[143, 202-204]. Tensin 1 is closely associated with integrins and interacts with a number of adhesion regulatory proteins such as Axl, EGFR, Src, FAK, p130Cas and Paxillin through SH2 and PTB domains[205, 206]. Another BioID candidate, PDLIM7 (also known as ENIGMA), is a cytoskeletal protein that has loosely been identified with adhesions by proteomics and is considered a mechanosensory protein that binds YAP to regulate nuclear localization [84, 207]. Additionally, Tabariès *et al*. (2019) implicated PDLIM7 in efficient breast cancer metastasis to the liver[208]. A zyxin family member, Thyroid Hormone Receptor Interactor 6, has also been localized to adhesions and functions in regulation of adhesion in concert with p130Cas[209]. The potential association of these proteins with LPP could involve direct, or indirect, binding recruitment through LIM domains or the variable regions on LPP[210]. Of note, multiple P-body and stress granule proteins were also identified (Pabpc4, Cpeb4, R3hdm1, Marf1, Dcp1a, Tnrc6a/b, and Cnot1). Interestingly, these cellular components are cytosolic and have not previously been reported in association with LPP, thus further investigation of potential association is needed.

To establish the functional relevance of the putative binding partners in adhesion dynamics, several *in vitro* assays will be employed. ShRNAs targeting each proximal protein of interest will

be expressed in 2776 cells; these cells will subsequently be assessed for phenocopy of LPP using single-cell migration speed in response to TGFβ. Furthermore, functional validation of binding partners *in vivo* using splenic injection and quantification of liver metastases will be needed (other cell models could be used for validation *in vivo* to test lung and liver spontaneous metastases). By functionally validating these candidate choices, we hope to better understand the LPP interactome, the key proteins involved in cancer progression, and what mechanisms LPP employs for regulation of cell migration. Use of a BioID approach with invadopodia isolation is a next step to separate LPP function at adhesion versus invadopodia structures.

To pursue this future direction, I generated NMuMG-ErbB2 cells expressing BirA fused to several phosphorylation mutants of LPP. These phosphorylation mutants could be used to parse an LPP interactome for invadopodia structures when paired with conditions that promote invadopodia formation. For example, an interactome comparison between BirA-LPP-WT and BirA-LPP-D (Y245F/Y301F/Y302F) would differentiate proteins present in invadopodia structures versus adhesions. The difficulty in pursuing these studies will be to enrich the MS sample with invadopodia structures, and thus, the number of proteins labeled while in invadopodia. This could be achieved either through invadopodia isolation (shearing of the perpendicular cell protrusion from a porous surface) or increasing the number of invadopodia by culturing cells on a substrate stiffness that induces the highest number of invadopodia during biotin treatment. Both methods would require testing to optimize the amount of protein isolated for MS experiments. If invadopodia-specific labeling can be enriched, then a proximity interactome of LPP within invadopodia could be generated. This would be the first invadopodia interactome generated using the BioID method and would have the potential to identify novel protein targets for involvement in cancer invasion.

We have established a potential interaction using a BioID approach that placed LPP in the same interactome as ShcA (p46/52 isoforms) (accepted JBC, E. Voorand author contributions, Kiepas *at al.* **The ShcA adaptor protein cooperates with LPP to mediate adhesion dynamics and invadopodia formation**). Using this BioID data, we have shown that LPP and ShcA cooperatively promote cell migration and adhesion dynamics. Moreover, a novel role for ShcA at invadopodia was discovered. Under TGFβ stimulation, invadopodia are formed in NMuMG-ErbB2 cells and with loss of ShcA expression, cells are no longer able to form invadopodia. Similar to LPP, this phenotype is also apparent with mutation of 3 key phosphorylation sites of ShcA

(Y239/Y240/Y313). These findings demonstrate potential functional cooperation between ShcA and LPP at both adhesions and invadopodia.

LPP in Triple-Negative breast cancer disease models

Compellingly, LPP overexpression is associated with worse overall survival across all breast cancer subtypes (Figure 4.1A). Thus far, the role of LPP in breast cancer metastasis has been established in Her2+ models[82, 83, 106]. We have since elucidated a similar role for LPP in TNBC. In the MDA-MB-231 and 4T1-2776 TN models, LPP regulates cell migration speed (data not shown) and invasion (Figure 4.1B, C) in response to TGFβ stimulation. Of note, TGFβ stimulation changes the appearance of the 4T1-derivative cell model degradative pattern from distinct invadopodia holes to larger areas of semi-degraded gelatin (Fig. 4.1E). This change in degradative pattern is partly reverted with LPP KD approaches (Fig. 4.1E) and may account for the discrepancy between the surface area degraded for the +/– TGFβ stimulation of the 4T1-2776 with LPP KD. The 4T1 parental cell line and 4T1-526 models recapitulate these migration responses and show similar trends in invasion with loss of LPP (data not shown). Regarding migration and invasion, each of these cell types increase migratory and degradative invadopodia formation in response to TGFβ stimulation. These results extend the model systems LPP is implicated in and demonstrates the influence of TGFβ on TNBCs.

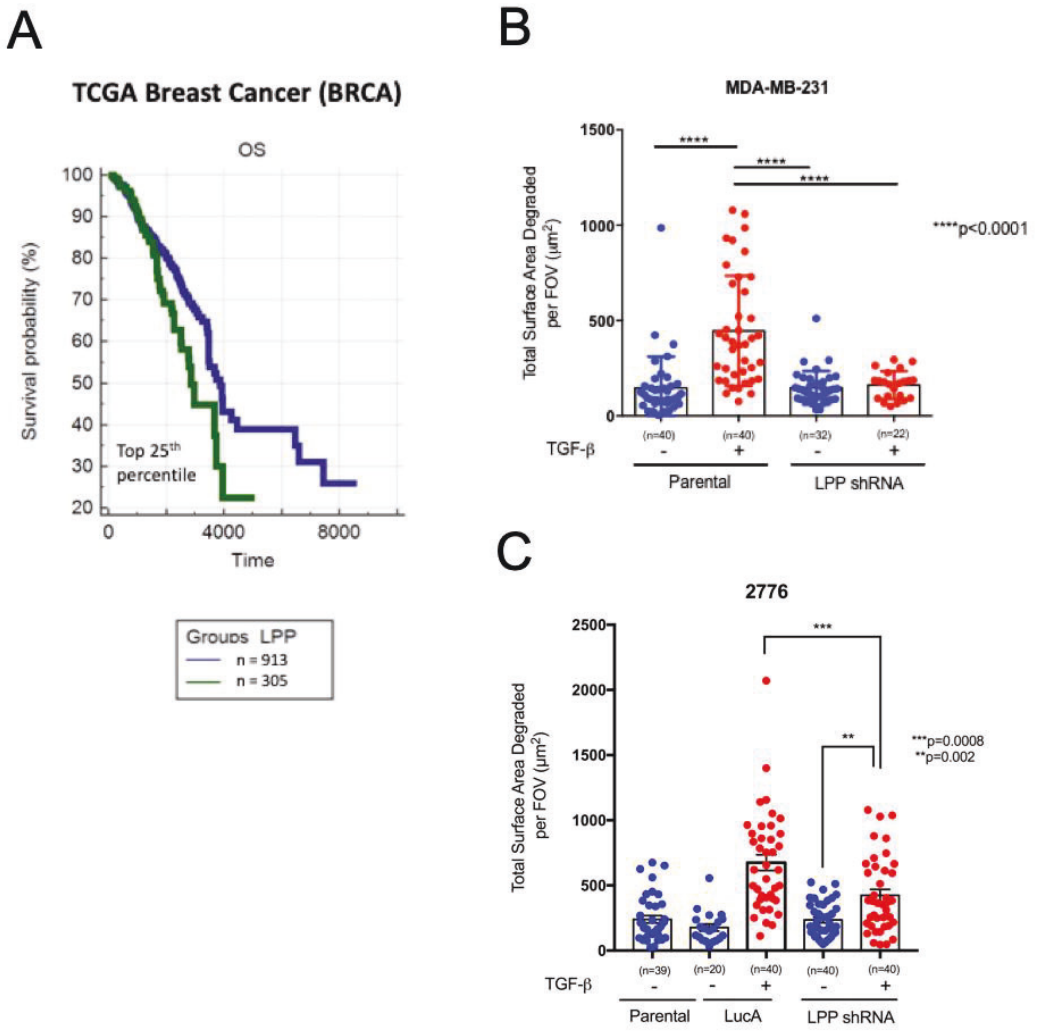

Figure 4.1 Implications of LPP expression in TNBC. **(A)** TCGA breast cancer data across all breast subtypes sorted by LPP expression determines overall patient survival (OS). **(B)** Degradative activity of MDA-MB-231 (n=138) and 2776 (n=179) **(C)** cells stimulated with TGFβ for 24 h and with shRNA against LPP (**, $P < 0.001$, ***, P<0.0008, ****, P<0.0001, two-tailed Student's *t*-test).

LPP is a mechanosensing protein

Tissue stiffness increases during breast cancer progression[159]. How cancer cells interpret increasing stiffness of the microenvironment to regulate migration and invasion is largely unexplored. To begin with, current biological studies have not comprehensively studied stiffness; often studies use the term "soft" and "hard" stiffness to interpret cell phenotypes, but the full range of stiffness experienced by cells *in vivo* have not been thoroughly studied[168, 211, 212]. To address this, we developed a platform to test cell phenotypes using PDMS. When coated with ECM, cell migratory and invasive responses were quantified. With this platform, we discovered that NMuMG-ErbB2 cells modulate cell speed according to underlying stiffness across a range of 100 kPa (Figure 4.2A). Our data suggests that on low and high stiffness, cells migrate slowly, likely due to ineffective traction forces on soft and hyperstabilization of adhesions on stiff (Figure 4.2A), similar to the classic biphasic model of fibroblast cell speed response to stiffness [162, 213-216]. These results suggest that cell speed is maximized around 40 kPa, an intermediate stiffness, and are distinct from MDA-MB-231 cell response to stiffness (Figure 3.8A, B). These discrepancies may be due to cell type-dependent responses. As suggested by Pathak *et. al*, the classical biphasic dependence on stiffness can be disrupted by cell types with higher force-generating ability or different number of receptors for force generation[217]. Therefore, further testing of multiple cell types would help assess potential cell-type dependency of mechanosensitivity to surfaces with different stiffnesses.

With the NMuMG-ErbB2 cell model, TGFβ treatment increases cell speed, but does not change the trend of relative response across stiffness (Figure 4.2A). These finding suggest there is an optimal range of stiffness for NMuMG-ErbB2 cell migration. Indeed, the results from testing HCC1954, 4T1-2776 and 4T1-526 breast cancer cell invadopodia activity aligns with the notion that an optimal range of stiffness also exists for invadopodia. These results are supported by previous studies that show MMP activity can be increased on soft matrices and breast carcinoma cells peak in activity on hard matrices[167, 218]. By profiling the migratory and invasive profile of several cell lines across a stiffness series, we have shown that multiple cancer cell types are capable of sensing many physiological stiffnesses and that some cell responses may be inherent to cancer cells.

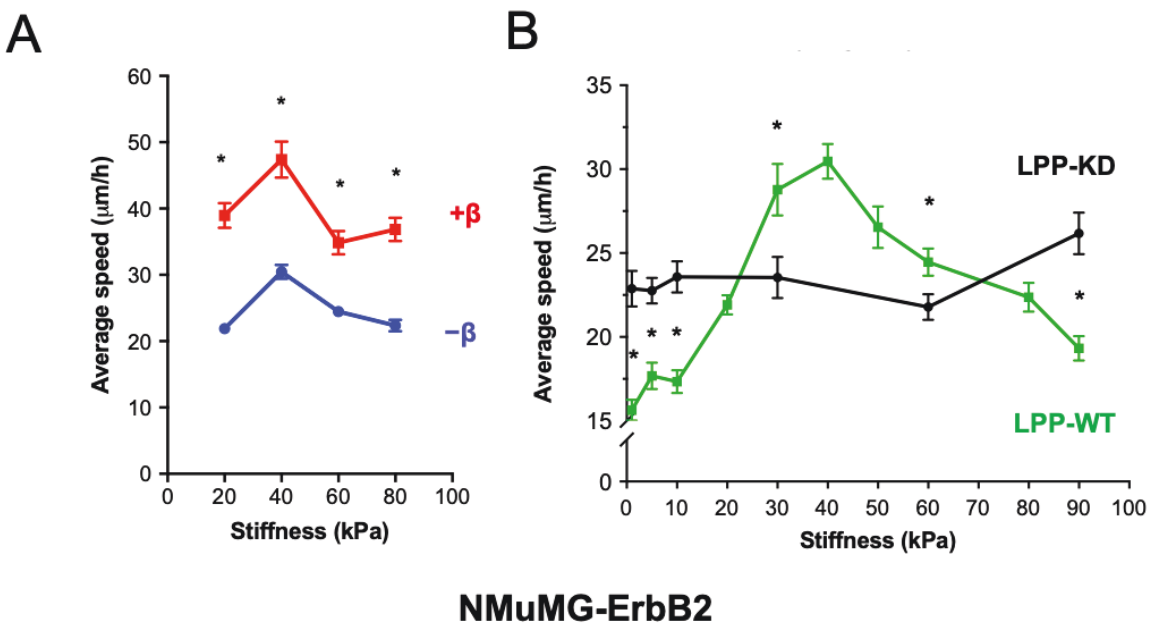

Figure 4.2 LPP is a mechanosensitive protein that regulates breast cancer cell migration in response to stiffness. **(A)** Average cell speed of NMuMG-ErbB2 on PDMS of different stiffness in the presence (red) or absence (blue) of TGFβ. **(B)** NMuMG-ErbB2 singe-cell tracking of cell speed on multiple stiffness. Both WT (green) and LPP KD (black) cells were tested. Data generated by Alex Kiepas. (*, P<0.05, two-tailed student's t-test).

LPP has been implicated as a mechanosensitive protein and our preliminary data suggests that LPP functions as a mechanoregulator. When LPP expression is reduced in NMuMG-ErbB2 cells, cells no longer modulate their speed in response to stiffness and maintain the same speed regardless of underlying stiffness (Figure 4.2B). With this data in mind, future studies will be directed to testing the pattern of invadopodia response with LPP KD of both Her2+ and TNBC models. Based on the BioID interactome, LPP has been placed next to several mechanosensing and mechanoregulatory proteins. Our hypothesis is that LPP may also act as a mechanoregulatory protein at invadopodia.

Biophysical conditioning of breast cancer cells *in vivo*

Breast cancer can metastasize to many different areas of the body with unique inherent tissue stiffness and biophysical (specifically, mechanical) properties. It is well studied that flexibility and adaptability of cancer cells is a means for cell survival in diverse and harsh environments during the metastatic process. With this in mind, we sought to test whether cancer

cell priming by mechanical cues alters cell adaptability to newly encountered stiffness cues, such as those encountered during primary tumour growth and metastasis. Our initial hypothesis was that, due to mechanical conditioning, cell migration and invasion would be maximized on surfaces that mimic the tissue stiffness cancer cells were extracted from. This hypothesis originated from the idea that cancer cells can adapt, and are even selected for survival and general fitness, at metastatic sites. From our observations, the migratory and invasive behavior of MDA-MB-231 cells encountering new stiffness is indeed altered by past stiffness priming, or conditioning, but contrary to our hypothesis, the migratory and invasive capacities were not maximized on the stiffness representing brain tissue. Instead of having maximal activity on 1 kPa, cells conditioned on a soft substrate had a unique pattern of response when compared to cells cultured on a stiff substrate.

Specifically, we have discovered that cells taken directly from soft mouse brain tissue (*ex vivo*) have a different pattern of behavior in comparison to cells serially cultured on stiff plastic. Moreover, the *ex vivo* pattern of migratory behavior can be either maintained or reverted with one week of culture on a stiffness mimicking brain tissue or cultured on stiff plastic, respectively. To note, the specific local stiffness experienced by the *in vivo* conditioned cells is unknown. Thus, phenotype heterogeneity was expected for the population of *ex vivo* cells, especially because *in vivo* conditioning involves many factors such as biochemical and cell-to-cell influence and communication. A future direction will be to control stiffness conditioning with cell culture on PDMS for extended periods of time. Moreover, comparison will be made to cells conditioned at other breast metastatic sites of distinct stiffness, such as bone, the liver and the mammary fat pad at several stiffnesses associated with different levels of tumour burden. It will be interesting to note whether the same pattern of response to a stiffness range will hold irrespective of site from which cancer cells are explanted from. Will the stiff environment of bone metastases condition a pattern of biophysical response unique from the soft conditioning in brain tissue? Mechanomemory may also impact how efficiently cells change the mode of migration used. For example, the switch between single-cell, collective or amoeboid migration could be studied to understand the impact of mechanical training.

Memory for biophysical environments has many implications for cancer metastasis. For example, priming of primary tumour cells in a stiff environment during disease progression could alter future cell migratory and invasive phenotypes; cells primed in a certain stiffness could have

selective advantage during seeding of a metastatic site; and priming could induce, for example via epigenetic regulation, other cell phenotypes associated with efficient metastasis, such as drug-resistance[219]. Therefore, the impact of mechanomemory on actin cytoskeleton structures is an important factor to consider and research.

Conclusions

With these experiments, we have shed light on the interactome of LPP at dynamic adhesions and explored the impact of substrate stiffness on cell migration and invasion. From the BioID of LPP, we can conclude that specific actin cytoskeleton proteins are enriched at highly dynamic adhesions with TGFβ treatment, including, Kank1, Sorbs1, Ppp2r2d, Pdlim7, Trip6 and Tns1. Furthermore, many of these identified proteins have mechano-sensory or -regulatory roles that may provide additional evidence to implicate LPP as a mechanoregulatory protein in complex. We have concluded from the studies of migration and invasion of breast cancer cells across a disease-relevant stiffness range that multiple breast cancer cell models have a distinct pattern of response. Specifically, on lower (<5 kPa) and higher (>90 kPa) stiffness, invadopodia-mediated invasion is most active. Breast cancer cell models were also shown to be sensitive to a large range of stiffness. Most interestingly, we have shown that the activity of adhesion and invadopodia actin cytoskeleton structures has been changed with biophysical conditioning, such that cells have memory for culture at a specific stiffness. From these observations, we have concluded that *ex vivo* brain cells and 1 kPa conditioned cells have a highly migratory phenotype, while cells taken *ex vivo* and conditioned on plastic or serially cultured on plastic have a more invasive phenotype when introduced to new stiffness. Collectively, in this thesis I have sought to understand the mechanisms regulating cell adhesions and invadopodia at both the protein level and biophysical level in the context of breast cancer metastasis.

REFERENCES

1. Committee, C.C.S.S.A., *Canadian Cancer Statistics 2019*. 2019: Toronto, ON: Canadian Cancer Society.
2. Cancer, W.H.O.I.A.f.R.o., *Latest Global Cancer Data: Cancer burden rises to 18.1 million new cases and 9.6 million cancer deaths in 2018*. 2018.
3. Sorlie, T., et al., *Gene expression patterns of breast carcinomas distinguish tumor subclasses with clinical implications.* Proc Natl Acad Sci U S A, 2001. **98**(19): p. 10869-74.
4. Sorlie, T., et al., *Repeated observation of breast tumor subtypes in independent gene expression data sets.* Proc Natl Acad Sci U S A, 2003. **100**(14): p. 8418-23.
5. Prat, A., et al., *Phenotypic and molecular characterization of the claudin-low intrinsic subtype of breast cancer.* Breast Cancer Res, 2010. **12**(5): p. R68.
6. Ali, H.R., et al., *Genome-driven integrated classification of breast cancer validated in over 7,500 samples.* Genome Biol, 2014. **15**(8): p. 431.
7. Curtis, C., et al., *The genomic and transcriptomic architecture of 2,000 breast tumours reveals novel subgroups.* Nature, 2012. **486**(7403): p. 346-52.
8. Holm, K., et al., *Molecular subtypes of breast cancer are associated with characteristic DNA methylation patterns.* Breast Cancer Res, 2010. **12**(3): p. R36.
9. Ronneberg, J.A., et al., *Methylation profiling with a panel of cancer related genes: association with estrogen receptor, TP53 mutation status and expression subtypes in sporadic breast cancer.* Mol Oncol, 2011. **5**(1): p. 61-76.
10. Szyf, M., *DNA methylation signatures for breast cancer classification and prognosis.* Genome Med, 2012. **4**(3): p. 26.
11. Wang, Y., et al., *Clonal evolution in breast cancer revealed by single nucleus genome sequencing.* Nature, 2014. **512**(7513): p. 155-60.
12. Beca, F. and K. Polyak, *Intratumor Heterogeneity in Breast Cancer.* Adv Exp Med Biol, 2016. **882**: p. 169-89.
13. Turashvili, G. and E. Brogi, *Tumor Heterogeneity in Breast Cancer.* Front Med (Lausanne), 2017. **4**: p. 227.

14. Holbro, T. and N.E. Hynes, *ErbB receptors: directing key signaling networks throughout life.* Annu Rev Pharmacol Toxicol, 2004. **44**: p. 195-217.
15. Yarden, Y. and M.X. Sliwkowski, *Untangling the ErbB signalling network.* Nat Rev Mol Cell Biol, 2001. **2**(2): p. 127-37.
16. Dankort, D., et al., *Multiple ErbB-2/Neu Phosphorylation Sites Mediate Transformation through Distinct Effector Proteins.* J Biol Chem, 2001. **276**(42): p. 38921-8.
17. Dankort, D., et al., *Grb2 and Shc adapter proteins play distinct roles in Neu (ErbB-2)-induced mammary tumorigenesis: implications for human breast cancer.* Mol Cell Biol, 2001. **21**(5): p. 1540-51.
18. Jones, R.B., et al., *A quantitative protein interaction network for the ErbB receptors using protein microarrays.* Nature, 2006. **439**(7073): p. 168-74.
19. Lemmon, M.A., *Ligand-induced ErbB receptor dimerization.* Exp Cell Res, 2009. **315**(4): p. 638-48.
20. Olayioye, M.A., et al., *The ErbB signaling network: receptor heterodimerization in development and cancer.* EMBO J, 2000. **19**(13): p. 3159-67.
21. Garrett, T.P., et al., *The crystal structure of a truncated ErbB2 ectodomain reveals an active conformation, poised to interact with other ErbB receptors.* Mol Cell, 2003. **11**(2): p. 495-505.
22. Slamon, D.J., et al., *Human breast cancer: correlation of relapse and survival with amplification of the HER-2/neu oncogene.* Science, 1987. **235**(4785): p. 177-82.
23. Slamon, D.J., et al., *Studies of the HER-2/neu proto-oncogene in human breast and ovarian cancer.* Science, 1989. **244**(4905): p. 707-12.
24. Bargmann, C.I., M.C. Hung, and R.A. Weinberg, *Multiple independent activations of the neu oncogene by a point mutation altering the transmembrane domain of p185.* Cell, 1986. **45**(5): p. 649-57.
25. Ursini-Siegel, J., et al., *Insights from transgenic mouse models of ERBB2-induced breast cancer.* Nat Rev Cancer, 2007. **7**(5): p. 389-97.
26. Guy, C.T., R.D. Cardiff, and W.J. Muller, *Activated neu induces rapid tumor progression.* J Biol Chem, 1996. **271**(13): p. 7673-8.
27. Muller, W.J., et al., *Single-step induction of mammary adenocarcinoma in transgenic mice bearing the activated c-neu oncogene.* Cell, 1988. **54**(1): p. 105-15.

28. Siegel, P.M., et al., *Novel activating mutations in the neu proto-oncogene involved in induction of mammary tumors.* Mol Cell Biol, 1994. **14**(11): p. 7068-77.
29. Siegel, P.M. and W.J. Muller, *Mutations affecting conserved cysteine residues within the extracellular domain of Neu promote receptor dimerization and activation.* Proc Natl Acad Sci U S A, 1996. **93**(17): p. 8878-83.
30. Siegel, P.M., et al., *Elevated expression of activated forms of Neu/ErbB-2 and ErbB-3 are involved in the induction of mammary tumors in transgenic mice: implications for human breast cancer.* EMBO J, 1999. **18**(8): p. 2149-64.
31. Shi, Y. and J. Massague, *Mechanisms of TGF-beta signaling from cell membrane to the nucleus.* Cell, 2003. **113**(6): p. 685-700.
32. Zhang, Y.E., *Non-Smad pathways in TGF-beta signaling.* Cell Res, 2009. **19**(1): p. 128-39.
33. Rahimi, R.A. and E.B. Leof, *TGF-beta signaling: a tale of two responses.* J Cell Biochem, 2007. **102**(3): p. 593-608.
34. Muraoka, R.S., et al., *Blockade of TGF-beta inhibits mammary tumor cell viability, migration, and metastases.* J Clin Invest, 2002. **109**(12): p. 1551-9.
35. Giampieri, S., et al., *Localized and reversible TGFbeta signalling switches breast cancer cells from cohesive to single cell motility.* Nat Cell Biol, 2009. **11**(11): p. 1287-96.
36. Padua, D. and J. Massague, *Roles of TGFbeta in metastasis.* Cell Res, 2009. **19**(1): p. 89-102.
37. Tian, M., J.R. Neil, and W.P. Schiemann, *Transforming growth factor-beta and the hallmarks of cancer.* Cell Signal, 2011. **23**(6): p. 951-62.
38. Wang, S.E., et al., *Transforming growth factor beta engages TACE and ErbB3 to activate phosphatidylinositol-3 kinase/Akt in ErbB2-overexpressing breast cancer and desensitizes cells to trastuzumab.* Mol Cell Biol, 2008. **28**(18): p. 5605-20.
39. Massague, J., S.W. Blain, and R.S. Lo, *TGFbeta signaling in growth control, cancer, and heritable disorders.* Cell, 2000. **103**(2): p. 295-309.
40. de Caestecker, M.P., E. Piek, and A.B. Roberts, *Role of transforming growth factor-beta signaling in cancer.* J Natl Cancer Inst, 2000. **92**(17): p. 1388-402.
41. Blobe, G.C., W.P. Schiemann, and H.F. Lodish, *Role of transforming growth factor beta in human disease.* N Engl J Med, 2000. **342**(18): p. 1350-8.

42. Wang, S.E., et al., *Transforming growth factor beta induces clustering of HER2 and integrins by activating Src-focal adhesion kinase and receptor association to the cytoskeleton.* Cancer Res, 2009. **69**(2): p. 475-82.
43. Northey, J.J., et al., *Signaling through ShcA is required for transforming growth factor beta- and Neu/ErbB-2-induced breast cancer cell motility and invasion.* Mol Cell Biol, 2008. **28**(10): p. 3162-76.
44. Northey, J.J., et al., *Distinct phosphotyrosine-dependent functions of the ShcA adaptor protein are required for transforming growth factor beta (TGFbeta)-induced breast cancer cell migration, invasion, and metastasis.* J Biol Chem, 2013. **288**(7): p. 5210-22.
45. Seton-Rogers, S.E., et al., *Cooperation of the ErbB2 receptor and transforming growth factor beta in induction of migration and invasion in mammary epithelial cells.* Proc Natl Acad Sci U S A, 2004. **101**(5): p. 1257-62.
46. Ueda, Y., et al., *Overexpression of HER2 (erbB2) in human breast epithelial cells unmasks transforming growth factor beta-induced cell motility.* J Biol Chem, 2004. **279**(23): p. 24505-13.
47. Siegel, P.M., et al., *Transforming growth factor beta signaling impairs Neu-induced mammary tumorigenesis while promoting pulmonary metastasis.* Proc Natl Acad Sci U S A, 2003. **100**(14): p. 8430-5.
48. Muraoka, R.S., et al., *Increased malignancy of Neu-induced mammary tumors overexpressing active transforming growth factor beta1.* Mol Cell Biol, 2003. **23**(23): p. 8691-703.
49. Siegel, R.L., K.D. Miller, and A. Jemal, *Cancer statistics, 2015.* CA Cancer J Clin, 2015. **65**(1): p. 5-29.
50. Valastyan, S. and R.A. Weinberg, *Tumor metastasis: molecular insights and evolving paradigms.* Cell, 2011. **147**(2): p. 275-92.
51. Klein, C.A., *Parallel progression of primary tumours and metastases.* Nat Rev Cancer, 2009. **9**(4): p. 302-12.
52. Yates, L.R., et al., *Genomic Evolution of Breast Cancer Metastasis and Relapse.* Cancer Cell, 2017. **32**(2): p. 169-184 e7.
53. Society, A.C., *Survival rates for breast cancer*.

54. Clark, A.G. and D.M. Vignjevic, *Modes of cancer cell invasion and the role of the microenvironment.* Curr Opin Cell Biol, 2015. **36**: p. 13-22.
55. Yamaguchi, H. and J. Condeelis, *Regulation of the actin cytoskeleton in cancer cell migration and invasion.* Biochim Biophys Acta, 2007. **1773**(5): p. 642-52.
56. Blouw, B., et al., *The invadopodia scaffold protein Tks5 is required for the growth of human breast cancer cells in vitro and in vivo.* PLoS One, 2015. **10**(3): p. e0121003.
57. Bowden, E.T., et al., *An invasion-related complex of cortactin, paxillin and PKCmu associates with invadopodia at sites of extracellular matrix degradation.* Oncogene, 1999. **18**(31): p. 4440-9.
58. Provenzano, P.P. and P.J. Keely, *The role of focal adhesion kinase in tumor initiation and progression.* Cell Adh Migr, 2009. **3**(4): p. 347-50.
59. Horwitz, R. and D. Webb, *Cell migration.* Curr Biol, 2003. **13**(19): p. R756-9.
60. Mayor, R. and S. Etienne-Manneville, *The front and rear of collective cell migration.* Nat Rev Mol Cell Biol, 2016. **17**(2): p. 97-109.
61. Wang, W., et al., *Single cell behavior in metastatic primary mammary tumors correlated with gene expression patterns revealed by molecular profiling.* Cancer Res, 2002. **62**(21): p. 6278-88.
62. Ahmed, F., et al., *GFP expression in the mammary gland for imaging of mammary tumor cells in transgenic mice.* Cancer Res, 2002. **62**(24): p. 7166-9.
63. Ewald, A.J., *Pulling cells out of tumours.* Nat Cell Biol, 2017. **19**(3): p. 147-149.
64. Condeelis, J. and J.E. Segall, *Intravital imaging of cell movement in tumours.* Nat Rev Cancer, 2003. **3**(12): p. 921-30.
65. Sahai, E., *Mechanisms of cancer cell invasion.* Curr Opin Genet Dev, 2005. **15**(1): p. 87-96.
66. Thiery, J.P., *Epithelial-mesenchymal transitions in tumour progression.* Nat Rev Cancer, 2002. **2**(6): p. 442-54.
67. Friedl, P. and K. Wolf, *Tumour-cell invasion and migration: diversity and escape mechanisms.* Nat Rev Cancer, 2003. **3**(5): p. 362-74.
68. Eddy, R.J., et al., *Tumor Cell Invadopodia: Invasive Protrusions that Orchestrate Metastasis.* Trends Cell Biol, 2017. **27**(8): p. 595-607.

69. Murphy, D.A. and S.A. Courtneidge, *The 'ins' and 'outs' of podosomes and invadopodia: characteristics, formation and function.* Nat Rev Mol Cell Biol, 2011. **12**(7): p. 413-26.
70. Lohmer, L.L., et al., *Invadopodia and basement membrane invasion in vivo.* Cell Adh Migr, 2014. **8**(3): p. 246-55.
71. Leong, H.S., et al., *Invadopodia are required for cancer cell extravasation and are a therapeutic target for metastasis.* Cell Rep, 2014. **8**(5): p. 1558-70.
72. Gligorijevic, B., et al., *N-WASP-mediated invadopodium formation is involved in intravasation and lung metastasis of mammary tumors.* J Cell Sci, 2012. **125**(Pt 3): p. 724-34.
73. Eckert, M.A. and J. Yang, *Targeting invadopodia to block breast cancer metastasis.* Oncotarget, 2011. **2**(7): p. 562-8.
74. Zaidel-Bar, R., et al., *Functional atlas of the integrin adhesome.* Nat Cell Biol, 2007. **9**(8): p. 858-67.
75. Geiger, B. and K.M. Yamada, *Molecular architecture and function of matrix adhesions.* Cold Spring Harb Perspect Biol, 2011. **3**(5).
76. Mitra, S.K., D.A. Hanson, and D.D. Schlaepfer, *Focal adhesion kinase: in command and control of cell motility.* Nat Rev Mol Cell Biol, 2005. **6**(1): p. 56-68.
77. Mitra, S.K. and D.D. Schlaepfer, *Integrin-regulated FAK-Src signaling in normal and cancer cells.* Curr Opin Cell Biol, 2006. **18**(5): p. 516-23.
78. Alexandrova, A.Y., et al., *Comparative dynamics of retrograde actin flow and focal adhesions: formation of nascent adhesions triggers transition from fast to slow flow.* PLoS One, 2008. **3**(9): p. e3234.
79. Wendt, M.K. and W.P. Schiemann, *Therapeutic targeting of the focal adhesion complex prevents oncogenic TGF-beta signaling and metastasis.* Breast Cancer Res, 2009. **11**(5): p. R68.
80. Sulzmaier, F.J., C. Jean, and D.D. Schlaepfer, *FAK in cancer: mechanistic findings and clinical applications.* Nat Rev Cancer, 2014. **14**(9): p. 598-610.
81. Xue, C., et al., *Epidermal growth factor receptor overexpression results in increased tumor cell motility in vivo coordinately with enhanced intravasation and metastasis.* Cancer Res, 2006. **66**(1): p. 192-7.

82. Ngan, E., et al., *A complex containing LPP and alpha-actinin mediates TGFbeta-induced migration and invasion of ErbB2-expressing breast cancer cells.* J Cell Sci, 2013. **126**(Pt 9): p. 1981-91.
83. Ngan, E., et al., *LPP is a Src substrate required for invadopodia formation and efficient breast cancer lung metastasis.* Nat Commun, 2017. **8**: p. 15059.
84. Byron, A. and M.C. Frame, *Adhesion protein networks reveal functions proximal and distal to cell-matrix contacts.* Curr Opin Cell Biol, 2016. **39**: p. 93-100.
85. Mueller, S.C., et al., *A novel protease-docking function of integrin at invadopodia.* J Biol Chem, 1999. **274**(35): p. 24947-52.
86. Albiges-Rizo, C., et al., *Actin machinery and mechanosensitivity in invadopodia, podosomes and focal adhesions.* J Cell Sci, 2009. **122**(Pt 17): p. 3037-49.
87. Lochter, A., et al., *The significance of matrix metalloproteinases during early stages of tumor progression.* Ann N Y Acad Sci, 1998. **857**: p. 180-93.
88. Wagenaar-Miller, R.A., L. Gorden, and L.M. Matrisian, *Matrix metalloproteinases in colorectal cancer: is it worth talking about?* Cancer Metastasis Rev, 2004. **23**(1-2): p. 119-35.
89. Ala-aho, R. and V.M. Kahari, *Collagenases in cancer.* Biochimie, 2005. **87**(3-4): p. 273-86.
90. Bjorklund, M. and E. Koivunen, *Gelatinase-mediated migration and invasion of cancer cells.* Biochim Biophys Acta, 2005. **1755**(1): p. 37-69.
91. Clark, E.S. and A.M. Weaver, *A new role for cortactin in invadopodia: regulation of protease secretion.* Eur J Cell Biol, 2008. **87**(8-9): p. 581-90.
92. Balzer, E.M., et al., *c-Src differentially regulates the functions of microtentacles and invadopodia.* Oncogene, 2010. **29**(48): p. 6402-8.
93. Bowden, E.T., et al., *Co-localization of cortactin and phosphotyrosine identifies active invadopodia in human breast cancer cells.* Exp Cell Res, 2006. **312**(8): p. 1240-53.
94. Artym, V.V., et al., *Dynamic interactions of cortactin and membrane type 1 matrix metalloproteinase at invadopodia: defining the stages of invadopodia formation and function.* Cancer Res, 2006. **66**(6): p. 3034-43.
95. Petit, M.M., et al., *LPP, the preferred fusion partner gene of HMGIC in lipomas, is a novel member of the LIM protein gene family.* Genomics, 1996. **36**(1): p. 118-29.

96. Gorenne, I., et al., *LPP, a LIM protein highly expressed in smooth muscle.* Am J Physiol Cell Physiol, 2003. **285**(3): p. C674-85.
97. Macalma, T., et al., *Molecular characterization of human zyxin.* J Biol Chem, 1996. **271**(49): p. 31470-8.
98. Grunewald, T.G. and E. Butt, *The LIM and SH3 domain protein family: structural proteins or signal transducers or both?* Mol Cancer, 2008. **7**: p. 31.
99. Hirata, H., H. Tatsumi, and M. Sokabe, *Mechanical forces facilitate actin polymerization at focal adhesions in a zyxin-dependent manner.* J Cell Sci, 2008. **121**(Pt 17): p. 2795-804.
100. Hirata, H., H. Tatsumi, and M. Sokabe, *Zyxin emerges as a key player in the mechanotransduction at cell adhesive structures.* Commun Integr Biol, 2008. **1**(2): p. 192-5.
101. Willier, S., et al., *Defining the role of TRIP6 in cell physiology and cancer.* Biol Cell, 2011. **103**(12): p. 573-91.
102. Wu, C., *Migfilin and its binding partners: from cell biology to human diseases.* J Cell Sci, 2005. **118**(Pt 4): p. 659-64.
103. Grunewald, T.G., S.M. Pasedag, and E. Butt, *Cell Adhesion and Transcriptional Activity - Defining the Role of the Novel Protooncogene LPP.* Transl Oncol, 2009. **2**(3): p. 107-16.
104. Petit, M.M., et al., *LPP, an actin cytoskeleton protein related to zyxin, harbors a nuclear export signal and transcriptional activation capacity.* Mol Biol Cell, 2000. **11**(1): p. 117-29.
105. Petit, M.M., S.M. Meulemans, and W.J. Van de Ven, *The focal adhesion and nuclear targeting capacity of the LIM-containing lipoma-preferred partner (LPP) protein.* J Biol Chem, 2003. **278**(4): p. 2157-68.
106. Ngan, E., et al., *Emerging roles for LPP in metastatic cancer progression.* J Cell Commun Signal, 2018. **12**(1): p. 143-156.
107. Wehland, J., M. Osborn, and K. Weber, *Cell-to-substratum contacts in living cells: a direct correlation between interference-reflexion and indirect-immunofluorescence microscopy using antibodies against actin and alpha-actinin.* J Cell Sci, 1979. **37**: p. 257-73.

108. Hirooka, S., et al., *Localization of the invadopodia-related proteins actinin-1 and cortactin to matrix-contact-side cytoplasm of cancer cells in surgically resected lung adenocarcinomas.* Pathobiology, 2011. **78**(1): p. 10-23.
109. Hansen, S.D. and R.D. Mullins, *VASP is a processive actin polymerase that requires monomeric actin for barbed end association.* J Cell Biol, 2010. **191**(3): p. 571-84.
110. Krause, M., et al., *The Ena/VASP enigma.* J Cell Sci, 2002. **115**(Pt 24): p. 4721-6.
111. Knight, B., et al., *Visualizing muscle cell migration in situ.* Curr Biol, 2000. **10**(10): p. 576-85.
112. Langanger, G., et al., *Ultrastructural localization of alpha-actinin and filamin in cultured cells with the immunogold staining (IGS) method.* J Cell Biol, 1984. **99**(4 Pt 1): p. 1324-34.
113. Xue, F., D.M. Janzen, and D.A. Knecht, *Contribution of Filopodia to Cell Migration: A Mechanical Link between Protrusion and Contraction.* Int J Cell Biol, 2010. **2010**: p. 507821.
114. Feramisco, J.R., *Microinjection of fluorescently labeled alpha-actinin into living fibroblasts.* Proc Natl Acad Sci U S A, 1979. **76**(8): p. 3967-71.
115. Le Clainche, C. and M.F. Carlier, *Regulation of actin assembly associated with protrusion and adhesion in cell migration.* Physiol Rev, 2008. **88**(2): p. 489-513.
116. Choi, C.K., et al., *Actin and alpha-actinin orchestrate the assembly and maturation of nascent adhesions in a myosin II motor-independent manner.* Nat Cell Biol, 2008. **10**(9): p. 1039-50.
117. Honda, K., *The biological role of actinin-4 (ACTN4) in malignant phenotypes of cancer.* Cell Biosci, 2015. **5**: p. 41.
118. Li, B., et al., *The lipoma preferred partner LPP interacts with alpha-actinin.* J Cell Sci, 2003. **116**(Pt 7): p. 1359-66.
119. Keicher, C., et al., *Phosphorylation of mouse LASP-1 on threonine 156 by cAMP- and cGMP-dependent protein kinase.* Biochem Biophys Res Commun, 2004. **324**(1): p. 308-16.
120. Zhang, H., et al., *Lasp1 gene disruption is linked to enhanced cell migration and tumor formation.* Physiol Genomics, 2009. **38**(3): p. 372-85.

121. Goicoechea, S.M., D. Arneman, and C.A. Otey, *The role of palladin in actin organization and cell motility.* Eur J Cell Biol, 2008. **87**(8-9): p. 517-25.
122. Jin, L., et al., *Angiotensin II, focal adhesion kinase, and PRX1 enhance smooth muscle expression of lipoma preferred partner and its newly identified binding partner palladin to promote cell migration.* Circ Res, 2007. **100**(6): p. 817-25.
123. Otey, C.A., et al., *The palladin/myotilin/myopalladin family of actin-associated scaffolds.* Int Rev Cytol, 2005. **246**: p. 31-58.
124. Parast, M.M. and C.A. Otey, *Characterization of palladin, a novel protein localized to stress fibers and cell adhesions.* J Cell Biol, 2000. **150**(3): p. 643-56.
125. Petit, M.M., et al., *The tumor suppressor Scrib selectively interacts with specific members of the zyxin family of proteins.* FEBS Lett, 2005. **579**(22): p. 5061-8.
126. Pearson, H.B., et al., *The polarity protein Scrib mediates epidermal development and exerts a tumor suppressive function during skin carcinogenesis.* Mol Cancer, 2015. **14**: p. 169.
127. Elsum, I.A., et al., *Scrib heterozygosity predisposes to lung cancer and cooperates with KRas hyperactivation to accelerate lung cancer progression in vivo.* Oncogene, 2014. **33**(48): p. 5523-33.
128. Pearson, H.B., et al., *SCRIB expression is deregulated in human prostate cancer, and its deficiency in mice promotes prostate neoplasia.* J Clin Invest, 2011. **121**(11): p. 4257-67.
129. Feigin, M.E., et al., *Mislocalization of the cell polarity protein scribble promotes mammary tumorigenesis and is associated with basal breast cancer.* Cancer Res, 2014. **74**(11): p. 3180-94.
130. Anastas, J.N., et al., *A protein complex of SCRIB, NOS1AP and VANGL1 regulates cell polarity and migration, and is associated with breast cancer progression.* Oncogene, 2012. **31**(32): p. 3696-708.
131. Savi, F., et al., *miR-296/Scribble axis is deregulated in human breast cancer and miR-296 restoration reduces tumour growth in vivo.* Clin Sci (Lond), 2014. **127**(4): p. 233-42.
132. Takizawa, N., et al., *Supervillin modulation of focal adhesions involving TRIP6/ZRP-1.* J Cell Biol, 2006. **174**(3): p. 447-58.
133. Crowley, J.L., et al., *Supervillin reorganizes the actin cytoskeleton and increases invadopodial efficiency.* Mol Biol Cell, 2009. **20**(3): p. 948-62.

134. Bhuwania, R., et al., *Supervillin couples myosin-dependent contractility to podosomes and enables their turnover.* J Cell Sci, 2012. **125**(Pt 9): p. 2300-14.
135. Silacci, P., et al., *Gelsolin superfamily proteins: key regulators of cellular functions.* Cell Mol Life Sci, 2004. **61**(19-20): p. 2614-23.
136. Reinhard, M., T. Jarchau, and U. Walter, *Actin-based motility: stop and go with Ena/VASP proteins.* Trends Biochem Sci, 2001. **26**(4): p. 243-9.
137. Holt, M.R., D.R. Critchley, and N.P. Brindle, *The focal adhesion phosphoprotein, VASP.* Int J Biochem Cell Biol, 1998. **30**(3): p. 307-11.
138. Krause, M., et al., *Ena/VASP proteins: regulators of the actin cytoskeleton and cell migration.* Annu Rev Cell Dev Biol, 2003. **19**: p. 541-64.
139. Kwiatkowski, A.V., F.B. Gertler, and J.J. Loureiro, *Function and regulation of Ena/VASP proteins.* Trends Cell Biol, 2003. **13**(7): p. 386-92.
140. Philippar, U., et al., *A Mena invasion isoform potentiates EGF-induced carcinoma cell invasion and metastasis.* Dev Cell, 2008. **15**(6): p. 813-28.
141. Toyoda, A., et al., *Aberrant expression of human ortholog of mammalian enabled (hMena) in human colorectal carcinomas: implications for its role in tumor progression.* Int J Oncol, 2009. **34**(1): p. 53-60.
142. Dertsiz, L., et al., *Differential expression of VASP in normal lung tissue and lung adenocarcinomas.* Thorax, 2005. **60**(7): p. 576-81.
143. Janssens, V., et al., *PP2A binds to the LIM domains of lipoma-preferred partner through its PR130/B'' subunit to regulate cell adhesion and migration.* J Cell Sci, 2016. **129**(8): p. 1605-18.
144. Smith, M.A., et al., *LIM domains target actin regulators paxillin and zyxin to sites of stress fiber strain.* PLoS One, 2013. **8**(8): p. e69378.
145. Hoffman, L.M., et al., *Stretch-induced actin remodeling requires targeting of zyxin to stress fibers and recruitment of actin regulators.* Mol Biol Cell, 2012. **23**(10): p. 1846-59.
146. Uemura, A., et al., *The LIM domain of zyxin is sufficient for force-induced accumulation of zyxin during cell migration.* Biophys J, 2011. **101**(5): p. 1069-75.
147. Yoshigi, M., et al., *Mechanical force mobilizes zyxin from focal adhesions to actin filaments and regulates cytoskeletal reinforcement.* J Cell Biol, 2005. **171**(2): p. 209-15.

148. Hooper, C.L., P.R. Dash, and S.Y. Boateng, *Lipoma preferred partner is a mechanosensitive protein regulated by nitric oxide in the heart.* FEBS Open Bio, 2012. **2**: p. 135-44.
149. Hooper, C.L., et al., *Modulation of stretch-induced myocyte remodeling and gene expression by nitric oxide: a novel role for lipoma preferred partner in myofibrillogenesis.* Am J Physiol Heart Circ Physiol, 2013. **304**(10): p. H1302-13.
150. Jin, L., et al., *Mechanical properties of the extracellular matrix alter expression of smooth muscle protein LPP and its partner palladin; relationship to early atherosclerosis and vascular injury.* J Muscle Res Cell Motil, 2009. **30**(1-2): p. 41-55.
151. Kumar, S. and V.M. Weaver, *Mechanics, malignancy, and metastasis: the force journey of a tumor cell.* Cancer Metastasis Rev, 2009. **28**(1-2): p. 113-27.
152. Acerbi, I., et al., *Human breast cancer invasion and aggression correlates with ECM stiffening and immune cell infiltration.* Integr Biol (Camb), 2015. **7**(10): p. 1120-34.
153. Provenzano, P.P., et al., *Collagen density promotes mammary tumor initiation and progression.* BMC Med, 2008. **6**: p. 11.
154. Levental, K.R., et al., *Matrix crosslinking forces tumor progression by enhancing integrin signaling.* Cell, 2009. **139**(5): p. 891-906.
155. Northey, J.J., L. Przybyla, and V.M. Weaver, *Tissue Force Programs Cell Fate and Tumor Aggression.* Cancer Discov, 2017. **7**(11): p. 1224-1237.
156. Kharaishvili, G., et al., *The role of cancer-associated fibroblasts, solid stress and other microenvironmental factors in tumor progression and therapy resistance.* Cancer Cell Int, 2014. **14**: p. 41.
157. Wei, S.C., et al., *Matrix stiffness drives epithelial-mesenchymal transition and tumour metastasis through a TWIST1-G3BP2 mechanotransduction pathway.* Nat Cell Biol, 2015. **17**(5): p. 678-88.
158. Nguyen, T.V., et al., *Sorafenib resistance and JNK signaling in carcinoma during extracellular matrix stiffening.* Biomaterials, 2014. **35**(22): p. 5749-59.
159. Athanasiou, A., et al., *Breast lesions: quantitative elastography with supersonic shear imaging--preliminary results.* Radiology, 2010. **256**(1): p. 297-303.
160. Wu, P.H., et al., *A comparison of methods to assess cell mechanical properties.* Nat Methods, 2018. **15**(7): p. 491-498.

161. Lele, T.P., A. Brock, and S.R. Peyton, *Emerging Concepts and Tools in Cell Mechanomemory.* Ann Biomed Eng, 2019.
162. Lo, C.M., et al., *Cell movement is guided by the rigidity of the substrate.* Biophys J, 2000. **79**(1): p. 144-52.
163. Bershadsky, A.D., N.Q. Balaban, and B. Geiger, *Adhesion-dependent cell mechanosensitivity.* Annu Rev Cell Dev Biol, 2003. **19**: p. 677-95.
164. Geiger, B., J.P. Spatz, and A.D. Bershadsky, *Environmental sensing through focal adhesions.* Nat Rev Mol Cell Biol, 2009. **10**(1): p. 21-33.
165. Ross, T.D., et al., *Integrins in mechanotransduction.* Curr Opin Cell Biol, 2013. **25**(5): p. 613-8.
166. Geiger, B., et al., *Transmembrane crosstalk between the extracellular matrix--cytoskeleton crosstalk.* Nat Rev Mol Cell Biol, 2001. **2**(11): p. 793-805.
167. Parekh, A., et al., *Sensing and modulation of invadopodia across a wide range of rigidities.* Biophys J, 2011. **100**(3): p. 573-582.
168. Alexander, N.R., et al., *Extracellular matrix rigidity promotes invadopodia activity.* Curr Biol, 2008. **18**(17): p. 1295-1299.
169. Jerrell, R.J. and A. Parekh, *Matrix rigidity differentially regulates invadopodia activity through ROCK1 and ROCK2.* Biomaterials, 2016. **84**: p. 119-129.
170. Jerrell, R.J. and A. Parekh, *Cellular traction stresses mediate extracellular matrix degradation by invadopodia.* Acta Biomater, 2014. **10**(5): p. 1886-96.
171. Golji, J. and M.R.K. Mofrad, *The talin dimer structure orientation is mechanically regulated.* Biophys J, 2014. **107**(8): p. 1802-1809.
172. Margadant, F., et al., *Mechanotransduction in vivo by repeated talin stretch-relaxation events depends upon vinculin.* PLoS Biol, 2011. **9**(12): p. e1001223.
173. Chen, Y. and N.V. Dokholyan, *Insights into allosteric control of vinculin function from its large scale conformational dynamics.* J Biol Chem, 2006. **281**(39): p. 29148-54.
174. Sawada, Y., et al., *Force sensing by mechanical extension of the Src family kinase substrate p130Cas.* Cell, 2006. **127**(5): p. 1015-26.
175. Shi, Q. and D. Boettiger, *A novel mode for integrin-mediated signaling: tethering is required for phosphorylation of FAK Y397.* Mol Biol Cell, 2003. **14**(10): p. 4306-15.

176. Lawson, C.D. and K. Burridge, *The on-off relationship of Rho and Rac during integrin-mediated adhesion and cell migration.* Small GTPases, 2014. **5**: p. e27958.
177. Chaturvedi, L.S., H.M. Marsh, and M.D. Basson, *Src and focal adhesion kinase mediate mechanical strain-induced proliferation and ERK1/2 phosphorylation in human H441 pulmonary epithelial cells.* Am J Physiol Cell Physiol, 2007. **292**(5): p. C1701-13.
178. Kippenberger, S., et al., *Signaling of mechanical stretch in human keratinocytes via MAP kinases.* J Invest Dermatol, 2000. **114**(3): p. 408-12.
179. Pickup, M.W., J.K. Mouw, and V.M. Weaver, *The extracellular matrix modulates the hallmarks of cancer.* EMBO Rep, 2014. **15**(12): p. 1243-53.
180. Labernadie, A., et al., *Protrusion force microscopy reveals oscillatory force generation and mechanosensing activity of human macrophage podosomes.* Nat Commun, 2014. **5**: p. 5343.
181. Eckert, M.A., et al., *ADAM12 induction by Twist1 promotes tumor invasion and metastasis via regulation of invadopodia and focal adhesions.* J Cell Sci, 2017. **130**(12): p. 2036-2048.
182. Ruff, M., et al., *The Disintegrin and Metalloprotease ADAM12 Is Associated with TGF-beta-Induced Epithelial to Mesenchymal Transition.* PLoS One, 2015. **10**(9): p. e0139179.
183. Wisdom, K.M., et al., *Matrix mechanical plasticity regulates cancer cell migration through confining microenvironments.* Nat Commun, 2018. **9**(1): p. 4144.
184. Nasrollahi, S., et al., *Past matrix stiffness primes epithelial cells and regulates their future collective migration through a mechanical memory.* Biomaterials, 2017. **146**: p. 146-155.
185. Swift, J., et al., *Nuclear lamin-A scales with tissue stiffness and enhances matrix-directed differentiation.* Science, 2013. **341**(6149): p. 1240104.
186. Heo, S.J., et al., *Biophysical Regulation of Chromatin Architecture Instills a Mechanical Memory in Mesenchymal Stem Cells.* Sci Rep, 2015. **5**: p. 16895.
187. Yao, M., et al., *Mechanical activation of vinculin binding to talin locks talin in an unfolded conformation.* Sci Rep, 2014. **4**: p. 4610.
188. Kong, F., et al., *Cyclic mechanical reinforcement of integrin-ligand interactions.* Mol Cell, 2013. **49**(6): p. 1060-8.

189. Chaudhuri, O., et al., *Extracellular matrix stiffness and composition jointly regulate the induction of malignant phenotypes in mammary epithelium.* Nat Mater, 2014. **13**(10): p. 970-8.

190. Yu, H., J.K. Mouw, and V.M. Weaver, *Forcing form and function: biomechanical regulation of tumor evolution.* Trends Cell Biol, 2011. **21**(1): p. 47-56.

191. Samuel, M.S., et al., *Actomyosin-mediated cellular tension drives increased tissue stiffness and beta-catenin activation to induce epidermal hyperplasia and tumor growth.* Cancer Cell, 2011. **19**(6): p. 776-91.

192. Schrader, J., et al., *Matrix stiffness modulates proliferation, chemotherapeutic response, and dormancy in hepatocellular carcinoma cells.* Hepatology, 2011. **53**(4): p. 1192-205.

193. Tan, F., et al., *Matrix stiffness mediates stemness characteristics via activating the Yes-associated protein in colorectal cancer cells.* J Cell Biochem, 2018.

194. Tan, Y., et al., *Matrix softness regulates plasticity of tumour-repopulating cells via H3K9 demethylation and Sox2 expression.* Nat Commun, 2014. **5**: p. 4619.

195. Hirata, E., et al., *Intravital imaging reveals how BRAF inhibition generates drug-tolerant microenvironments with high integrin beta1/FAK signaling.* Cancer Cell, 2015. **27**(4): p. 574-88.

196. Chang, C.C., et al., *Regulation of metastatic ability and drug resistance in pulmonary adenocarcinoma by matrix rigidity via activating c-Met and EGFR.* Biomaterials, 2015. **60**: p. 141-50.

197. Tokuda, E.Y., C.E. Jones, and K.S. Anseth, *PEG-peptide hydrogels reveal differential effects of matrix microenvironmental cues on melanoma drug sensitivity.* Integr Biol (Camb), 2017. **9**(1): p. 76-87.

198. Choi, H., et al., *SAINT: probabilistic scoring of affinity purification-mass spectrometry data.* Nat Methods, 2011. **8**(1): p. 70-3.

199. Tabaries, S., et al., *Lyn modulates Claudin-2 expression and is a therapeutic target for breast cancer liver metastasis.* Oncotarget, 2015. **6**(11): p. 9476-87.

200. Yang, C., et al., *Mechanical memory and dosing influence stem cell fate.* Nat Mater, 2014. **13**(6): p. 645-52.

201. Yang, Y., et al., *Biophysical Regulation of Cell Behavior-Cross Talk between Substrate Stiffness and Nanotopography.* Engineering (Beijing), 2017. **3**(1): p. 36-54.

202. Yu, M., et al., *Force-Dependent Regulation of Talin-KANK1 Complex at Focal Adhesions.* Nano Lett, 2019. **19**(9): p. 5982-5990.
203. Sun, Z., et al., *Kank2 activates talin, reduces force transduction across integrins and induces central adhesion formation.* Nat Cell Biol, 2016. **18**(9): p. 941-53.
204. Ichikawa, T., et al., *Vinexin family (SORBS) proteins play different roles in stiffness-sensing and contractile force generation.* J Cell Sci, 2017. **130**(20): p. 3517-3531.
205. Stutchbury, B., et al., *Distinct focal adhesion protein modules control different aspects of mechanotransduction.* J Cell Sci, 2017. **130**(9): p. 1612-1624.
206. Clarke, J.H., et al., *The function of phosphatidylinositol 5-phosphate 4-kinase gamma (PI5P4Kgamma) explored using a specific inhibitor that targets the PI5P-binding site.* Biochem J, 2015. **466**(2): p. 359-67.
207. Elbediwy, A., et al., *Enigma proteins regulate YAP mechanotransduction.* J Cell Sci, 2018. **131**(22).
208. Tabaries, S., et al., *Afadin cooperates with Claudin-2 to promote breast cancer metastasis.* Genes Dev, 2019. **33**(3-4): p. 180-193.
209. Yi, J., et al., *Members of the Zyxin family of LIM proteins interact with members of the p130Cas family of signal transducers.* J Biol Chem, 2002. **277**(11): p. 9580-9.
210. Kadrmas, J.L. and M.C. Beckerle, *The LIM domain: from the cytoskeleton to the nucleus.* Nat Rev Mol Cell Biol, 2004. **5**(11): p. 920-31.
211. Engler, A.J., et al., *Matrix elasticity directs stem cell lineage specification.* Cell, 2006. **126**(4): p. 677-89.
212. Cassereau, L., et al., *A 3D tension bioreactor platform to study the interplay between ECM stiffness and tumor phenotype.* J Biotechnol, 2015. **193**: p. 66-9.
213. Galbraith, C.G., K.M. Yamada, and M.P. Sheetz, *The relationship between force and focal complex development.* J Cell Biol, 2002. **159**(4): p. 695-705.
214. DiMilla, P.A., K. Barbee, and D.A. Lauffenburger, *Mathematical model for the effects of adhesion and mechanics on cell migration speed.* Biophys J, 1991. **60**(1): p. 15-37.
215. Doyle, A.D., et al., *One-dimensional topography underlies three-dimensional fibrillar cell migration.* J Cell Biol, 2009. **184**(4): p. 481-90.
216. Peyton, S.R. and A.J. Putnam, *Extracellular matrix rigidity governs smooth muscle cell motility in a biphasic fashion.* J Cell Physiol, 2005. **204**(1): p. 198-209.

217. Pathak, A., *Modeling and predictions of biphasic mechanosensitive cell migration altered by cell-intrinsic properties and matrix confinement.* Phys Biol, 2018. **15**(6): p. 065001.
218. Gu, Z., et al., *Soft matrix is a natural stimulator for cellular invasiveness.* Mol Biol Cell, 2014. **25**(4): p. 457-69.
219. Sun, W., C.T. Lim, and N.A. Kurniawan, *Mechanistic adaptability of cancer cells strongly affects anti-migratory drug efficacy.* J R Soc Interface, 2014. **11**(99).

APPENDIX

Table S1. Parameters tested for designing PDMS and polyacrylamide substrates and coating with 488-gelatin

Parameter Tested	Successful 488-Gelatin Coating
Gelatin concentration* (1) Range of %w/v (gelatin/water)	X
Plate Format* (1) 24, 48, 96 well plates (2) Corning, MatTek, and Eppendorf	X
Additional Protein or Chemical Layers* (1) fibronectin or poly-L-lysine	X
Sulfo-SANPAH Crosslinker* (1) UV Source for activation: wavelength, intensity, duration, distance form UV source (2) Number of UV activation cycles	X
Gelatin Coating Incubation* (1) length of incubation time and temperature	X
PDMS Stiffness* (1) low versus high stiffness	X
Buffers and pH* (1) Range of HEPEs buffer concentration and pH	X
Substrate Thickness and Microscopy (1) Mounted versus unmounted substrate* (2) Upright versus inverted microscopy* (3) Substrate casting on glass versus plastic (4) Curation of PDMS at RT versus 100 °C (5) PDMS thickness	✓
Number/Type/Order of Chemical Crosslinkers/Activators (1) Glutaraldehyde* (2) sulfo-SANPAH* (3) PEI (4) Piranha (5) $NaBH_4$ (6) Plasma Oxidation*	✓

*Parameters tested for both PDMS and polyacrylamide

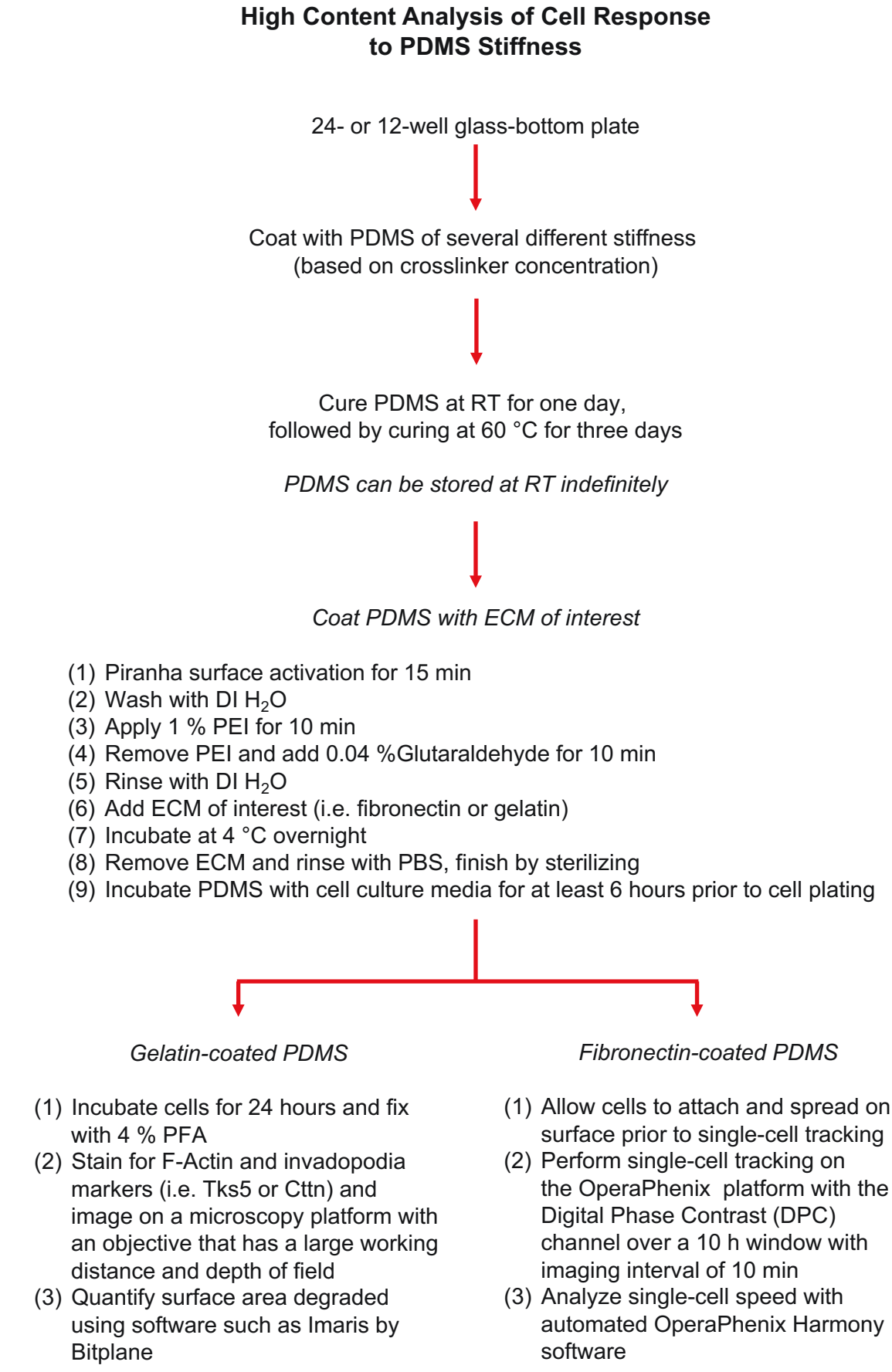

Figure S1. Schematic of experimental design for high content analysis of cell response to PDMS stiffness.

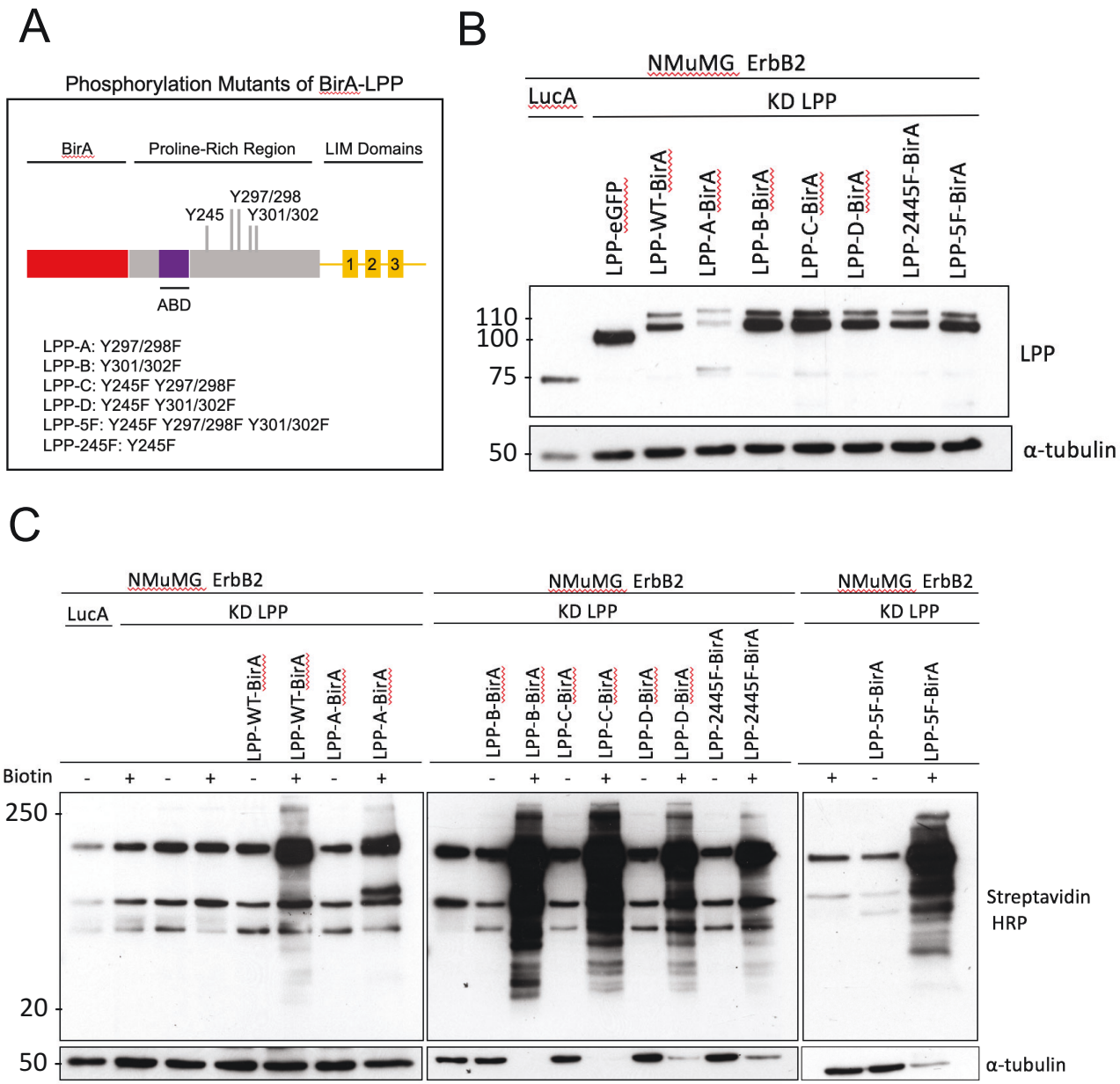

Figure S2. Immunoblot analysis of BioID construct expression in NMuMG-ErbB2 breast cancer cells. **(A)** Schematic depicting fusion of LPP phosphorylation mutants to BirA. **(B)** LPP variants were fused to BirA and protein expression levels were compared to endogenous (LucA) and eGFP-LPP. LPP A, B, C, D, 245F, and 5F represent variations in phosphorylation site mutation; A: Y297F/Y298F, B: Y301F/Y302F, C: Y245F/Y297F/Y298F, D: Y245F/Y301F/Y302F, 245F: Y245F, and 5F: Y245F/Y297F/Y297F/Y301F/Y302F. **(C)** Cells were incubated with 50 μM biotin for 24 hours and collected for lysis. Whole cell lysates (input) and streptavidin pulldown (biotinylated proteins) were blotted. An antibody specific to LPP was used to detect the fusion protein expression, while Streptavidin fused to HRP was used to detect all biotinylated proteins. α-tubulin was used as the loading control for each set of immunoblots.

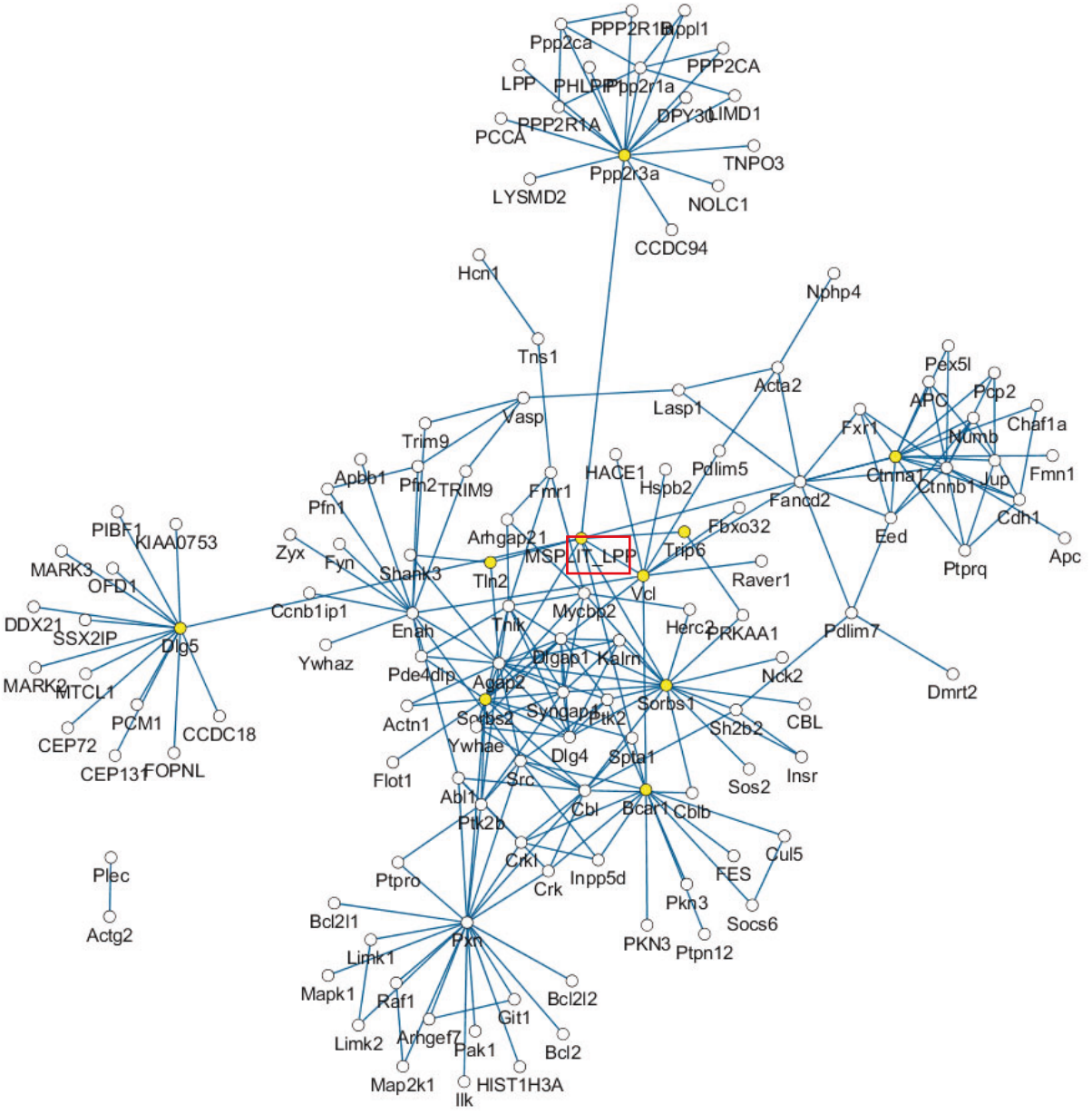

*Yellow nodes represent primary nodes

Figure S3. LPP protein interaction network from a BioGRID database and combined with an LPP BioID data set. Prioritized proteins identified with the BioID of LPP are represented as the yellow nodes. These yellow nodes represent the first subshell of interactors. The second subshell in the network taken from a BioGRID database, represented by white nodes, are known protein interactions of the BioID identified proteins (yellow nodes).

Table S2. Enriched BioID interactors of LPP-WT with TGFβ treatment

Enriched in WT LPP + TGFβ Condition

Prey	SAINT Score
Tns1	1.00
Tln2	1.00
Vcl	0.73
Pxn	0.55
Kank1	0.50
Kank2	0.59
Shroom2	0.32
Ctnna1	0.80
Bcar1	0.38
Sorbs1	0.77
Enah	0.39
Trip6	0.95
Pdlim7	0.55
Dok1	0.47
Arhgap21	0.47
Arpc4	0.43
Rassf8	0.46

Table S3. Enriched BioID interactors of LPP-ΔABD with TGFβ treatment

Enriched in ΔABD LPP + TGFβ Condition

Prey	SAINT Score
Actg2	1.00
Acta2	1.00
G3bp2	0.35
Ppp2r3a	1.00
Cdgap (Arhgap31)	0.45

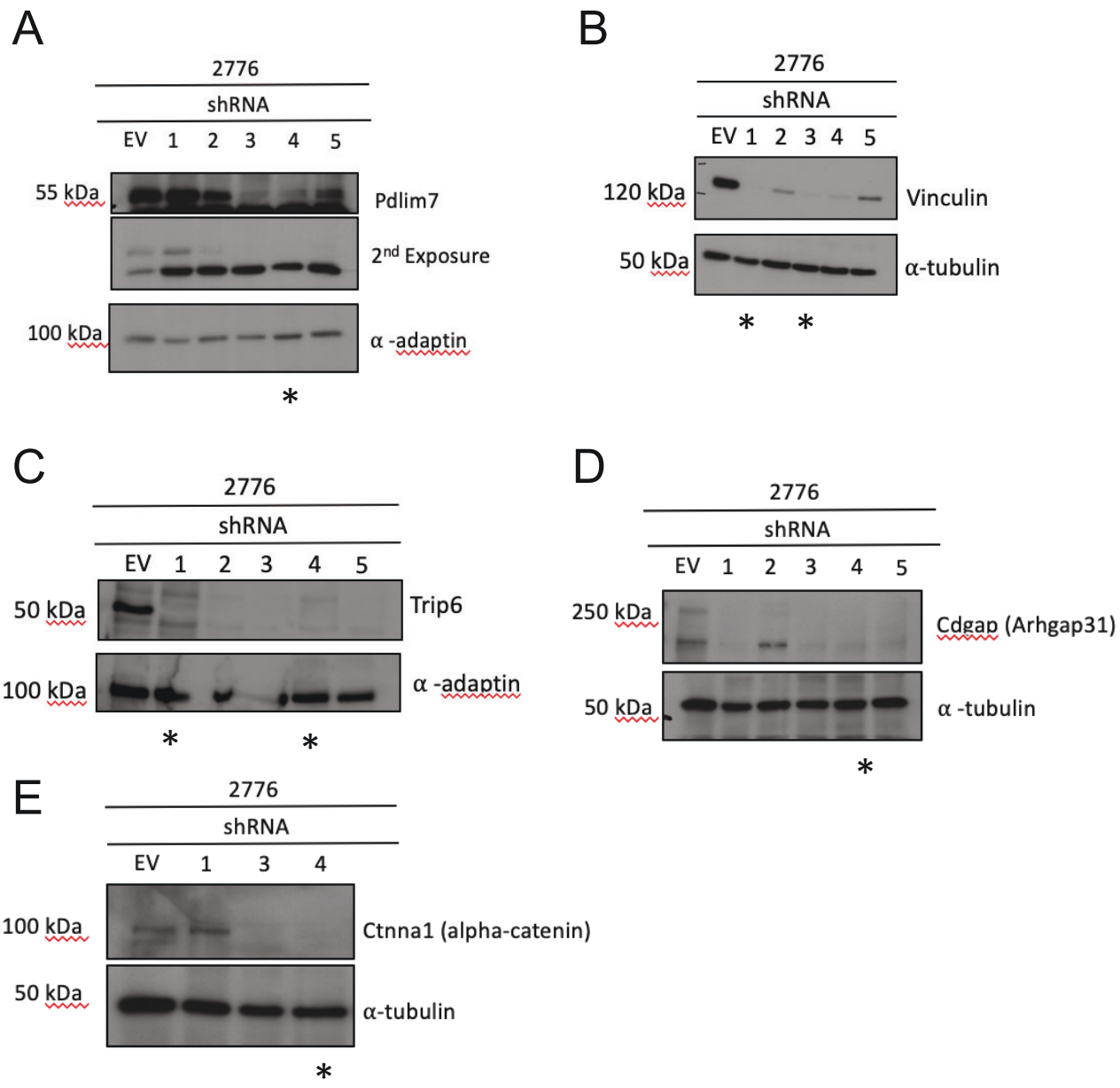

Figure S4. Immunoblots of 2776 cells with shRNA against prioritized LPP BioID candidates. Antibodies against **(A)** Pdlim7, **(B)** Vinculin, **(C)** Trip6, **(D)** Cdgap, and **(E)** Ctnna1 were used to identify successful KD of protein expression. Both α-adaptin and α-tubulin were used as loading controls. Immunoblots were validated twice and the shRNA denoted with an * represent shRNA which were successful in both biological replicates.

A

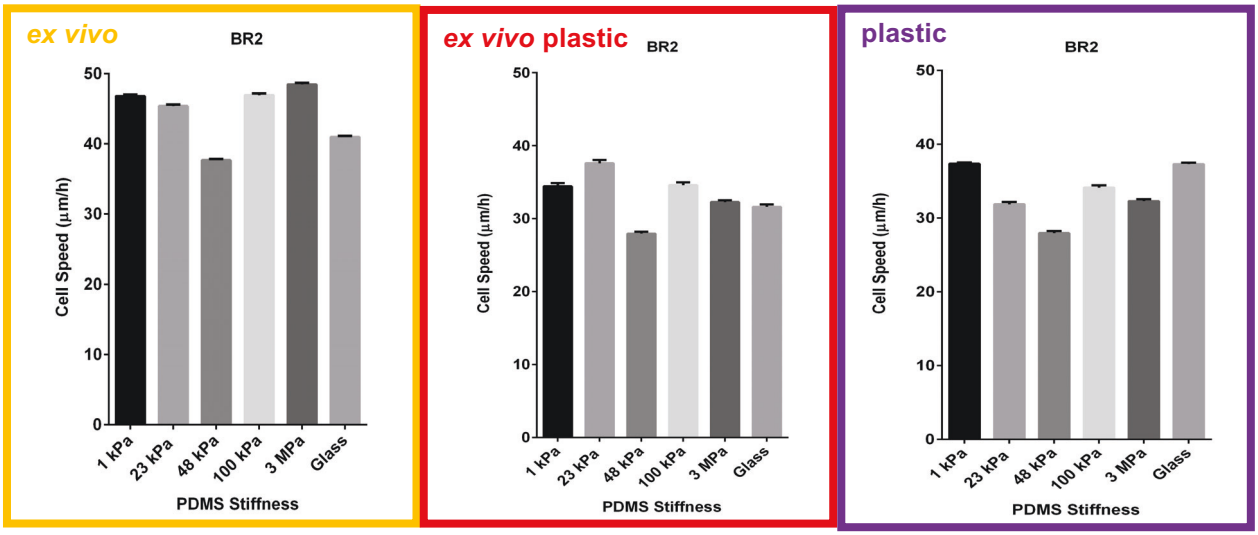
ex vivo
BR2
Cell Speed (µm/h)
50
40
30
20
10
0
1 kPa
23 kPa
48 kPa
100 kPa
3 MPa
Glass
PDMS Stiffness
ex vivo plastic
BR2
Cell Speed (µm/h)
PDMS Stiffness
plastic
BR2
Cell Speed (µm/h)
PDMS Stiffness

B

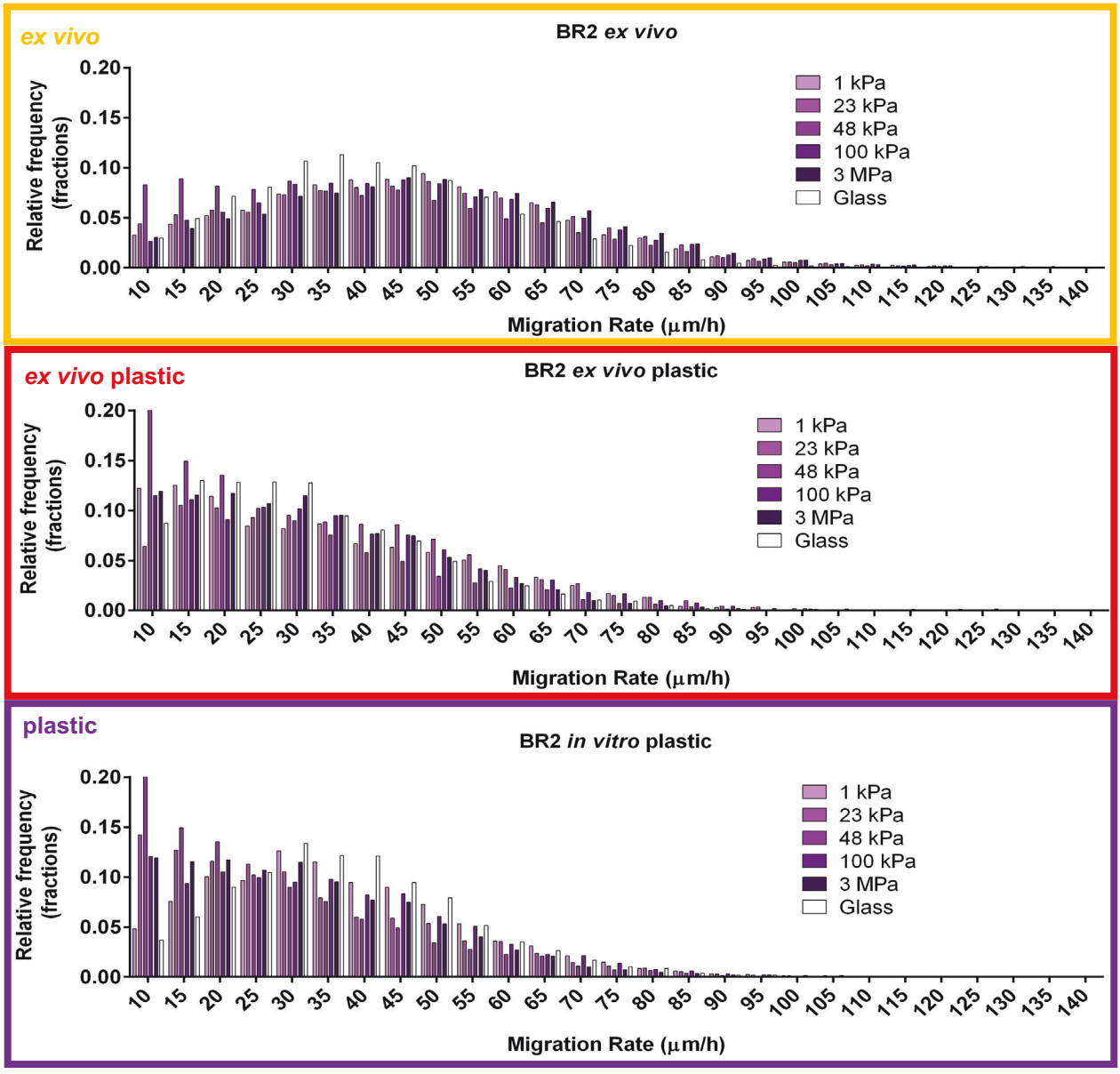
ex vivo
BR2 ex vivo
Relative frequency (fractions)
0.20
0.15
0.10
0.05
0.00
1 kPa
23 kPa
48 kPa
100 kPa
3 MPa
Glass
10 15 20 25 30 35 40 45 50 55 60 65 70 75 80 85 90 95 100 105 110 115 120 125 130 135 140
Migration Rate (µm/h)
ex vivo plastic
BR2 ex vivo plastic
Relative frequency (fractions)
Migration Rate (µm/h)
plastic
BR2 in vitro plastic
Relative frequency (fractions)
Migration Rate (µm/h)

Figure S5. Second biological replicate of MDA-MB-231 migration response to stiffness after biophysical conditioning. MDA-MB-231 *ex vivo* cells were taken either directly *ex vivo* from mouse brain tissue or were cultured for one week on plastic and subsequently cultured on PDMS of different stiffness (*ex vivo* and *ex vivo* plastic, respectively). The migration speed of these cells were compared to MDA-MB-231 serially cultured on plastic (plastic) and placed on PDMS of different stiffness. **(A)** Average cell speed (μm/h) of MDA-MB-231 from distinct biophysical environments (*ex vivo*, *ex vivo* plastic and plastic) on PDMS of 1 kPa, 23 kPa, 48 kPa, 100 kPa, 3 MPa, and Glass. **(B)** Frequency distribution of cell migration speed (A) with a bin size of 5 μm/h.